UNIVERSITY OF DEUSTO

Engineering for the Information Society and Sustainable Development

NOVEL OPTIMIZATION METHODS AND MODEL FOR IMPROVING SUSTAINABILITY AND EFFICIENCY IN LAST-MILE LOGISTICS

Erick Rodríguez Esparza

A dissertation submitted in partial fulfillment of the
requirements for the degree of Doctor of Philosophy

Supervised by Dr. Antonio D. Masegosa Arredondo and Dr. Enrique Onieva Caracuel

Bilbao, Biscay, 2024

UNIVERSITY OF DEUSTO

Engineering for the Information Society and Sustainable Development

NOVEL OPTIMIZATION METHODS AND MODEL FOR IMPROVING SUSTAINABILITY AND EFFICIENCY IN LAST-MILE LOGISTICS

Candidate:

Erick Rodríguez Esparza

Advisor: **Dr. Antonio D. Masegosa Arredondo**

Advisor: **Dr. Enrique Onieva Caracuel**

Bilbao, Biscay, 2024

Novel Optimization Methods and Model for Improving Sustainability and Efficiency in Last-Mile Logistics

Author: Erick Rodríguez Esparza
Advisor: Antonio David Masegosa Arredondo
Advisor: Enrique Onieva Caracuel

Text printed in Bilbao
First edition, 2024

To my mom and dad, for all your love, support and patience. I will always be indebted to you. Thanks to you I am who I am.

Abstract

This thesis delves into the challenges in Last-Mile Logistics (LML) optimization in urban environments, intensified by the rapid growth of e-commerce and the consequential demands on logistics systems, particularly highlighted during the rapid increase in online shopping and the transformative effects of the COVID-19 pandemic. It emphasizes the role of LML in connecting businesses with consumers, which is significantly impacting urban infrastructure and logistics efficiency.

This remarkable growth has posed challenges for logistics service providers (LSPs) in the LML sector, where efficiency and timely delivery are crucial. This shift also has significant social implications, particularly evident in urban environments.

Specifically, LSPs face the fact that LML is the most resource-intensive and costly segment of the delivery process, accounting for approximately 28% to 41% of the total delivery costs. Moreover, factors such as failed deliveries, lower delivery success rates in certain areas, and consumer environmental concerns further exacerbate these costs.

Furthermore, delivering goods in urban environments presents additional obstacles, such as complex traffic management, limited parking availability, and convoluted delivery routes. The increasing number of delivery vehicles increases urban congestion, dominates infrastructure use, and disrupts traffic flow, thereby affecting vehicle circulation and compromising the safety of pedestrians and cyclists, ultimately impacting overall urban mobility.

As the number of freight vehicles in cities increases, LML operations significantly influence urban sustainability. Addressing these challenges requires innovative solutions that streamline the delivery process, reduce travel distances, and mitigate economic, environmental, and social impacts.

Among the proposed solutions to address the challenges and impacts of LML, three strategic policies are gaining considerable attention and yielding positive results: Vehicle Fleet Electrification, Demand Aggregation Infrastructure, and Enhanced Traffic Management. These policies aim to address various aspects of LML optimization. However, each of these policies presents unique challenges, necessitating the development of new tools and technologies to assist LSPs, public authorities, and infrastructure managers. This thesis aims to contribute to these advanced optimization methods and models, which will improve efficiency, sustainability, and resilience in LML.

The use of optimization methods in this thesis to address the challenges associated with the three policies is explained. To overcome the challenges posed by the vehicle fleet electrification policy, this thesis employs advanced optimization techniques to develop intelligent route planning solutions that minimize distances and reduce delivery times. Specifically, the focus is on the Capacitated Electric Vehicle Routing Problem (CEVRP),

which entails strategic planning of Electric Vehicle (EV) routes regarding their limited load and range. A significant gap in current CEVRP methodologies is their lack of scalability and robustness, especially when handling scenarios with high customer density. Therefore, a key contribution is the development of the Hyper-heuristic Adaptive Simulated Annealing with Reinforcement Learning (HHASA_{RL}) algorithm for solving the CEVRP, which demonstrates significant progress over existing methods in the state-of-the-art by identifying optimal solutions for high-dimensional instances on the IEEE WCCI2020 competition benchmark.

To overcome the challenges presented by the demand aggregation infrastructure policy, this thesis delves into the intricacies of the Stationary Parcel Locker (SPL) Location Problem. SPLs are physical facilities consisting of automated storage units placed in accessible locations, and the problem lies in determining the optimal locations to install the lockers and their setup in terms of size and volume. However, a significant gap in current SPL models is their lack of consideration for dynamic customer behavior and realistic constraints, including limited locker capacity, stochastic demand distributions, and variable costs and collection periods. Therefore, another key contribution is the development of the new Constrained Locker Location Problem under the Threshold Luce Model (CLLPTLM), which incorporates these mentioned factors and the probability of customer acceptance, offering realistic solutions. It was solved using an adapted Genetic Algorithm (GA) using data from synthetic and real datasets.

To overcome the challenges inherent in the enhanced traffic management policy, this thesis focuses on vehicle segmentation in image-based vehicle traffic monitoring. This monitoring process involves analyzing traffic camera video to identify and detect vehicles, aiming to estimate the state of roads. It enables real-time assessment of traffic flow, density, and patterns, providing valuable data to inform and optimize traffic control measures. However, current methodologies have gaps in the accuracy and adaptability of vehicle segmentation, especially in adjusting to various environmental conditions and incorporating real-time data for traffic management. Therefore, the final contribution of this thesis is the Hyper-heuristic Genetic Algorithm based on Thompson Sampling with Diversity (HH-GATSD), which demonstrates robustness and adaptability in vehicle segmentation within vehicle monitoring. The proposed method incorporates sophisticated optimization techniques to dynamically segment vehicles in traffic camera video frames, allowing for precise and adaptive estimation of road occupancy.

This dissertation underscores the potential for leveraging Metaheuristics (MHs) and Hyper-heuristics (HHs) in crafting solutions for the LML to improve sustainability in operational challenges for LSPs and society, mitigating economic, environmental, and social impacts. Future research directions are suggested, particularly in refining these algorithms and models to adapt to more complex and varied urban logistics scenarios, further integrating technological advancements to build smarter and more responsive urban logistics systems.

Acknowledgements

First and foremost, I want to thank my family. None of this would've been possible without the opportunities, constant support, understanding, and unconditional love that I've received from my mom and dad. Their presence, even from afar, has been my greatest inspiration and motivation to complete this journey. Your sacrifices, guidance, and belief in me have laid the foundation for my success in completing this doctoral thesis.

To my brothers, Omar and Josué, I extend my heartfelt gratitude for always being there for me, despite the distance that separates us. Your presence drives me to strive to be a better brother and a good example for you. I hope to continue making you proud.

Moving on, I want to thank my supervisors, Antonio Masegosa and Enrique Onieva, for offering me this opportunity, the freedom, and the constant trust they've placed in me throughout this journey. I'm grateful for their support for each of my ideas and projects, no matter how crazy they were. They were always there to provide me with their knowledge and feedback, helping me to realize them.

I'm also thankful to my former master's supervisor and dear friend, Diego Oliva, for continuing to collaborate with me. His support has extended beyond the academic; he's been a friend and mentor.

I wish to express my deepest gratitude to the people who've accompanied me and put up with me patiently during this process of over three years. My gratitude extends to my coworkers, friends, and former colleagues at DeustoTech (Oscar J., Armando M., Hamed A., Alexandra B., Elisa A., Ana G., Paddy J., Hugo L., Jenny F., Luis D., Leire S., Salomey O., Iván G., Ignacio F., Manuel A., Aritz M., Lorenzo P., Oleksandr H., and Danyal M.). Our conversations during meals and coffee breaks, full of laughter, advice, and motivation, have been a fundamental pillar in my day-to-day life.

Furthermore, I extend my sincere gratitude to Eleni I. Vlahogianni for giving me the opportunity to carry out my research stay, which has been a profoundly enriching experience. I also want to express my deep appreciation to my colleagues and friends (Emmanouil K., Konstantinos K., Charis C., Eleni M., and Panagiotis F.) at the National Technical University of Athens, who shared this journey with me and made it an incredible ride.

Lastly, I want to thank that special group of friends I met in Bilbao, who have become much more than friends to me; I already consider them my family (Maxime T., Karolina Ć., David M., Lizeth C., Mikel R., Ricky G., Quentin D., Nicolas S., Davide R., Valeria O., Khadja P., Elif O., Ezgi U., Fabio G., Eduarda D., Nacho G., Pedro L., Lorenza D., Panagiotis R., and Sarah H.). Thank you for all the shared experiences, the trips we've taken together, the countless times going out for beers, and for all the affection I've felt from you. Every moment spent with you has been valuable and has left an unforgettable

mark on my heart.

Finally, I'm deeply grateful to my other family in Mexico: Carlos G., Flavio M., Miguel J., Armando S., Marco F., Alejandro O., Laura Z., Fernando R., Juanma N., Saúl M., Jesús E., Oscar R., and Nayeli G. Your presence in my life over the years has been invaluable. Despite the distance, the love and friendship we share remain strong, reminding me of the lifelong bonds that keep us connected. Your support, friendship, and the conversations we've shared have been a constant source of motivation and comfort.

Contents

List of Figures i

List of Tables iii

Acronyms v

1 Introduction 1
- 1.1 Motivation and Scope . . . 4
- 1.2 Objectives and Specific Objectives: . . . 6
- 1.3 Research Methodology . . . 6
- 1.4 Contributions and Publications . . . 8
- 1.5 Research Context . . . 10
  - 1.5.1 Research Support and Funding . . . 10
  - 1.5.2 Research Stay . . . 10
- 1.6 Structure of the Thesis . . . 10

2 Background and Related Work 13
- 2.1 Logistics . . . 13
  - 2.1.1 Logistics Management . . . 14
  - 2.1.2 Transportation Operations . . . 16
  - 2.1.3 Last-Mile Logistics . . . 17
- 2.2 Optimization . . . 18
  - 2.2.1 Metaheuristics . . . 21
  - 2.2.2 Hyper-heuristics . . . 24
- 2.3 Optimization Problems and Methods for Last-Mile Logistics . . . 26
  - 2.3.1 Capacitated Electric Vehicle Route Optimization . . . 26
  - 2.3.2 Stationary Parcel Locker Location problem . . . 27
  - 2.3.3 Image-Based Vehicle Traffic Monitoring Optimization . . . 29

3 A New Hyper-Heuristic for the Capacitated Electric Vehicle Routing Problem 31
- 3.1 Introduction . . . 31
  - 3.1.1 Challenges in Last-Mile Operations . . . 31
  - 3.1.2 Objectives and Contributions . . . 32
- 3.2 Methodology . . . 32
  - 3.2.1 Capacitated Electric Vehicle Routing Problem . . . 32

3.2.2 Theoretical Bases . . . 35
3.2.3 Simulated Annealing . . . 35
3.2.4 Multi-Armed Bandit Reinforcement Learning Methods . . . 36
3.2.5 Heuristics for Vehicle Routing Problem . . . 37
3.2.6 Hyper-heuristic Adaptive Simulated Annealing and Reinforcement Learning . . . 38
3.3 Experimental Framework . . . 43
3.3.1 Benchmark Description . . . 43
3.3.2 Experimental Setup . . . 45
3.4 Results and Discussion . . . 45
3.4.1 Comparison of the Statistical Results . . . 45
3.4.2 Non-Parametric Analysis . . . 47
3.4.3 Analysis of the Selection of Heuristics of the Hyper-Heuristic Proposals 48
3.4.4 Comparison of Additional Energy Used . . . 51
3.4.5 Graphical Analysis of the Solution . . . 52
3.5 Conclusions . . . 53

4 A New Model for Stationary Parcel Locker Location Problem under Realistic Constraints 55
4.1 Introduction . . . 55
4.1.1 Challenges in Last-Mile Operations . . . 55
4.1.2 Objectives and Contributions . . . 56
4.2 Methodology . . . 56
4.2.1 Model Formulation . . . 57
4.2.2 Proposed Method . . . 60
4.3 Experimental Framework . . . 61
4.3.1 Instance Generator for the Synthetic Dataset . . . 62
4.3.2 Experimental Setup . . . 64
4.4 Results and Discussion . . . 67
4.4.1 Synthetic Dataset Results . . . 67
4.4.2 Real-World Dataset Results . . . 72
4.5 Conclusions . . . 77

5 A Robust Hyper-Heuristic Approach for Vehicle Segmentation 79
5.1 Introduction . . . 79
5.1.1 Challenges in Last-Mile Operations . . . 79
5.1.2 Objectives and Contributions . . . 80
5.2 Methodology . . . 80
5.2.1 Multilevel Image Segmentation . . . 80
5.2.2 Hyper-heuristic Genetic Algorithm based on Thompson Sampling with Diversity . . . 83
5.3 Experimental Framework . . . 87
5.3.1 Datasets . . . 87
5.3.2 Experimental Setup . . . 90
5.3.3 Methodology for Vehicle Segmentation . . . 91

5.3.4 Metrics . . . 93
5.3.5 Non-parametric Test . . . 96
5.4 Results and Discussion . . . 96
5.4.1 Experiments with IEEE CEC2017 Benchmark . . . 96
5.4.2 Experiments in Multilevel Segmentation . . . 101
5.4.3 Experiments with Traffic Video Frames for the Vehicle Segmentation 102
5.5 Conclusions and Future Work . . . 107

6 Conclusions and Future Work 109
6.1 Summary of Contributions . . . 109
6.2 Limitations and Future Work . . . 111
6.3 Other Publications . . . 112

List of Figures

1.1 LML: The final leg of the supply chain connecting businesses with end consumers. . . . 1
1.2 The research methodology flowchart of this thesis comprises four interconnected stages, forming a cyclical and iterative process. . . . 7

2.1 Hierarchy of supply chain, logistics and transportation. . . . 15
2.2 Physical flow of logistic processes. . . . 16
2.3 Transport Networks Example. . . . 17
2.4 Diversity of LML services. . . . 18
2.5 The design optimization process. . . . 19
2.6 Classification of optimization algorithms. . . . 21
2.7 Actions of a metaheuristic algorithm. a) Exploration. b) Exploitation. . . . 23
2.8 Classification of metaheuristic algorithms. . . . 23
2.9 Classification of hyper-heuristic algorithms. . . . 24

3.1 Example of CEVRP with four routes. (A) stops twice in the same charging station, (B) does not stop in any station, (C) stops in two different stations and (D) stops in a single station. . . . 34
3.2 The general flowchart of HHASA$_{RL}$ . . . 39
3.3 Local search flowchart of HHASA$_{RL}$ . . . 41
3.4 Graphs of the vectors of the selected heuristics and the rewards of all the local searches of the four proposals of this work for the E101 instance. . . . 49
3.5 Graphs of the vectors of the selected heuristics and the rewards of all the local searches of the four proposals of this work for the X916 instance. . . . 50
3.6 Solutions generated by HHASA$_{TS}$ for instances E51, E101, X685, and X1001. The symbols •, ○, and • represent the depot, customers, and charging stations, respectively. . . . 53

4.1 A static parcel locker paradigm. . . . 56
4.2 Example of the fixed lockers problem under the CLLPTLM model. a) fixed parcel lockers problem. b) solution using the CLLPTLM. . . . 60
4.3 General flowchart and encoding of the locker set. . . . 60
4.4 Flowchart of the adapted GA. . . . 62
4.5 Distribution of the position of the customers: a) uniform distribution; b) standard Gaussian distribution; c) shifted Gaussian distribution; d) mixture of two Gaussian distributions. . . . 64

4.6 Geographical locations of the SPLs with the solutions obtained for the instance B3 with $p = 1$ and $Max_C = 7$. 67
4.7 Convergence curve for the B3 instance with $p = 0.8$ and $Max_C = 5$: a) uniform distribution; b) standard Gaussian distribution; c) shifted Gaussian distribution; d) mixture of two Gaussian distributions. 70
4.8 Demand Cost Sensitivity Analysis of the B3 instance for the four distributions. 73
4.9 Geographical locations of the SPLs with the solutions obtained for the real-world dataset with $p = 1$. a) $Max_C = 5$. b) $Max_C = 7$. c) $Max_C = 10$. . . 74
4.10 Convergence curve for the real-world dataset with $p = 0.8$ and a) $Max_C = 5$, b) $Max_C = 7$, c) $Max_C = 10$. 75
4.11 Demand Cost Sensitivity Analysis of the real-world dataset. 76

5.1 Flowchart of the proposed HHGATSD. 84
5.2 Set of benchmark images and their corresponding histograms depicting the distribution of pixel intensities. The histograms offer insights into the frequency of intensity values in each image, providing additional information about the image features. 89
5.3 Examples of frames captured from the road traffic surveillance camera. . . 90
5.4 Flowchart of the proposed method for vehicle segmentation in a traffic surveillance camera. 91
5.5 Convergence curves for all algorithms during a specific run of 50-dimensional instances. The curves employ a logarithmic scale for enhanced presentation quality. 100
5.6 Visual Examples of the Proposed Methodology. 105
5.7 Visual Examples of the Proposed Methodology. 106

List of Tables

3.1 Details of the CEVRP benchmark set 44
3.2 Results of the proposed algorithm applied to small instances of the benchmark 46
3.3 Results of the proposed algorithm applied to large instances of the benchmark 47
3.4 Average Friedman's rankings and Holm's p values (0.05) of the four proposed HHs for the CEVRP benchmark. 48
3.5 Average Friedman's rankings and Holm's p values (0.05) of the comparison with the state-of-the-art for the CEVRP benchmark. 48
3.6 Difference in energy consumption between the average distance values and the minimum distance found so far. 52

4.1 Notations for the CLLPTLM model 58
4.2 Computational results of the B1 instance under all combinations (p, Max_C). 68
4.3 Computational results of the B2 instance under all combinations (p, Max_C). 69
4.4 Computational results of the B3 instance under all combinations (p, Max_C). 69
4.5 Cost results for the B1 instance under all combinations (p, Max_C). 71
4.6 Cost results for the B2 instance under all combinations (p, Max_C). 71
4.7 Cost results for the B3 instance under all combinations (p, Max_C). 72
4.8 Computational results of the real-world dataset under all combinations (p, Max_C). 73
4.9 Cost results for the real-world dataset under all combinations (p, Max_C). . 75

5.1 Summary of the CEC2017 Benchmark Functions 88
5.4 Average Friedman's Rankings and Holm's p Values (0.05) for the CEC2017 Benchmark Functions in 30 and 50 Dimensions. 97
5.2 Statistical Results of the CEC2017 Benchmark Functions in 30 Dimensions. 98
5.3 Statistical Results of the CEC2017 Benchmark Functions in 50 Dimensions. 99
5.5 Average Friedman's Rankings and Holm's p Values (0.05) for the BSDS500. 101
5.6 Average Computation Times (in seconds) for the BSDS500 and Traffic Video Frames. 102
5.7 Stadistical Results and Average Friedman's Rankings and Holm's p Values (0.05) for traffic video frames. 103
5.8 Statistical Results of the Performance Metrics in Vehicle Segmentation. . . 104

Acronyms

- **AVG: AV**era**G**e
- **BACO: B**ilevel **A**nt **C**olony **O**ptimization
- **BLPSO: B**iogeography-based **L**earning **P**article **S**warm **O**ptimization
- **BSD: B**ernstain-**S**earch **D**ifferential Evolution
- **BLX: BL**end Crossover
- **CEVRP: C**apacitated **E**lectric **V**ehicle **R**outing **P**roblem
- **CLLPTLM: C**onstrained **L**ocker **L**ocation **P**roblem under the **T**hreshold **L**uce **M**odel
- **DE: D**ifferential **E**volution
- $\mathbf{D}_{TD}$ Normalized **T**rue **D**iversity
- ϵ**-G: E**psilon **G**reedy
- **EV: E**lectric **V**ehicle
- **EVRP: E**lectric **V**ehicle **R**outing **P**roblem
- **FSIM: F**eature **S**imilarity **I**ndex **M**etric
- **GA: G**enetic **A**lgorithm
- **GRASP: G**reedy **R**andomized **A**daptive **S**earch **P**rocedure
- **GWO: G**rey **W**olf **O**ptimizer
- **HH: H**yper-**H**euristic
- **HHO: H**arris **H**awks **O**ptimization
- $\mathbf{HHASA}_{RL}$**: H**yper-**H**euristic **A**daptive **S**imulated **A**nnealing with **R**einforcement **L**earning
- **HHGATSD: H**yper-**H**euristic **G**enetic **A**lgorithm based on **T**hompson **S**ampling with **D**iversity

- **JADE:** Self-**A**daptive **D**ifferential **E**volution
- **LLH:** **L**ow-**L**evel **H**euristic
- **LLPTL:** **L**ocker **L**ocation **P**roblem under the **T**hreshold **L**uce
- **LML:** **L**ast-**M**ile **L**ogistics
- **LSP:** **L**ogistic **S**ervice **P**rovider
- **MAB:** **M**ulti-**A**rmed **B**andit
- **MCET:** **M**inimum **C**ross-**E**ntropy **T**hresholding
- **MH:** **M**eta**h**euristic
- **MIN:** **M**inimum
- **NMDF:** **N**ormalization with **M**aximum **D**iversity so **F**ar
- **PSNR:** **P**eak **S**ignal to **N**oise **R**atio
- **PSO:** **P**article **S**warm **O**ptimization
- **RL:** **R**einforcement **L**earning
- **RMSE:** **R**oot **M**ean **S**quare **E**rror
- **RPCA:** **R**obust **P**rincipal **C**omponent **A**nalysis
- **SA:** **S**imulated **A**nnealing
- **STD:** **St**andard **D**eviation
- **SPL:** **S**tationary **P**arcel **L**ocker
- **SSIM:** **S**tructural **S**imilarity **I**ndex **M**etric
- **TLM:** **T**hreshold **L**uce **M**odel
- **TS:** **T**hompson **S**ampling
- **UPC1:** **U**pper **C**onfidence **B**ound 1
- **VNS:** **V**ariable **N**eighborhood **S**earch
- **VRP:** **V**ehicle **R**outing **P**roblem

1

Introduction

The expansion of the e-commerce industry has significantly changed consumer behavior and the logistics landscape. Last-Mile Logistics (LML), the final leg of the supply chain, has emerged as a critical and challenging aspect, particularly with the surge in online purchases [1, 2]. This growing significance of LML in the e-commerce sector parallels the global rise in online transactions [3]. As depicted in Figure 1.1, LML plays an integral role in connecting businesses with final consumers.

Figure 1.1: LML: The final leg of the supply chain connecting businesses with end consumers.

In 2018, e-commerce increased by 23.3% [4], and this trend accelerated further during the COVID-19 pandemic because of the mobility restrictions [5, 6]. This transformative period led to a staggering 74% increase in e-commerce websites and a notable shift of 52% of consumers away from physical stores [7].

However, this remarkable growth has posed challenges for Logistics Service Providers (LSPs) in the LML sector, where efficiency and timely delivery are crucial. This growth also has significant societal impacts resulting in significant effects, especially in urban environments [7, 8].

To be more specific, LSPs face substantial challenges in the LML sector because it constitutes the most resource-intensive and time-consuming phase in the delivery process, comprising up to 28% of the total delivery cost [9] and, in some instances, soaring to 41% [10]. Factors such as failed deliveries, low delivery rates in specific areas, and heightened consumer concerns about the environmental impact contribute to these costs [11]. To address these challenges, innovative solutions are essential to optimize the delivery process, reduce travel distances, and mitigate economic, environmental, and social impacts.

Urban environments present additional obstacles to LML, including traffic management issues, limited parking availability, and convoluted delivery routes. Moreover, meeting delivery timelines is particularly challenging in these environments, given the expectation for fast and accurate delivery schedules [12].

Addressing the social challenges and impacts of the LML sector involves recognizing the consequences of intensified infrastructure usage. The surge in delivery vehicles not only results in heightened congestion but also leads to the substantial occupation of urban infrastructure, contributing to the saturation of available space. This increased occupation of roads and public spaces disrupts traffic flow and poses challenges for pedestrians and cyclists, impacting overall urban mobility [13].

The rise in congestion and infrastructure occupation due to the influx of delivery vehicles contribute to increased pollutant emissions which directly affects public health. Prolonged exposure to congested and polluted urban environments can contribute to respiratory issues and aggravate existing health problems. Furthermore, the increased noise generated by the growing fleet of delivery vehicles adds another layer of concern. Noise pollution is often underestimated, adversely affecting physical and mental well-being, leading to stress, sleep disturbances, and other health-related issues for residents in these areas [14].

In addition to immediate health concerns, the environmental footprint of LML operations is a significant consideration. The heightened CO_2 emissions from the expanding delivery fleet contribute to air pollution and climate change. Mitigating these emissions is imperative to address broader environmental challenges and achieve sustainability objectives [15].

To confront these challenges in LML, solutions should come from different areas such as urban planning strategies, environmental regulations, and innovative transportation solutions. Creating sustainable and resilient urban logistics systems is fundamental to balancing the need for efficient LML with the well-being of urban environments and their inhabitants.

Among the solutions proposed to address the challenges and impacts of LML, three policies are gaining considerable traction and yielding positive outcomes:

1. **Vehicle Fleet Electrification:** This policy seeks to tackle environmental issues by transitioning the delivery vehicle fleet to Electric Vehicles (EVs). The advantages of this electrification include a significant reduction in carbon emissions and

air pollution, thus contributing to better air quality in urban areas. Furthermore, electrification proves advantageous for LSPs by reducing operational costs related to fuel and maintenance. However, it faces several challenges, such as the need to develop charging infrastructures, manage the high initial costs of EVs, and strategically plan routes, considering aspects like charging time, autonomy limitations, and the location of charging points [16].

2. **Demand Aggregation Infrastructure:** This policy encompasses solutions such as parcel lockers, collaborative warehouses, and microhubs, aiming to streamline delivery operations. Among these, parcel lockers prove to be the most successful. They can reduce the number of failed deliveries, leading to increased efficiency and customer satisfaction. Furthermore, they help to minimize travel distances and optimize routes, benefiting LSPs by lowering costs and improving delivery accuracy. Additionally, it alleviates traffic congestion by decreasing the number of delivery vehicles in urban environments, thereby reducing emissions. However, challenges such as the costly initial investment, security concerns, and ensuring consumer acceptance need to be addressed, particularly in urban and densely populated areas where finding suitable locations for parcel lockers can be complex [17].

3. **Enhanced Traffic Management:** This policy focuses on implementing advanced traffic management systems to mitigate the impact of the growing volume of vehicles dedicated to LML. Advantages of enhanced traffic management include improved traffic flow, reduced congestion, and better urban mobility, contributing to the reduction in stress caused by traffic, noise, and air pollution in urban areas. Furthermore, LSPs can benefit from this policy since it can increase delivery efficiency and reduce travel times. To implement this type of policy, the deployment of smart sensors, such as traffic counters and cameras, is required. While traditional traffic counters may necessitate roadworks that need to disrupt traffic, emerging technologies like traffic cameras, often already deployed by the traffic management authorities, offer a less intrusive and more cost-effective solution. However, challenges include the development of automated methods to extract valuable information from these devices [18].

To address the challenges posed by these policies, it is required to develop new tools and technologies to assist LSPs, public authorities, and infrastructure managers. This thesis aims to contribute to the development of these new tools and technologies, which will in turn contribute to enhancing the efficiency, sustainability, and resilience of LML.

In this chapter, Section 1.1 sets out the motivation for this research and the research questions that have emerged from it. Subsequently, the research objectives and methodology are presented in Sections 1.2 and 1.3, respectively. The contributions and scientific publications are then summarized in Section 1.4. Finally, the research context and the outline of this thesis are provided in Sections 1.5 and 1.6, respectively.

1.1 Motivation and Scope

In recent years, the logistics sector, including LML, has seen a significant increase in data availability, driven by ongoing digitalization and the widespread adoption of technologies like the Internet of Things. This influx of data presents both opportunities and challenges for the logistics industry [19].

Amidst this data-driven landscape, Artificial Intelligence (AI) has emerged as a powerful tool across various fields, revolutionizing problem-solving and decision-making processes. AI technologies, such as machine learning, optimization algorithms, and predictive analytics, provide unmatched capabilities in analyzing data fostering better-informed decision-making. The logistics industry is also benefiting from the impact of AI technologies in addressing these challenges by leveraging the abundant data available [20].

Among the different methodologies found within AI, optimization methods are the ones that can offer a better response to the challenges presented by the policies mentioned above: fleet electrification, demand aggregation infrastructure, and enhanced traffic management. In particular, Metaheuristics (MHs) and Hyper-heuristics (HHs) [21, 22], two prominent optimization approaches, offer adaptive and efficient solutions for tackling dynamic and combinatorial problems prevalent in LML operations.

MHs are high-level strategies that guide the search process to explore large solution spaces efficiently. They prioritize the balance between solution quality and computational efficiency, ensuring that even the most complex problems receive competent solutions quickly. On the other hand, HHs represent a layer above MHs, focusing not on direct problem-solving but on intelligently selecting or generating heuristics to solve a problem at hand. Although these are approximate methods, a significant amount of experimental evidence suggests that these algorithms can provide good solutions within reasonable time and resources [23].

The utilization of optimization methods in this thesis to tackle the challenges associated with the three policies outlined in the preceding section is explained below:

1. To overcome the challenges posed by the vehicle fleet electrification policy, this thesis employs advanced optimization techniques to develop intelligent route planning solutions that minimize distances and reduce delivery times. Specifically, the focus is on the **Capacitated Electric Vehicle Routing Problem (CEVRP)**, which entails strategic planning of EV routes regarding their limited load and range. The objective is to minimize route distances while accommodating the limitations related to the energy storage and the capacity of the EVs, thus tackling the intricacies of optimizing delivery routes within these constraints. However, a significant gap in current CEVRP methodologies is their lack of scalability and robustness, particularly in handling high customer dimensions [24]. This gap highlights the need for new methods capable of scaling effectively to meet the demands of more complex and expansive urban logistics scenarios. This research gap is addressed in this dissertation.

2. To overcome the challenges presented by the demand aggregation infrastructure policy, this thesis addresses the intricacies of the **Stationary Parcel Locker (SPL)**

Location Problem. SPLs are physical facilities, consisting of automated storage units placed in accessible locations in urban environments to enhance delivery efficiency and operational flexibility [25]. The objective of the problem lies in determining the optimal locations to install the lockers and their setup in terms of size and volume to maximize efficiency. However, a significant gap in current SPL methodologies is their lack of consideration for dynamic customer behavior and real-world constraints, such as the dynamic behavior of customer demands, the limited capacity of lockers, or base their conclusions on unrealistic assumptions about customer behavior and the practical constraints associated with collection periods. This dissertation aims to bridge the identified gap in research.

3. To overcome the challenges inherent in the enhanced traffic management policy, this thesis focuses on the vehicle segmentation of **Image-Based Vehicle Traffic Monitoring**. This monitoring process involves analyzing video from traffic cameras to identify and detect vehicles to estimate automatically the state of the network (e.g. density level, congestion, etc.), a crucial step for effective traffic management. It enables real-time traffic flow, density, and patterns assessment, providing valuable data to inform and optimize traffic control measures [26, 27]. However, current methodologies exhibit gaps in the precision and adaptability of vehicle segmentation, particularly in adjusting to diverse environmental conditions and incorporating real-time data for traffic management. This dissertation tackles the identified research gap.

Summarizing, multiple research questions derived from the motivations presented above:

1. Is it possible to develop a new optimization method based on HHs that are more efficient and scalable than existing state-of-the-art methods for solving the CEVRP, addressing the challenges associated with high-dimensional instances?

2. Could a more realistic model for the SPL problem be developed that incorporates stochastic demand, costs, locker capacities, dynamic collection periods, and the prediction of customer acceptance choices?

3. Is the Genetic Algorithm (GA) a competitive method to solve this more realistic and complex model of the SPL problem?

4. Can an efficient HH algorithm be developed for optimizing vehicle segmentation in image-based traffic monitoring that accounts for the variability of environmental conditions and real-time traffic management requirements?

These research questions lay the groundwork for the subsequent objectives and methodology, guiding the development of novel optimization frameworks and algorithms tailored to address the unique challenges of LML.

1.2 Objectives and Specific Objectives:

The main objective of this dissertation is to leverage the potential of MHs and HHs to develop new optimization methods and models that contribute to addressing relevant challenges in LML related to the electrification of the fleet, demand aggregation, and enhanced traffic management.

- **Objective 1:** Develop an advanced HH algorithm specifically designed to tackle high-dimensional instances of the CEVRP more efficiently. *This objective corresponds to the first research question.*
- **Objective 2:** Develop a new model for the SPL problem that incorporates stochastic demand distributions, locker capacities, dynamic costs and collection periods, and the probability of customer acceptance options to achieve more realistic and effective solutions for the location of parcel lockers. *This objective corresponds to the second research question.*
- **Objective 3:** Adapt the GA to effectively solve the new model for the SPL problem that incorporates more realistic factors. *This objective corresponds to the third research question.*
- **Objective 4:** Develop a more efficient HH algorithm for vehicle segmentation in image-based traffic monitoring to accurately and adaptively estimate road occupancy, considering the variability of environmental conditions and real-time traffic management requirements. *This objective corresponds to the fourth research question.*

1.3 Research Methodology

The research scope of this thesis is rapidly evolving due to ongoing technological advancements and the continuous generation of knowledge in the LML optimization field. As a result, an iterative research methodology has been employed, allowing for periodic state-of-the-art reviews. The primary objective behind this cyclical process is to leverage knowledge acquired in its initial phases to design increasingly original contributions, aiming to enhance understanding and knowledge in the specific areas addressed by this thesis. This cyclical process has undergone multiple iterations over the three years of this doctoral thesis. Figure 1.2 illustrates the different phases of this research methodology, briefly described below.

1. **Review and Analysis of the State-of-the-art:** The initial stage of the research methodology focuses on conducting a comprehensive review and analysis of the state-of-the-art related to LML optimization. This stage involves examining relevant publications in journals, conference proceedings, and other scholarly sources to identify existing gaps, challenges, and emerging trends in the field. Through this process, insights are gained into the complexities of LML operations and the limitations of current methodologies.

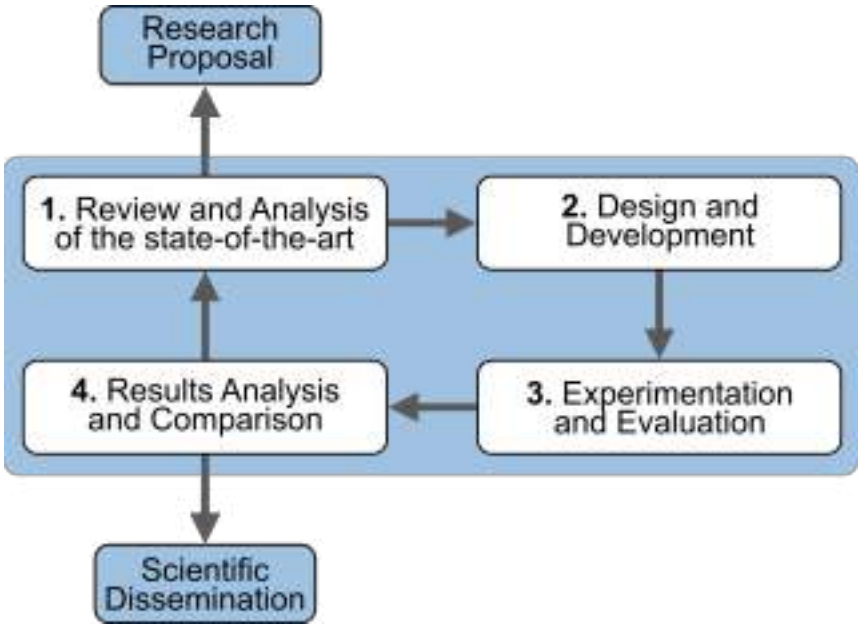

Figure 1.2: The research methodology flowchart of this thesis comprises four interconnected stages, forming a cyclical and iterative process.

It is crucial in determining the research direction and formulating research questions that address issues in LML optimization. It is the foundation for subsequent stages by providing a thorough understanding of the theoretical and practical landscape of the field. The knowledge gained during this stage was used to develop the research proposal in the first year of the PhD.

2. **Design and Development:** In this stage, different proposals are designed and developed to effectively address the gaps and challenges identified during the literature review stage. A holistic approach is followed, using previously acquired knowledge to generate innovative solutions. This approach helps to stay at the forefront of the ever-evolving state-of-the-art landscape and makes the proposals more robust and effective.

   This stage involves iterative refinement of proposed solutions through prototyping, simulation, and experimentation. Emphasis is placed on ensuring that the developed frameworks are robust, scalable, and adaptable to diverse urban environments and operational contexts.

3. **Experimentation and Evaluation:** During this stage, the effectiveness and performance of the solutions developed in the previous stage are thoroughly evaluated through systematic experimentation. Experiments are designed, and appropriate evaluation metrics and statistical analyses are defined, aligning with the research objectives.

   The solutions that have been implemented are carefully analyzed to measure their impact on performance indicators. All experimental results are gathered and examined meticulously to optimize the solutions. Feedback from experimentation is used

iteratively to make further improvements and optimizations, ensuring continuous development and enhancement of the research results.

4. **Results Analysis and Comparison:** The final stage of the research methodology is to analyze the results and compare them with other benchmarks and state-of-the-art approaches in the literature to determine the effectiveness of the proposed solutions and draw meaningful conclusions. This stage synthesizes the results, identifies patterns or trends, and critically evaluates the implications of the research results for the theory and practice of LML optimization.

   The proposed methodologies are analyzed comparatively, highlighting their strengths and limitations. From this analysis, recommendations for future research and practical applications are formulated. The knowledge generated is shared through academic publications, presentations, and collaborations with industry stakeholders, thus contributing to the knowledge advancement and practice in urban logistics.

1.4 Contributions and Publications

The work undertaken in this thesis contributes significantly to the field of LML optimization, addressing key challenges and presenting innovative solutions. The following highlights the pivotal contributions of this thesis and the associated scientific achievements that have emerged throughout the research:

- **Contribution 1:** This research presents the Hyper-heuristic Adaptive Simulated Annealing with Reinforcement Learning (HHASA_{RL}) approach to address LML challenges using EVs. Addressing CEVRP, HHASA_{RL} combines a multi-armed bandit method with self-adaptive Simulated Annealing to schedule proactive battery recharging, which contributes to improved travel times and route distribution efficiency. HHASA_{RL} has demonstrated its effectiveness by improving multiple best-known minimal solutions and achieving the best average values for high-dimensional instances, as demonstrated in the benchmark proposed for the IEEE WCCI2020 [28] competition. *This contribution is described in Chapter 3 and the associated scientific publication is:*

  Title: A new Hyper-heuristic based on Adaptive Simulated Annealing and Reinforcement Learning for the Capacitated Electric Vehicle Routing Problem.
  Authors: E. Rodríguez-Esparza, A. D Masegosa, D. Oliva, and E. Onieva
  Journal: Expert Systems with Applications (IF = 8.5 $\rightarrow$ Q1)
  Status: Published. DOI:

- **Contribution 2:** This study introduces and elaborates on a comprehensive methodology for enhancing LML through strategic SPL implementation, combining the "first select then merge" approach and the advanced Locker Location Problem with Constraints on the Luce Threshold Model (CLLPTLM). Initially, the research tackles the Locker Location Problem under the Threshold Luce (LLPTL) model, optimizing locker selection using a binary GA and subsequently employing the Blend Crossover

(BLX) method to maximize profit by merging and relocating lockers, considering customer usage probabilities [29]. Further development introduces the CLLPTLM, an enhanced version incorporating realistic constraints, employing an adapted GA to optimize LSP profitability. These methodologies demonstrate significant potential to boost delivery company profits, optimize resource allocation, and enhance delivery efficiency. The effectiveness and adaptability of these approaches are validated through computational experiments using both synthetic and real datasets, supported by a thorough sensitivity analysis to measure the impact of various parameters. *This contribution is described in Chapter 4 and the associated scientific publications are:*

Title: A two-phase metaheuristic approach for the parcel locker location problem: First select then merge.
Authors: E. Rodríguez-Esparza, E. Kampitakis, A. D Masegosa, E. Onieva and E. I. Vlahogianni
Conference: 8th International Conference on Models and Technologies for Intelligent Transportation Systems (MT-ITS), 2023
Status: Published. DOI: 10.1109/MT-ITS56129.2023.10241703

Title: Optimizing Parcel Locker Locations under Capacity and Pick-up Time Constraints.
Authors: E. Rodríguez-Esparza, E. Kampitakis, A. D Masegosa, E. Onieva and E. I. Vlahogianni
Journal: European Journal of Operational Research (IF = 6.4 → Q1)
Status: Under review

- **Contribution 4:** This study presents the approach of the Hyper-heuristic Genetic Algorithm based on Thompson Sampling with Diversity (HHGATSD), offering a novel and efficient solution for addressing complex optimization and versatility challenges, specifically in image segmentation for image-based traffic monitoring applications. HHGATSD has demonstrated remarkable effectiveness and robustness across various benchmarks, including the IEEE CEC2017 function set and the Berkeley Segmentation Dataset. Furthermore, the methodology has been particularly successful in vehicle segmentation from road traffic camera videos, leading to significant advancements in enhanced traffic management [30]. *This contribution is addressed in Chapter 5 and the associated scientific publication is:*

  Title: Optimizing Road Traffic Surveillance: A Robust Hyper-Heuristic Approach for Vehicle Segmentation.
  Authors: E. Rodríguez-Esparza, O. Ramos-Soto, A. D Masegosa, E. Onieva, D. Oliva, A. Arriandiaga, and A. Ghosh
  Journal: IEEE Access (IF = 3.9 → Q2)
  Status: Published. DOI: 10.1109/ACCESS.2024.3369039

1.5 Research Context

This section provides a detailed overview of the financial support, affiliations, and research stays that have contributed to the development and execution of this thesis.

1.5.1 Research Support and Funding

This research has been supported by the University of Deusto Research Training Grants Programme, by the Spanish Ministry of Science and Innovation through the research project PID2022-140612OB-I00 and PID2019-109393RA-I00, and by the Basque Government through the research grant IT1564-22. This research has also been funded and supported by the Deusto Smart Mobility Research Group and the Faculty of Engineering at the University of Deusto (Spain).

These sources of support have played a crucial role in facilitating the progress and success of the research efforts documented in this thesis.

1.5.2 Research Stay

During the second year of the doctoral program, an international research stay was conducted to enrich research activities and foster collaboration. The research stay took place at the National Technical University of Athens within the Department of Transportation Planning and Engineering, under the guidance of PhD Eleni I. Vlahogianni, Associate Professor. Lasting three months, from May to August 2022, the main objectives of the research stay were to collaborate with international experts in the field of transportation research, exchange knowledge, and obtain valuable feedback. The research stay provided valuable opportunities to network, learn, and advance the research agenda in collaboration with experts in the field. As a result of the research stay, an in-depth exploration of urban freight transport, transport modeling, and parcel lockers was carried out, resulting in conference proceedings and publications of journal articles [29].

1.6 Structure of the Thesis

The following chapters of this thesis dissertation are delineated below, providing a comprehensive overview of the organizational framework and content that will be explained:

[label=**Chapter 0:**,left=0pt, start=2]Provides an overview of the background and related work of the three LML optimization problems addressed in this thesis. It defines and clarifies the key terms and concepts used throughout the thesis, laying the groundwork for the proposed methodologies and solutions. Presents the novel HH developed for the CEVRP that improves the scalability and efficiency of state-of-the-art algorithms for this problem. Therefore, this chapter aligns with *Specific Objective 1*. Presents a new model for the SPL location problem that incorporates more realistic constraints than the state-of-the-art and probability of customer acceptance consideration. Therefore, this chapter aligns with *Specific Objective 2 and 3*. Presents the new HH designed for image-based vehicle traffic monitoring that

improves the accuracy and efficiency of vehicle detection in dynamic traffic environments. Therefore, this chapter aligns with *Specific Objective 4*. Summarizes the main and specific objectives of this doctoral thesis, highlights the key contributions of this research, and suggests potential areas of future investigation.

2

Background and Related Work

This chapter provides a detailed overview of the key concepts underpinning the contributions of this thesis. Concretely, it focuses with a special emphasis on Last-Mile Logistics (LML) and the importance of optimization, particularly through Metaheuristic (MH) and Hyper-heuristic (HH) algorithms, to solve complex logistics problems efficiently.

Section 2.1 provides an in-depth exploration of the evolution and importance of logistics, from its military origins to its role in modern business management. The section explores logistics management, transportation operations, and LML. In Section 2.2, the discussion transitions to optimization, highlighting its essential function and methodologies in logistics to enhance decision-making and operational efficiency, specifically focusing on MHs and HHs. Finally, Section 2.3 delves into optimization challenges and strategies specific to LML, addressing Capacitated Electric Vehicle Routing Problem (CEVRP) optimization, Stationary Parcel Locker (SPL) location problem, and image-based vehicle traffic monitoring to refine the effectiveness of modern logistics frameworks.

2.1 Logistics

The field of logistics, now a cornerstone of business management and industrial efficiency, traces its origins back to the critical demands of military operations. Military strategists recognized the life-and-death significance of precise resource and supply management on the battlefield, a concept that eventually evolved into modern logistics [31].

The origin of the word "logistics" is related to the term that the ancient Greeks designated with the word *logistikos* (which comes from the Greek *logistēs*, meaning "calculator" or "accountant") to military officers skilled in calculating the military activities of expeditions in wars and managing supplies, provisions, and resources [32].

The formal recognition of logistics as a science dates back to 1838 when Antoine-Henri Jomini, a French army general, authored the book "Summary of the Art of War". The

book focuses on the Napoleonic art of war and is considered the first documented work on logistics' subject. However, the true leap in logistics systems occurred during World War II. Throughout this conflict, the armed forces of the United States and its allies displayed superior efficiency compared to their German counterparts. In contrast, the German forces faced challenges in maintaining their warehouses, while their adversaries excelled in timely, accurate, and cost-effective supply operations. This era marked the beginning of innovative military logistics techniques and the evolution of logistics into both an art and a science [33].

This evolution eventually gave rise to the modern logistics systems we have today. Modern logistics encompass inbound and outbound processes, including supply chain management, transportation, distribution, and resource management. It is important to note that logistics is a key component of the broader supply chain framework, and the two concepts are closely interconnected [34].

To understand logistics, it is crucial to comprehend the supply chain. The supply chain is a comprehensive term that encompasses the planning, coordination, and management operations required to transform raw materials into finished products. This activity includes procurement, component manufacturing, assembly, distribution to end markets, and material handling and storage activities that are part of logistics [35].

Present-day logistics professionals use their skills and expertise to create efficient logistics systems that ensure the timely, accurate, and cost-effective delivery of products to consumers. Logistics is a competitive strategy in the contemporary business landscape that enables businesses to meet and exceed consumer expectations by effectively integrating supply chain components. It involves various activities and disciplines, including purchasing, planning, coordination, warehousing, distribution, and customer service [36].

2.1.1 Logistics Management

Logistics management emerged as a response to the increasing need for an integrated system that spans distribution route planning, warehouse management, and supply chain coordination. It is also closely related to other functions like marketing, sales, manufacturing, and information technology. According to the Council of Supply Chain Management Professionals (CSCMP), logistics management is defined as follows [33]:

> "Logistics management is that part of supply chain management that plans, implements, and controls the efficient, effective forward and reverse flow and storage of goods, services, and related information between the point of origin and the point of consumption in order to meet customers' requirements."

Logistics management is crucial for planning and execution at all levels, which include strategic, operational, and tactical aspects. Specifically, it involves managing inbound and outbound transportation, warehousing, fleet control, material handling, order fulfillment, logistics network planning, inventory management, supply and demand forecasting, and monitoring external logistics service providers [37]. The relationship between Supply Chain Management, Logistics Management, and Transportation Operations is illustrated in Figure 2.1.

Figure 2.1: Hierarchy of supply chain, logistics and transportation.

Additionally, logistics management aims to achieve a set of core objectives known as the 7R framework [33]:

- The Right goods (i.e. as ordered)
- In the Right quantity
- With the Right quality
- At the Right time
- At the Right place
- At the Right cost
- At the Right sustainable impact/footprint

These objectives serve as a comprehensive summary of what logistics strives to accomplish, emphasizing the importance of precision, timeliness, efficiency, and sustainability in goods and services management.

The logistics process involves the movement of materials into, within, and out of a company. This process is divided into three components: (1) inbound logistics, which deals with the storage and movement of materials received from suppliers; (2) materials management, which oversees the storage and transportation of materials within the company; and (3) outbound logistics, which involves the movement and storage of products from the point of final production to the customer [38].

Logistics deals with the movement of goods through two main types of flow: physical and information flow. Physical flow pertains to the actual movement of goods from the origin point to the final destination. Figure 2.2 shows the physical flow of goods, which starts from the manufacturing stage and ends with shipment to the customer [39]. On the other hand, information flow moves in the opposite direction, from downstream to

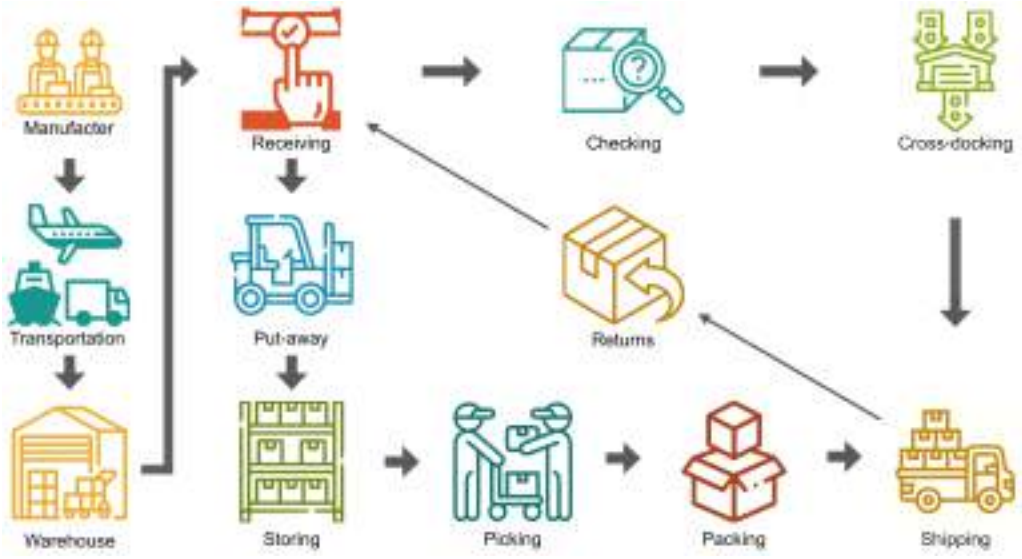

Figure 2.2: Physical flow of logistic processes.

upstream elements, and is essential in coordinating and optimizing the physical flow of goods.

In practice, physical and information flows are not unidirectional, as they flow in both directions. Reverse logistics refers to the process of moving products back through the supply chain, which includes returned goods, used products, and activities related to recovery, waste disposal, and packing returning to the system [40]. Figure 2.2 also shows the reverse logistics flow, starting from the shipping stage, continuing with the returns stage, and ending with receiving.

The main components of logistics systems to address the concept of physical flows can be classified systematically into functional areas, encompassing transportation and warehousing, material handling, and packaging.

2.1.2 Transportation Operations

Transportation is crucial in logistics, facilitating the movement of goods from their origin to their needed destination. The efficiency of transportation networks has a significant impact on logistics costs, which can account for a substantial portion of total expenses, ranging from one-third to two-thirds [41]. Efficient transportation ensures product availability at the right time and place, enhancing customer satisfaction, a key factor for marketing success. There are five primary modes of transport for moving goods from one place to another: road, rail, air, water, and pipeline. However, the suitability of each mode depends on the specific products and markets. Therefore, when making transportation decisions, it is important to consider factors such as the level of service demanded by the recipient, environmental sustainability objectives, and competitive aspects. These elements collectively determine the most suitable modes of transport [42].

Transport networks are categorized into subgroups, each with distinct characteristics. Planning long-distance routes differs significantly from organizing urban deliveries, with

each segment requiring specialized knowledge and terminology [43]. The visual representation of the transport network subgroup, including pre-haulage, long-haul, and end-haulage, is presented in Figure 2.3.

Long-Haul Transportation: This segment involves the movement of goods over significant distances. The specific distance that counts as "long" varies depending on the context of the transportation. Typically, it refers to distances that require different modes of transportation, such as road and sea transport.

Short-Haul Transportation (Drayage): This segment involves the movement of goods over shorter distances, usually as part of a larger freight movement. Drayage operations that transport goods from the point of origin to the first transfer point are known as first-mile transport or pre-haulage. Similarly, drayage operations between the last transfer point and the final destination are known as last-mile transport or end-haulage.

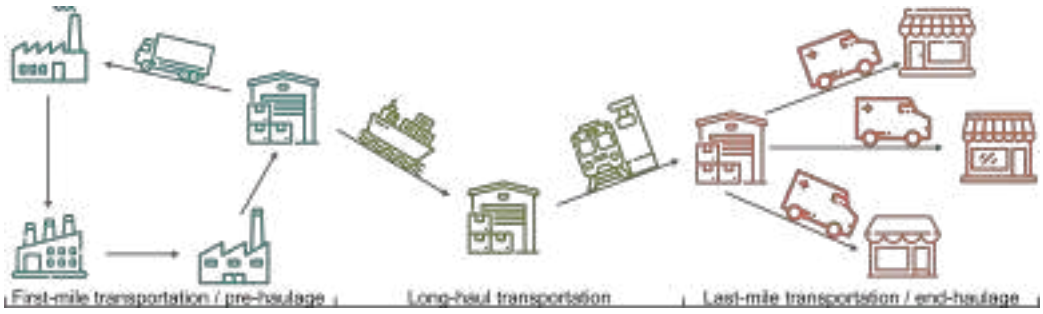

Figure 2.3: Transport Networks Example.

Within the broad scope of logistics, the efficient movement of goods through various modes of transport is only one part of the supply chain. However, as the final leg of this complex journey is approached, a critical and distinct phase known as LML is entered. It represents the last and often the most challenging step in the logistics chain, where products are transported from a distribution center to their final destination, usually the end consumer [44]. This phase requires meticulous planning, accuracy, and responsiveness, as it has a direct impact on customer satisfaction and overall operational efficiency. While the short-haul transport networks lay the foundation of the supply chain, the LML component is where the promises made to consumers are realized, making it a focal point of modern logistics operations.

2.1.3 Last-Mile Logistics

LML stands for the final phase of the distribution process, which involves transporting products from distribution centers or warehouses to their ultimate destination, such as the home or the workplace of customers. Distribution activity managers use two transportation modes: demand aggregation infrastructure and door-to-door delivery. Figure 2.4 showcases examples of transportation modes, including delivery trucks, bicycles, electric vehicles, and foot deliveries. These modes are particularly suitable for densely populated urban areas [45].

This final delivery phase is vital in fulfilling the promises made during the purchasing process, directly affecting customer satisfaction and brand loyalty. The effectiveness and

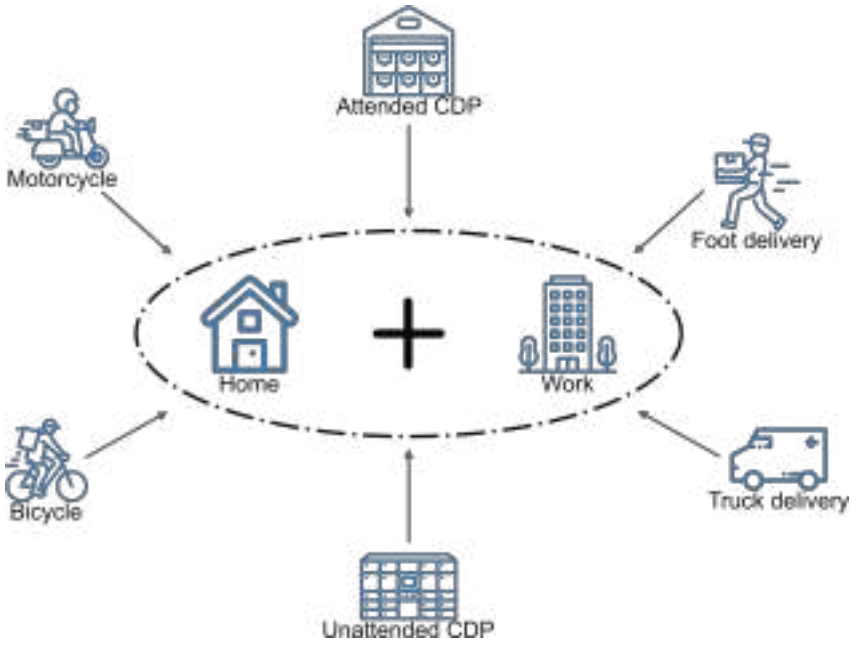

Figure 2.4: Diversity of LML services.

quality of this delivery stage are integral to the customer experience [46].

LML faces numerous challenges, particularly in urban mobility, including traffic management, parking limitations, and complex delivery routes. Precisely meeting delivery timelines is also challenging, given the expectation of the consumers for timely deliveries [47]. Furthermore, LML operations have a considerable impact on three different aspects of sustainability:

- **Economical:** Efficiency and cost-effectiveness in deliveries are essential for ensuring the profitability of the Logistics Service Providers (LSPs).
- **Social:** Addressing traffic congestion and its associated health impacts is crucial for urban well-being.
- **Environmental:** Mitigating CO_2 emissions and noise pollution is imperative, considering the significant environmental footprint of the transport sector.

The rise of e-commerce has spurred an increased demand for delivery solutions that are both efficient and sustainable. Consequently, advanced optimization methods are being explored to address these challenges. The following section will delve into these methods, specifically focusing on the three optimization problems discussed in this thesis: CEVRP, SPL location, and image-based vehicle traffic monitoring.

2.2 Optimization

Optimization is a tool in decision science and the analysis of physical systems, playing a crucial role in optimizing logistics processes. Its core aim is to identify the most favorable

solution within a given context. Solutions are achieved by adjusting problem parameters and optimizing an objective function while considering constraints or limitations. This function enables the comparison of various options within the search space to determine the "best solution" or optimal solution [39, 48].

The application of optimization spans various disciplines, such as mathematics, engineering, logistics, business strategy, and even medical and industrial applications [49]. For example, it is used in engineering to create efficient structures and systems. In logistics, optimization strategies are crucial for designing cost-effective delivery routes. In business, these techniques are helpful in resource allocation and maximizing profits.

The typical optimization process in engineering design is illustrated in Figure 2.5, which delineates problem specifications, including parameters, constants, objectives, and constraints. An optimization algorithm usually commences with a baseline design or initial point, iterating towards improvement. The iterative optimization process is highlighted in blue in the figure.

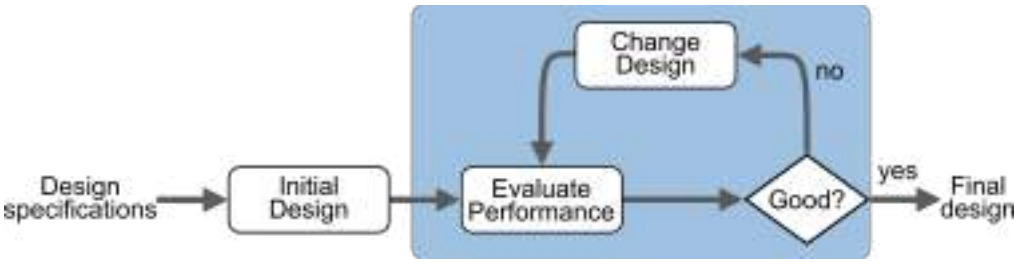

Figure 2.5: The design optimization process.

In mathematical modeling, optimization begins with defining a set S, known as the search space, encompassing all potential problem solutions. An objective function $f : S \rightarrow R$ assigns a cost $f(\mathbf{x})$ to each solution $\mathbf{x}$ within S [50]. The goal is to find an $\mathbf{x} \in S$ that minimizes $f(\mathbf{x})$, representing the optimal solution, expressed as:

$$\min_{\mathbf{x} \in S} f(\mathbf{x}) \tag{2.1}$$

Here, $\mathbf{x} = [x_1, x_2, x_3, \ldots x_n]$ represents a n-dimensional vector of variable values, where x_i denotes the ith design variable. The Equation 2.1 emphasizes the goal of finding the optimal solution by minimizing the objective function $f(\mathbf{x})$.

The objective is to find $\mathbf{x} \in S$ such that $f(\mathbf{x})$ is as small as possible, i.e., the best solution. This minimization process aims to identify the optimal solution within the defined search space, providing the foundation for effective decision-making in logistics [51].

To summarize, optimization problems have the following four fundamental components:

- **Objective function:** This is a mathematical expression used in optimization problems to determine the best values for decision variables. It represents the optimization criterion, which can be either maximized or minimized. It is also known as a cost function and is expressed as f. For instance, in logistics, the objective function could represent the cost of transportation or the time required for delivery.

- **Decision variables:** These are the unknowns or independent variables that can be adjusted or controlled to affect the objective function. There must be one or more design variables represented by the vector $\mathbf{x} = [x_1, x_2, \ldots, x_n]$.

- **Constraints:** These are the conditions or limitations that must be met in the problem. They are established using equality constraints (equations) or inequality constraints (inequalities) that restrict the range of values that the decision variables can take.

- **Domain of the decision variables:** This domain refers to the set of allowed or valid values for each variable. It defines the limits within which the decision variables can vary to find the optimal solutions.

The proper formulation of an optimization problem must meet the following conditions: (1) there must be at least one feasible solution, (2) the problem must have a unique solution, i.e., a clearly defined optimal solution, (3) small changes in the initial conditions of the problem should lead to proportional changes in the solution.

Optimization algorithms typically iterate, beginning with an initial guess and progressively refining it. Each algorithm differs in the transition between iterations. In this process, algorithms use information related to the objective function, constraint functions, and even the derivatives of these functions. Some algorithms keep a record of information collected in previous iterations, while others rely solely on local information available at the current point [52].

Regardless of the differences in their application, the algorithms must meet three fundamental properties mentioned below:

1. **Efficiency:** They should operate without requiring an excessive amount of storage resources and within a reasonable time.

2. **Precision:** They should be capable of finding solutions with a high degree of accuracy without being too sensitive to data errors or arithmetic rounding errors that may occur during execution on a computer.

3. **Robustness:** They should offer adequate performance on a range of problems within their class, regardless of the starting point.

There are two main types of algorithms: deterministic and stochastic. Deterministic algorithms use a rule-based approach, which is beneficial for problems with smooth and continuous objective functions. On the other hand, stochastic algorithms introduce randomness, making them more suitable for tackling complex problems with nonlinearities or multiple local optima. Figure 2.6 illustrates the classification and some of these approaches [53].

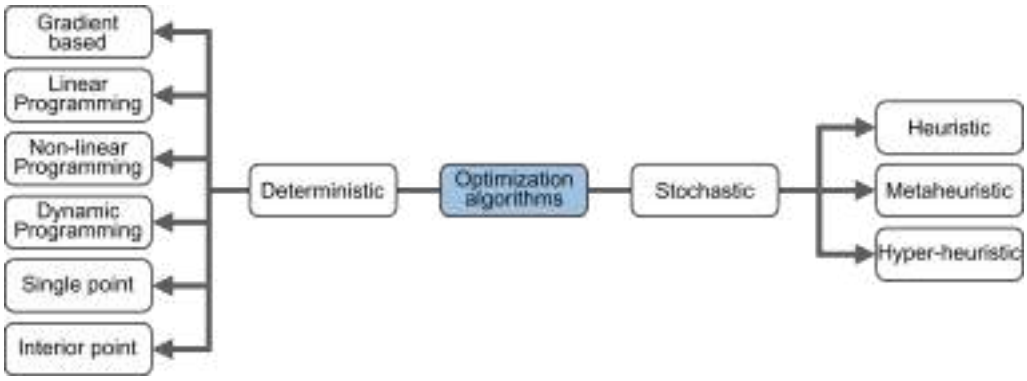

Figure 2.6: Classification of optimization algorithms.

Deterministic Algorithms: These methods utilize a predictable and logical approach to find optimal solutions. These classical methods follow a defined set of rules and procedures, ensuring the search is performed systematically and deterministically. Deterministic algorithms work particularly well in scenarios where the objective function is smooth and continuous [54]. However, these algorithms may face difficulties dealing with complex, nonlinear problems or those with multiple local optima. In such situations, they may become trapped in a local optimum and unable to explore the entire search space, which limits their ability to find the best possible solution.

Stochastic Algorithms: These methods incorporate elements of randomness in their search process. Instead of following a deterministic path, these algorithms introduce some uncertainty into their approach. This randomness enables them to explore the search space more extensively and flexibly, which is particularly useful in solving complex, nonlinear, or multiple local optima problems.

To summarize, stochastic algorithms are better suited for challenging optimization objectives, especially those that involve non-linear relationships or multiple local optima. This attribute is because they effectively explore complex search spaces and can uncover diverse optimal solutions. This inherent flexibility is particularly advantageous in logistics and supply chain management, where optimizing LML operations is crucial [55]. The following subsections will focus on the concepts of MHs and HHs.

2.2.1 Metaheuristics

MHs are optimization techniques that use randomness to address problems with a wide range of potential solutions in the search space. These algorithms generate a set of random solutions and iteratively improve them until a certain level of accuracy is reached. The advantage of using these algorithms is that they quickly move toward optimal solutions, efficiently solving complicated problems [56].

It is relevant to note that the distinction between the terms heuristics and MHs is minimal. The first thing is to define the meaning of heuristics. The term comes from Greek and means to know, find, discover, or guide a search. Heuristics uses a deterministic approach with various starting points at the start of the algorithms, even though they are classified as stochastic methods due to their use of random elements.

Heuristic techniques use trial-and-error strategies to determine which solution from a set of possible solutions will be examined next. They use the information generated by the algorithm to decide which candidate solution to try next. By doing so, complex problems can be solved in a reasonable time and at an acceptable computational cost, resulting in adequate solutions. It is important to note that even though these techniques do not guarantee the discovery of an optimal solution, they can still provide valuable solutions [57].

MHs are a higher category that generally work more effectively than heuristics. The term *meta−* suggests a "higher" level or "beyond", and these algorithms outperform simple heuristics. The key point of MHs is that they strike a balance between randomization and local search, making them suitable for global optimization [50].

These algorithms are often inspired by nature, as they are developed based on some abstraction from natural processes. The two fundamental components in any MH are the best possible solutions and randomization selection. The former ensures that the algorithm converges to the optimum, while the latter prevents solutions from getting stuck at local optima and enforces solution diversity. By effectively combining these two components, the search for the global optimum is generally guaranteed, but the best solution obtained from the algorithm may not be the global optimum [51]

MHs are the algorithm type that can solve complex problems without requiring information on the derivative of the objective function, meaning that they can tackle complex problems that are not necessarily convex, linear, or unimodal. These problems may involve linear or nonlinear constraints, and the decision variables may be continuous or discrete.

Exploration and exploitation are the two fundamental actions. During the exploration phase (Figure 2.7 a)), the algorithm searches the entire search space to identify areas with a high probability of containing the optimal solution. In other words, the algorithm explores unvisited regions, moving away from the current solution. On the other hand, the exploitation phase (Figure 2.7 b)) focuses on improving solutions close to the current solution by analyzing local regions of the search space [58]. The goal is to optimize the current solution or nearby regions that are considered promising. Exploitation aims to refine and improve the current solution. A proper balance between exploration and exploitation is necessary to ensure good algorithm performance in global optimization. Too much exploration can lead to excessive time expenditure in unpromising areas, while too much exploitation can result in stalling at local optima. Balancing and adjusting these two strategies is an essential feature of MHs.

The MHs fall into different categories, the most popular being population-based and trajectory-based. In logistics, trajectory-based algorithms can optimize a specific route, while population-based algorithms can manage and optimize a fleet of vehicles. Figure 2.8 provides examples of classical MHs for each category.

Trajectory-based: These algorithms work with a single solution in each iteration. The algorithms start with a simple solution and then employ search operators to explore the solution space and gradually improve the current solution. Each iteration yields a single neighbor solution. This solution can be accepted or rejected based on criteria, including whether it improves the fitness solution when evaluated on the objective function [59].

Population-based: These algorithms manage and maintain multiple solutions in

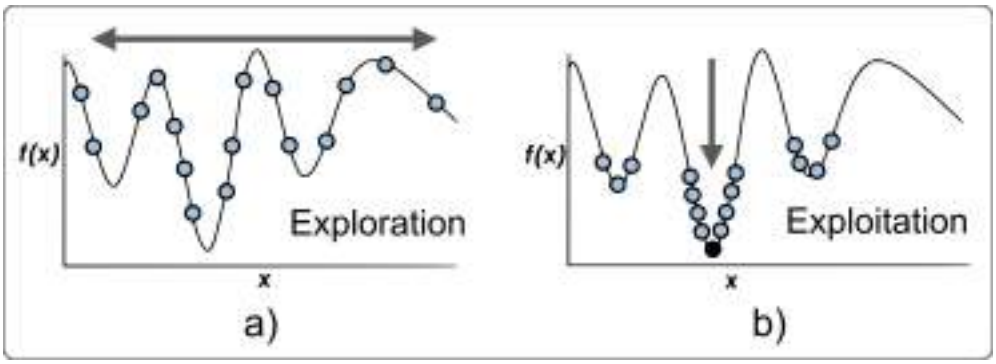

Figure 2.7: Actions of a metaheuristic algorithm. a) Exploration. b) Exploitation.

parallel instead of just one solution. At each iteration, these solutions interact and undergo operators, allowing exploration of the search space from multiple starting points. This approach enables the algorithm to find better solutions and avoid getting stuck in local optima [60].

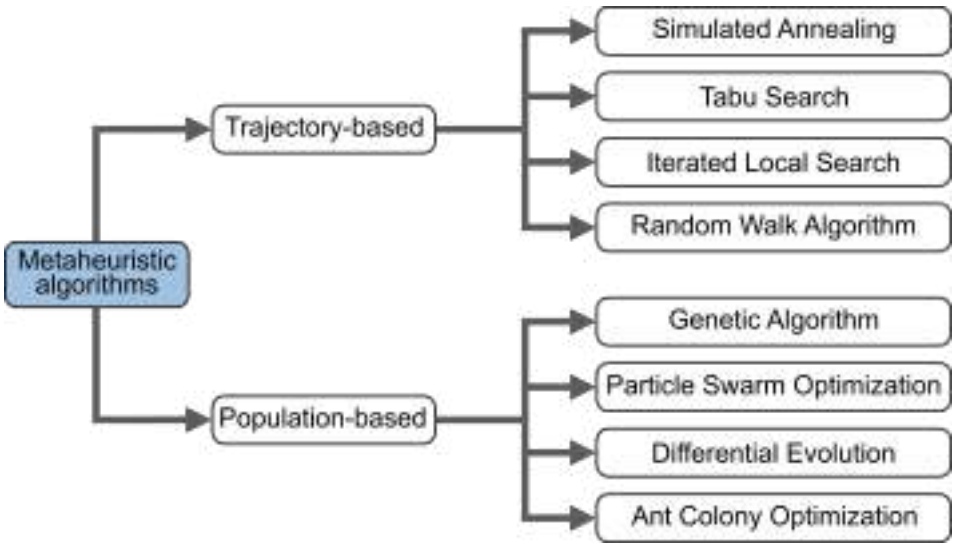

Figure 2.8: Classification of metaheuristic algorithms.

The choice between trajectory-based and population-based algorithms depends on the nature of the problem. Trajectory-based algorithms are suitable for problems where significant improvements can be obtained in a single solution that is modified at each iteration. On the other hand, population-based algorithms are more appropriate for complex or nonlinear problems, as they explore multiple starting points.

Although there is a wide variety of algorithms, each of which has different strengths and suitability for solving problems, it is significant to recognize one theorem that challenges the idea of a one-size-fits-all solution: the *No Free Lunch Theorem* [61].

This theorem, developed by Wolpert and Macready, essentially states that no optimization or search algorithm, whether deterministic or stochastic, can outperform all others on all possible problems [62]. In other words, while certain algorithms may be highly effective

for specific optimization problems, no method can guarantee superior performance across all problems.

According to Wolpert and Macready, the No Free Lunch theorem suggests that the effectiveness of metaheuristic algorithms depends on their ability to adapt to a specific problem to achieve better than random results. The practical relevance of this theorem is that it highlights the importance of algorithm adaptability when it comes to achieving success in solving complex problems [63].

2.2.2 Hyper-heuristics

HHs are advanced stochastic optimization strategies that go beyond MHs by automating the management of low-level algorithms, such as heuristics and MHs. Instead of focusing on the direct manipulation of specific algorithms, HHs seek to develop more generalized and robust search methodologies. Instead of focusing on the direct manipulation of specific algorithms, HHs look for suitable heuristic methods or sequences to solve complex optimization problems. This approach is dynamic as it is an "on-the-fly" method that adapts to the changing needs rather than a "tailor-made" technique [64].

The relatively novel term HH has been extended to refer to an automated methodology high-level search method or learning mechanism that helps select or generate heuristics or low-level heuristic (LLH) components such as move, neighborhood, or MH operators to solve complex optimization problems [65]. The distinguishing feature of HHs is that they operate in the heuristic search space, not directly in the problem solution search space [66].

HHs are mainly classified into two categories from the perspective of their nature: heuristic generators and heuristic selectors, as illustrated in Figure 2.9 according to Burke et al. [67]. Heuristic generators are a methodology that focuses on creating new algorithms or heuristics using principles or rules to generate adaptive heuristics. On the other hand, heuristic selectors are a methodology that focuses on selecting an existing set of heuristics and applying strategies to choose the most appropriate one for a specific case of a problem [28].

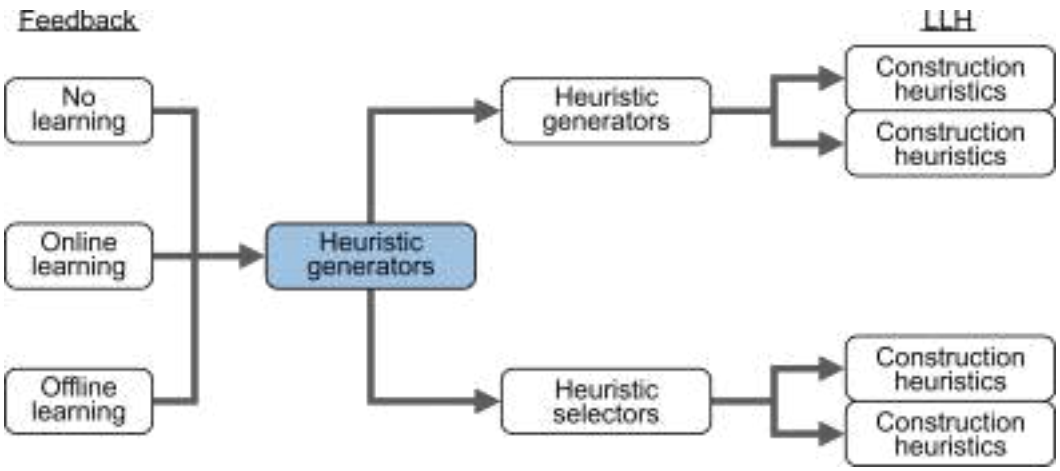

Figure 2.9: Classification of hyper-heuristic algorithms.

Within the classification of heuristic selection and generative heuristics, a significant subdivision focuses on design strategies for search and implementation. These strategies are constructive and perturbative, shown in Figure 2.9 as a second dimension of the classification. This categorization refers to the nature of the LLH used in either category [68, 69].

Constructive heuristics involve generating solutions progressively, starting from scratch, and building a complete solution through a predefined set of LLH. These approaches are particularly useful in creating new heuristics or generating effective strategies from existing components.

On the other hand, perturbative strategies modify or improve existing solutions and focus on complete solutions. This is usually an iterative process that continues until a termination criterion is met. These approaches are useful for improving existing solutions, adjusting heuristic strategies, and exploring different approaches without starting from scratch.

An HH is classified as a learning algorithm when it uses feedback on the performance of the LLH during the search process. This categorization of its feedback is illustrated in Figure 2.9 and explained below [67]:

No learning HHs: Do not use any prior information from the search process regarding their performance. Instead, choose a heuristic uniformly at random or in a predefined order from the existing set without keeping track of its prior performance. This approach avoids any bias and ensures equal opportunities for all heuristics to be selected.

Online learning HHs: Use prior information from the search process on the performance of the LLH. It learns while solving a specific instance of the problem. During the search process, it adjusts its choices of heuristics based on the observed performance, dynamically adapting itself to improve the efficiency and effectiveness of problem-solving in real-time.

Offline learning HHs: Also, use prior information from the search process. However, it learns from a set of training examples. A method is developed that generalizes to unseen problem instances based on previous experience. This approach seeks to improve the HH's ability to address a more applicable variety of instances based on features identified in training.

Despite these categorizations, there are hybrid methodologies that integrate both constructive and perturbative LLH. These methodologies take a combined approach, merging step-by-step construction strategies with techniques that introduce perturbations or modifications to existing solutions.

Operational efficiency is crucial in logistics, and advanced optimization techniques are essential in achieving it. Exact algorithms are not always the best option since they exhaustively explore all possible combinations to find optimal solutions. In contrast, MHs and HHs offer more flexible and adaptable approaches to tackle the complexity of optimization problems in this context.

MHs stand out for their ability to search for near-optimal solutions in a reasonable amount of time. This aspect is critical in LML, where the dynamics and variability of operating conditions require agile and efficient responses. In contrast, exact algorithms can become computationally expensive as the complexity and number of variables increase. Hence, MHs allow for effective solutions in a feasible time.

HHs, on the other hand, automate the management of LLH, which provides even more flexibility. The adaptability of HHs is crucial in LML, which is dynamic in nature. The challenges range from route optimization to efficient parcel locker management and real-time traffic conditions and require continuous adjustments. HHs are advantageous in this regard since they enable automation and optimization of algorithm selection, making them suitable for specific situations.

2.3 Optimization Problems and Methods for Last-Mile Logistics

This section focuses on three critical policies that play a crucial role in improving the efficiency, sustainability, and adaptability of modern transportation and logistics systems in the multifaceted landscape of LML. The policies are related to the optimization problems of CEVRP, SPL location, and image-based vehicle traffic monitoring. To provide a comprehensive overview, the exploration begins by examining the state-of-the-art solutions for these problems, which significantly impact LML.

2.3.1 Capacitated Electric Vehicle Route Optimization

Optimizing EV routes is crucial for reducing costs and minimizing environmental impact in LML operations. This section offers an overview of recent developments and methodologies in the field, with a specific emphasis on CEVRP optimization.

When addressing the CEVRP, several significant works aim to optimize EV routing, considering limited travel ranges and the necessity for battery recharging during delivery routes. This problem can be viewed as a variant of the green Vehicle Routing Problems (VRP), initially proposed by Erdogan and Miller-Hooks in 2012 [70]. Their approach involved using a modified Clarke and Wright savings heuristic [71] and a density-based clustering algorithm [72] to find initial solutions, followed by an optimization phase. While pioneering, their approach primarily focuses on minimizing distance traveled while considering limited fueling capacity, raising questions about scalability and robustness, especially for large problem instances.

The scientific literature on Electric Vehicle Routing Problems (EVRP) has grown continuously. For example, Pelletier et al. carried out a comprehensive study of EVRP variants in 2015 [73], while in 2019, Erdelić and Carić conducted a survey that categorized articles based on fleet composition, objective function terms, recharging technologies, and constraints such as EV capacities and customer time windows. Their work reviewed exact, heuristic, MH, and hybrid approaches applied to solve different EVRP variants [74].

As seen from the works mentioned above on the state-of-the-art, different strategies have been developed to solve the problems related to EVs. Schneider et al. hybridized the Variable Neighborhood Search algorithm and the Tabu Search heuristic to extend the model to the EVRP, which included time windows for the customers [75].

Researchers have explored different versions of the EVRP, including EVRP with Time Windows and Multiple Recharging Options. In a recent study, Mao and his colleagues proposed an improved ant colony optimization algorithm by combining it with an insertion

heuristic and an enhanced local search. The study aimed to improve decision-making on partial recharging and battery swapping. [76].

Furthermore, recent developments in Reinforcement Learning (RL) techniques have been utilized to solve EVRP and its variations. For example, Shi et al. introduced an off-policy RL framework for EVRP in ride-hailing services [77], while Lin et al. proposed a deep RL framework for EVRPTW [78]. Additionally, Zhao et al. hybridized a deep RL model with a local search strategy for solving VRP and VRP with time windows [79]. Moreover, Bogyrbayeva et al. developed an RL framework to address complex routing problems in free-floating electric vehicle-sharing systems, displaying the potential of RL in this field. [80].

Keskin and Çatay used the same instances of the Solomon benchmark [81]. They considered the cases with a partial recharge of the battery when stopping at a recharging station and different objectives. Introducing new route modification heuristics to add/remove clients and stations using an adaptive large neighborhood search approach, they proposed two works [82]. Montoya et al. proposed an automated repair strategy that inserts stations into routes to ensure route viability and a modified multi-space sampling heuristic [83]. One year later, Montoya et al. formulated a recharging of the battery process as a nonlinear function and presented a hybrid metaheuristic combining an iterated local search and a heuristic concentration to solve the new variation of the problem called electric vehicle routing problem with nonlinear charging functions [84]. These contributions, along with the existing body of work, provide a diverse set of tools and insights for tackling the challenges posed by CEVRP. The innovative methods proposed by these researchers showcase the adaptability and versatility required for real-world applications, contributing significantly to the ongoing evolution of state-of-the-art methodologies in electric vehicle route optimization.

Despite these advancements, existing methodologies often exhibit stability and robustness challenges when scaling up to higher-dimensional problems, primarily tailored for EV routing scenarios with a maximum of 100 to 320 clients.

Having explored the state-of-the-art in EVRP optimization, it is evident that existing methodologies exhibit limitations in addressing the challenges posed by the CEVRP. With a focus on the green vehicle routing problem and its variants, including CEVRP, various studies have laid the groundwork, yet scalability and robustness challenges persist. In response to these gaps, the objective is to mitigate the stability concerns associated with scaling up to higher-dimensional problems. This research endeavors to provide a resilient and effective solution for optimizing EV routes within the LML paradigm, contributing to the ongoing evolution of state-of-the-art methodologies in this domain.

2.3.2 Stationary Parcel Locker Location problem

In recent years, numerous studies have investigated the effectiveness of SPLs in addressing LML challenges [85]. However, despite commendable efforts, many of these studies often overlook locker capacity limitations or draw conclusions based on unrealistic assumptions. This section offers a detailed exploration of the related work in SPL optimization, shedding light on existing gaps in the state-of-the-art and paving the way for novel methodologies and solutions.

In their pioneering work in 2018, Deutsch and Golany [86] focused on optimizing total benefits through SPL location. They introduced a mixed-integer linear programming model with binary variables. However, their exploration was limited to a single case study without considering locker capacity constraints and with deterministic customer choices.

Subsequently, Lin et al. [87] aimed to maximize the service level of an SPL network by predicting customer choices. They employed random utility theory through the multinomial logit model for customer demand prediction. While their research highlighted the strong dependence of SPL locations on customer choices, it overlooked facility capacity, a crucial factor influencing customer behavior.

On the other hand, Yang et al. [88] introduced a bilevel programming model to optimize parcel locker locations, aiming to maximize company profits and minimize customer travel costs using a bilevel GA. However, their study ignored critical factors such as customers' willingness to use the service, seasonal variations in ordering rates, and fixed locker sizes.

In a recent study in 2022, Luo et al. [89] tackled the multi-objective problem of SPL locations, aiming to maximize locker accessibility while minimizing total costs. Their approach used an integer linear programming model and an active learning Pareto evolutionary algorithm. While their approach was promising, the study made assumptions like uniform facility configuration, unlimited capacity, and unlimited time for customers to pick up orders.

Additionally, Che et al. [90] proposed a multi-objective optimization model for SPL facility planning, considering factors such as maximum coverage, minimum overlap, and minimum total idle capacity. Their method used a hybrid approach of the Taguchi method and non-dominant classification GA II. However, the study assumed that the total demand of a location would never exceed the maximum capacity of the assigned lockers and did not consider customer choices and preferences.

Lin et al. [91] employed the Threshold Luce Model (TLM) to estimate the probability of customers using SPL facilities to investigate optimal SPL locations. Their focus was on maximizing profit by accounting for income and installation costs. Rodriguez-Esparza et al. [29] extended this model using a two-stage process with metaheuristic algorithms. However, both studies overlooked locker capacity, assuming it to be unlimited.

Kahr [92] strategically located SPLs to accommodate discrete stochastic demand, maximizing efficiency and profitability. The study considered stochastic demand, locker availability, and various configurations of cabinets but did not account for stochastic processes in package pick-up or customers' stochastic decisions.

In 2023, Mancini et al. [93] modeled a service point location problem with stochastic demand and locker availability, aiming to maximize allocated parcels and minimize customer walking distance. However, the study did not include installation costs of service points in the objective function and assumed uniform service point capacities.

Yunusoglu and Gonca [94] optimized SPL locations and pricing decisions using a price-response function, demonstrating efficacy in optimizing locker placement and pricing based on customer demand.

While existing literature has made commendable efforts in optimizing SPL locations, many studies either overlook locker capacity limitations or base conclusions on unrealistic assumptions about customer behavior and practical constraints associated with pick-up periods.

Motivated by these gaps, this thesis aims to develop a more realistic model. It will consider stochastic demand, locker capacity, and the dynamism of pick-up periods. The proposal model will predict customer choices through a random utility theory model. The ultimate goal is to optimize SPL locations, providing a more accurate and effective solution for LML services.

2.3.3 Image-Based Vehicle Traffic Monitoring Optimization

Effective road traffic monitoring is crucial for optimal route planning and operational efficiency in the dynamic landscape of LML. Proficient traffic monitoring facilitates route optimization, and it plays an essential role in mitigating congestion, reducing travel times, and enhancing overall LML effectiveness. This subsection reviews recent advancements and methodologies in Image-Based Vehicle Traffic Monitoring optimization, focusing on traffic management and vehicle segmentation.

Traffic Management

Several heuristic proposals have been presented for traffic management. In 2022, Khassiba and Delahaye proposed a Simulated Annealing (SA) HH algorithm, applied to analyze delay-based and rerouting-based neighborhood operators [95]. In 2023, Liao et al. addressed the traffic assignment problem using a GA HH approach for real-time assignment of uncertain commuters [96]. They introduced a reactive assignment strategy as a LLH rule, which evolved through the proposed method. By training using a designed heuristic template, commuters can dynamically find optimal paths in real-time, maximizing traffic network throughput.

Also, in 2023, Zheng et al. designed a HH algorithm based on Tabu Search, incorporating a high-level heuristic strategy to more efficiently select underlying search operators to optimize vehicle routes by balancing distribution costs and customer satisfaction. This approach is applied to a model considering a time-dependent speed, reflecting vehicle travel speed and road traffic flow changes in urban traffic flow simulations [97].

Image Vehicle Segmentation

Numerous proposals have been put forth, each featuring unique approaches characterized by distinct and innovative task analyses. These approaches aim to enhance the accuracy and efficiency of vehicle segmentation, contributing to the advancement of computer vision applications, particularly in the context of autonomous driving, traffic management, and surveillance systems.

In 2019, Prakoso et al. conducted a comprehensive assessment of Otsu's thresholding, Fuzzy C-means, and K-means for vehicle segmentation applied to video frames, evaluating the effectiveness of these techniques using Mean Square Error (MSE) and Peak Signal-to-Noise Ratio (PSNR) as performance metrics [98].

Deep learning approaches have also been explored, with Hu et al. introducing a scale-insensitive convolutional neural network in 2018 for fast vehicle detection, achieving detection speeds of up to 37 FPS [99]. Similarly, Sindhu utilized YOLOv4 for rapid object

detection and vehicle identification in video streams from CCTV cameras [100]. A more recent 2023 proposal by Kashevnik et al. fused the EfficientNetB3 architecture with multiparallel residual blocks, drawing inspiration from the CenterNet architecture, for 3D localization and pose estimation of vehicles within a scene [101].

To the best of current knowledge, only a limited number of heuristic proposals (including MH and HH approaches) have been specifically designed to segment traffic vehicles. In 2020, Huang et al. [102] introduced a hyper-spherical hash algorithm as a high-dimensional heuristic enhancement for vehicle identification in intelligent traffic analysis. Notable examples include the utilization of the Haversine formula and a recent innovative approach known as the hyper-heuristic-based Encoder-Decoder using Gated Recurrent Units with an attention mechanism, as introduced by Priya et al. in their work presented this year [103].

In light of the existing gaps identified in the state-of-the-art image-based vehicle traffic Monitoring, there is a clear need for innovative solutions that address the challenges presented in vehicle segmentation and traffic management. The review of existing studies indicates that the domain is complex, and current methodologies have limitations. This thesis aims to address these gaps by proposing advanced methodologies and techniques in traffic image analysis, enhancing the precision and efficiency of the LML landscape.

3

A New Hyper-Heuristic for the Capacitated Electric Vehicle Routing Problem

3.1 Introduction

3.1.1 Challenges in Last-Mile Operations

The introduction in Chapter 1 highlighted the challenges that Last-Mile Logistics (LML) faces in urban areas due to traffic congestion and high demand for delivery services. E-commerce has further complicated the situation, increasing delivery volumes and expectations for prompt service. Optimizing the electrification of the vehicle fleet in the LML can improve efficiency, reduce costs, and mitigate CO_2 from delivery operations.

Electric Vehicles (EVs) offer a promising solution to reduce the environmental footprint of LML, but their integration comes with its own set of challenges, particularly in terms of route planning and energy management [104]. The Capacitated Electric Vehicle Routing Problem (CEVRP) encapsulates these challenges, demanding innovative solutions to optimize EV routes while considering battery constraints and recharging needs [75]. The evolving landscape of urban logistics necessitates adaptive and efficient strategies to tackle the nuanced complexities of LML with EVs, underscoring the importance of advanced optimization techniques in this realm [105].

However, a notable gap persists in the current methodologies applied to CEVRP: their limited scalability and robustness, especially when addressing high customer dimensions. This deficiency highlights the necessity for novel, scalable methods that can effectively adapt to the complexities of more expansive and intricate urban logistics landscapes.

3.1.2 Objectives and Contributions

This chapter introduces a novel Hyper-heuristic (HH) algorithm, the Hyper-Heuristic Adaptive Simulated Annealing and Reinforcement Learning (HHASA_{RL}), designed to address the multifaceted challenges of the CEVRP in LML. By hybridizing an adaptive Simulated Annealing (SA) technique with Reinforcement Learning (RL) strategies, this approach seeks to enhance the optimization process, offering a dynamic and effective solution to the CEVRP.

The primary objective is to develop and validate the HHASA_{RL} algorithm that can efficiently optimize routes for electric vehicles in urban delivery networks, considering battery capacity limitations and the need for periodic recharging in high-dimensional instances. This endeavor contributes to the logistics domain by providing a robust tool for optimizing LML with EVs, fostering sustainability and efficiency in urban logistics operations.

The methodology, detailed in Section 3.2, elucidates the components and operational mechanics of HHASA_{RL}, emphasizing its innovative integration of MHs and RL techniques. Following this, Section 3.3 delineates the experimental setup, illustrating the application of the algorithm to the IEEE WCCI2020 competition benchmark for CEVRP and its comparative analysis against existing state-of-the-art methods. The experimental results, discussed in Section 3.4, highlight the performance of the proposed HH and its implications for LML optimization with EVs. Concluding the chapter, Section 3.5 encapsulates the key findings, emphasizing the ongoing need for adaptive and intelligent solutions in the evolving landscape of urban logistics. This structured approach guarantees a thorough comprehension of the research, methodologies employed, and the resultant findings.

3.2 Methodology

This section presents the methodologies used to solve the CEVRP, which is a complex optimization challenge. It outlines the attributes of the CEVRP, including the load and battery capacities of EVs, as well as the encoding of charging stations. Additionally, it provides an overview of the HHASA_{RL} algorithm, outlining its core components and adaptive mechanisms. The algorithm utilizes advanced optimization techniques, and its potential to revolutionize route optimization in the context of LML is highlighted.

3.2.1 Capacitated Electric Vehicle Routing Problem

The CEVRP is an $\mathcal{NP}$-hard combinatorial optimization challenge that extends the classic VRP by integrating capacity constraints. Unlike the traditional VRP, the CEVRP considers unique attributes of EVs, such as specific load and battery capacities. The primary objective of the CEVRP is to determine the most efficient routes for a fleet of EVs, minimizing the total distance traveled. These vehicles must service a set of customers, fulfilling their demands while adhering to various constraints, including vehicle autonomy and the necessity for battery recharging [106, 74].

Mathematically, the CEVRP is represented on a complete, undirected graph $G(\boldsymbol{V}, \boldsymbol{A})$, where $\boldsymbol{V} = \{\boldsymbol{D} \cup \boldsymbol{C} \cup \boldsymbol{S}\}$ consists of nodes representing a set $\boldsymbol{C}$ of n_c customers, a set $\boldsymbol{S}$ of n_s external charging stations, and a central depot ($\boldsymbol{D}$). The set $\boldsymbol{A}$ contains arcs

(i, j), where $i, j \in \boldsymbol{V}$ and $i \neq j$. Each arc has a non-negative value d_{ij} representing the distance between nodes i and j. The energy consumption rate, denoted by h, determines the energy consumed by the EV as it travels along an arc (i, j), calculated as $e_{i,j} = h \cdot d_{ij}$.

Each customer node i is associated with a delivery demand q_i. All EVs in the fleet are identical, with maximum load (Max_C) and battery (Max_Q) capacities that cannot be exceeded. These EVs start and finish their routes at the depot, with the possibility of visiting charging stations multiple times. However, each customer must be visited exactly once.

The mathematical formulation of the CEVRP is presented in Equation 3.1a, which incorporates the constraints outlined in Equations 3.1b to 3.1j [107].

$$min \quad f(\boldsymbol{x}) = \sum_{i \in \boldsymbol{V}, j \in \boldsymbol{V}, i \neq j} d_{ij} \cdot x_{ij}, \tag{3.1a}$$

$$s.t. \quad \sum_{j \in \boldsymbol{V}, i \neq j} x_{ij} = 1, \qquad \forall i \in \boldsymbol{C}, \tag{3.1b}$$

$$\sum_{j \in \boldsymbol{V}, i \neq j} x_{ij} \leq 1, \qquad \forall i \in \boldsymbol{S}, \tag{3.1c}$$

$$\sum_{j \in \boldsymbol{V}, i \neq j} x_{ij} - \sum_{j \in \boldsymbol{V}, i \neq j} x_{ji} = 0, \qquad \forall i \in \boldsymbol{V}, \tag{3.1d}$$

$$u_j \leq u_i - c_i \cdot x_{ij} + Max_C \cdot (1 - x_{ij}), \qquad \forall i \in \boldsymbol{V}, \forall j \in \boldsymbol{V}, i \neq j, \tag{3.1e}$$

$$0 \leq u_i \leq Max_C, \qquad \forall i \in \boldsymbol{V}, \tag{3.1f}$$

$$y_j \leq y_i - hd_{ij} \cdot x_{ij} + Max_Q \cdot (1 - x_{ij}), \qquad \forall i \in \boldsymbol{I}, \forall j \in \boldsymbol{V}, i \neq j, \tag{3.1g}$$

$$y_j \leq Max_Q - hd_{ij} \cdot x_{ij}, \qquad \forall i \in \boldsymbol{S} \cup \{0\}, \forall j \in \boldsymbol{V}, i \neq j, \tag{3.1h}$$

$$0 \leq y_i \leq Max_Q, \qquad \forall i \in \boldsymbol{V}, \tag{3.1i}$$

$$x_{ij} \in \{0, 1\}, \qquad \forall i \in \boldsymbol{V}, \forall j \in \boldsymbol{V}, i \neq j, \tag{3.1j}$$

Here, Equation 3.1a delineates the objective function of the CEVRP, which aims to minimize the total travel distance for all EVs. The constraint in Equation 3.1b ensures that each customer is served exactly once, and the constraint in Equation 3.1c permits multiple visits to charging stations. Equation 3.1d establishes flow conservation, ensuring that the number of incoming arcs equals the number of outgoing arcs at every node. Equations 3.1e and 3.1f provide the capacity constraints, ensuring the load of the EV is non-negative upon arriving at any node, including the depot. The energy constraints in Equations 3.1g, 3.1h, and 3.1i maintain that the battery charge level of the EV does not fall below zero. Finally, Equation 3.1j specifies the binary decision variables (x_{ij}), where x_{ij} equals one if an EV travels the arc (i, j) and zero otherwise.

The variables u_i and y_i, respectively, represent the remaining charge capacity and the remaining energy level of the EV when it reaches the node $i \in \boldsymbol{V}$. Despite explicit constraints, all EVs must depart and return from the depot.

Route Representation and Charging Station Encoding

Figure 3.1 illustrates various scenarios of CEVRP routes for four EVs, denoted by A, B, C, and D. These examples provide insights into the variety of routing possibilities.

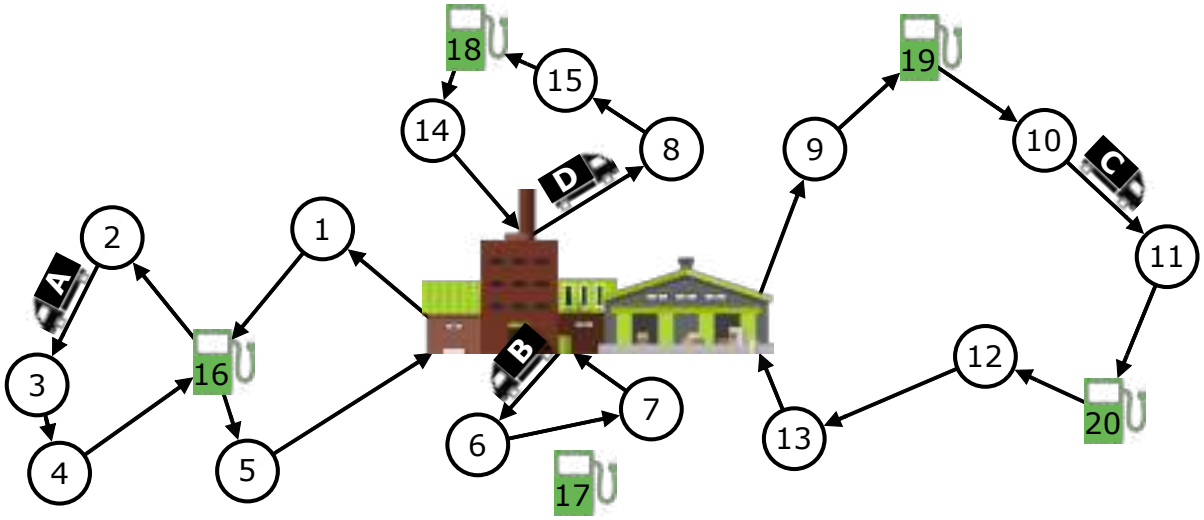

Figure 3.1: Example of CEVRP with four routes. (A) stops twice in the same charging station, (B) does not stop in any station, (C) stops in two different stations and (D) stops in a single station.

In these examples, route A demonstrates a situation where an EV visits the same charging station twice, which could be a strategic choice in certain situations. Route B shows an EV completing its journey without recharging, indicating efficient energy management or a shorter route. Route C represents a more complex journey, requiring stops at two different charging stations, illustrating the challenge of handling longer and more energy-demanding routes in some cases. Finally, route D portrays an EV that needs only a single charging stop before heading back to the depot, exemplifying a route with intermediate energy needs.

The encoding algorithm represents each route as a number sequence. The depot is denoted by the number 0, while numbers ranging from 1 to $n_c + n_s$ uniquely identify customers and charging stations along the route. The routes for EVs are demarcated by 0s, indicating the start and end at the depot. To incorporate recharging stations into the route, the encoding utilizes the number -1, which, within the sequence, is substituted with the index of the nearest charging station positioned between two customers.

For instance, consider EV A from Figure 3.1. Its encoding would be [0, 1, 16, 2, 3, 4, 16, 5, 0], where the underlined numbers signify the charging stations integrated into the route. The encoding for the four routes illustrated in Figure 3.1 is as follows:

- Route A: [0, 1, 16, 2, 3, 4, 16, 5, 0]
- Route B: [0, 6, 7, 0]
- Route C: [0, 8, 15, 18, 14, 0]
- Route D: [0, 9, 19, 10, 11, 20, 12, 13, 0]

3.2.2 Theoretical Bases

This section delineates the theoretical underpinnings and essential components of the HH proposed in this chapter. First, the SA algorithm and the Metropolis criterion are introduced. Following this, the algorithms addressing Multi-Armed Bandit (MAB) problems are detailed, succeeded by an exposition of prevalent improvement heuristics.

3.2.3 Simulated Annealing

In 1983, Kirkpatrick et al. proposed the SA algorithm that uses the physical process of annealing solid metals in metallurgy as a reference to solve global and combinatorial optimization problems [108].

SA generates a candidate solution in each iteration using improvement heuristics. The new candidate solution is then either accepted or rejected based on the Metropolis criterion, which uses the relative quality of the solution and the temperature as a probability of selecting worse solutions, promoting exploration of the search space [109]. This criterion helps to avoid stagnation at local optima and promotes the exploration of the search space. The Metropolis criterion is expressed in Equation 3.2.

$$p^k = \begin{cases} \exp\left(\frac{-\Delta}{T}\right), & \text{if} \quad \Delta > 0 \\ 1, & \text{if} \quad \Delta \leq 0 \end{cases} \tag{3.2}$$

The original pseudo-code for the SA algorithm can be found in Algorithm 1.

Algorithm 1 Pseudo-code of SA

```
Inputs: I_Iter, α, T_0, M_Acc
s ← Create initial solution
T ← T_0
while acc < M_Acc do
    for (k ← 1 to I_Iter) do
        s' ← Create neighbor solution(s)
        Δ = f(s') − f(s)
        if Δ ≤ 0 then
            s ← s'
        else
            if p^k > rand then
                s ← s'
            end if
        end if
        acc ← acc + 1
        k ← k+1;
    end for
    T = T · α
end while
Return: best solution found
```

where I_{Iter} is the number of iterations in which the local search continues at a particular temperature. α is the coefficient that controls the cooling schedule, and T_0 is the initial temperature equal to the current temperature (T) at the beginning of the algorithm. Finally, M_{Acc} represents the maximum number of function accesses allowed, as mentioned in [110].

3.2.4 Multi-Armed Bandit Reinforcement Learning Methods

Originating from the gambler dilemma in a set n-slot machines, the MAB problem in RL personifies the exploration-exploitation trade-off. The objective is to obtain the highest value of the accumulated reward between each spin and using one machine at a time, whether to continue playing with the current machine or to switch to another one [111, 112]. This problem optimizes its reward by acquiring knowledge through exploration and optimizing decisions based on that learning through exploitation.

Formally, the MAB problem of K-arms (actions or heuristics) is defined by $A_{i,n}$, which are random variables from $1 \leq i \leq K$ and $n \geq 1$. Here, i represents the index of the slot machine. This analogy extends to heuristics selection, where the most common methods, such as Epsilon Greedy (ϵ-G), Thompson Sampling (TS), and Upper Confidence Bound (UCB1), are employed to optimize the reward over iterations, balancing the known versus unknown and refining decision-making based on accrued knowledge.

Epsilon Greedy

The ϵ-G is a simple method used to balance exploration and exploitation when deciding between random exploration and exploitation. It is considered the greediest among the other two algorithms presented below. The ϵ value (which ranges from 0 to 1) determines the probability of choosing to explore. However, the constant is usually set to 0.1, indicating that it exploits most of the time with a small possibility of exploring [113]. The pseudo-code of this strategy is presented in Algorithm 2. The vector $\boldsymbol{R}$ keeps track of the accumulated rewards for each action or heuristic up to that moment.

Algorithm 2 Pseudo-code of ϵ-G

Inputs: ϵ, $\boldsymbol{R}$
if $(rand > \epsilon)$ **then**
  $heuristic \leftarrow$ Select a random action
else
  $heuristic \leftarrow$ Select the action with the $argmax(\boldsymbol{R})$
end if
Return: $heuristic$

Thompson Sampling

The TS approach is based on Bayesian principles and can produce more balanced and efficient results in some cases. It involves constructing a probability distribution, usually

a beta distribution, to represent the actual success rate of each action. This distribution is built using information from previously taken actions as training, creating an active exploration with a trial-and-error search of the behavior of the actions in each of the moves [114]. The algorithm then decides whether to reward or punish each action based on heuristic results, which increases the corresponding value of vector $\boldsymbol{R}$ or vector $\boldsymbol{P}$, respectively. This strategy generates other actions that probably maximize the reward, leading to future performance improvements. The pseudo-code for this approach is presented in Algorithm 3.

The probability of selecting a heuristic is proportional to the number of times the corresponding machine (action) completes successfully compared to failures. However, heuristics with a lower success/failure ratio may still be selected to enable exploration.

Algorithm 3 Pseudo-code of TS

Inputs: $\boldsymbol{R}$, $\boldsymbol{P}$
for (i $\leftarrow$ 1 to $num_{actions}$) **do**
  $\theta_i \leftarrow Beta(R_i + 1, P_i + 1)$ sample from Beta distribution
end for
$heuristic \leftarrow$ Select the action with the $argmax(\boldsymbol{\theta})$
Return: *heuristic*

Upper Confidence Bound 1

The UCB1 algorithm is a decision-making algorithm grounded in the principle of optimism in the face of uncertainty. When uncertain about which action to take, the algorithm adopts an optimistic stance, assuming optimistically that the chosen action is correct. The main idea behind UCB1 is to consistently select the heuristic with the highest upper bound, effectively striking a balance between exploration and exploitation, one critical characteristic of the algorithm [115].

UCB1 reduces exploration systematically to reduce uncertainty over time. As the number of turns or shots of the machines increases, the exploration rate decreases exponentially. In other words, the algorithm gives a boost to the least explored machine, even if its estimated average is low, especially if the gambler has been playing for a while. This distinctive characteristic allows it to define its exploration-exploitation combinations without depending on any parameters.

The pseudo-code of UCB1 is outlined in Algorithm 4. The vector $\boldsymbol{R}$ represents the accumulated rewards for each action, and the vector $\boldsymbol{S}$ indicates the number of times each heuristic has been selected.

3.2.5 Heuristics for Vehicle Routing Problem

In the realm of VRP, heuristics are instrumental in constructing initial solutions and refining them through neighborhood searches. Constructive heuristics are iterative methods used to generate initial solutions by building routes and adding elements sequentially until

Algorithm 4 Pseudo-code of UCB1

Inputs: k, $\boldsymbol{R}$, $\boldsymbol{S}$
if $(k \leq num_{actions})$ **then**
  $heuristic \leftarrow k$
else
  for (i $\leftarrow$ 1 to $num_{actions}$) **do**
    $\phi_i \leftarrow R_i/S_i + \frac{\sqrt{2 \cdot \log(k)}}{S_i}$
  end for
end if
$heuristic \leftarrow$ Select the action with the $argmax(\boldsymbol{\phi})$
$S_{heuristic} \leftarrow$ Is increased by 1
Return: $heuristic$, $\boldsymbol{S}$

a complete solution is formed. These solutions are built greedily and often deviate from the optimal solution significantly [116].

On the other hand, improvement heuristics explore the neighborhood of the current solution, searching for a better solution by applying perturbation operators. The local search process ends when no improved solution is found in the neighborhood, resulting in a state called a local optimum.

In the VRP literature, the following perturbation heuristics are commonly used:

- *Swap*: Two randomly selected nodes exchange positions, either within the same route or on different routes.
- *Reversion*: Starting from two nodes, the number string is inverted, regardless of whether they are on the same route or not.
- 2*Opt*: Two randomly chosen arcs are replaced with two new ones, with the option to reverse the direction of the route upon reconnection.
- *Insertion*: Two nodes are selected, and the first node is inserted in the position following the second selected node.

3.2.6 Hyper-heuristic Adaptive Simulated Annealing and Reinforcement Learning

This section delves into the intricate workings of the HHASA$_{RL}$ algorithm, commencing with an overview of the components that constitute the general HH flowchart. It then explores the local search block, which is subdivided into four crucial sub-blocks: *RL Method*, *Generate*, *Repair*, and *Adjust Station*.

To elucidate the process of heuristic selection within HHASA$_{RL}$, an analogy is drawn with the MAB problem, where heuristics are likened to bandit arms, each associated with its rewards. The challenge of balancing exploration and exploitation of the search space is adeptly managed using RL techniques, which dynamically adjust scores of the heuristic based on their performance throughout the iterative process.

This innovative application of the MAB concept empowers the algorithm with enhanced decision-making capabilities during local search phases. The RL method, integrated into the local search block (Section 3.2.6), plays a crucial role in selecting heuristics that effectively balance the exploration-exploitation dilemma to optimize problem-solving efficiency.

General Description

Figure 3.2 graphically represents the HHASARL general methodology of the algorithm, which adopts the classical input parameters of the classical SA algorithm(as expounded in Section 3.2.3), including T, $MAcc$, I_{Iter}, and α. Additional parameters, $limit$ and the variable h_{up}, are introduced to modulate the temperature dynamics of the proposal. The $limit$ parameter acts as a threshold, defining the maximum iteration count for h_{up} without solution enhancement. Upon reaching this threshold, the temperature T is increased.

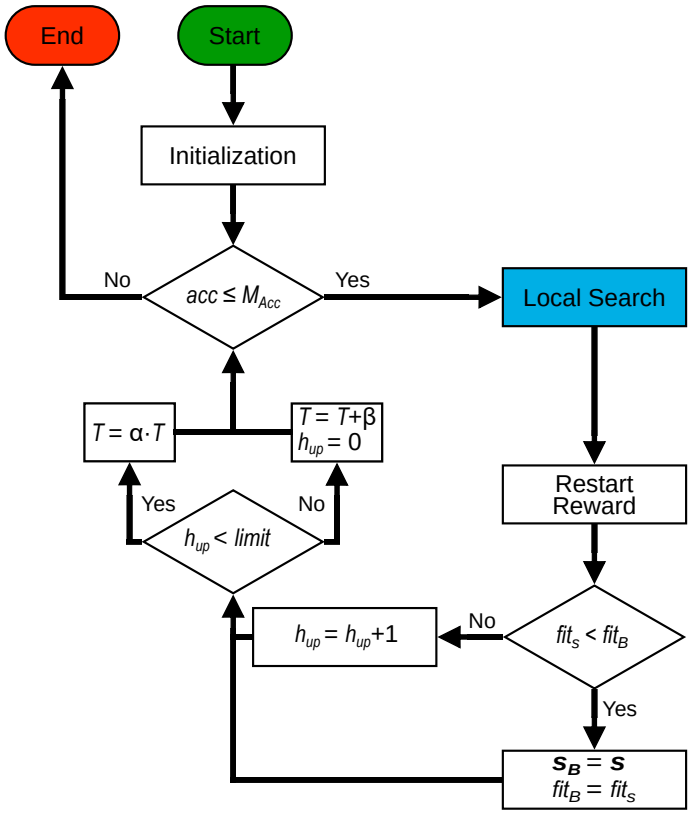

Figure 3.2: The general flowchart of HHASA$_{RL}$

The dynamic temperature adjustment of the algorithm, orchestrated by β, is critical in striking a balance between exploration, through accepting suboptimal solutions to discover new search areas, and exploitation, by favoring solutions that surpass the global optimum during the cooling phase. This nuanced temperature control facilitates the adaptability of the algorithm to varying search space characteristics, promoting exploratory or exploitative behavior as needed to improve solution quality in the CEVRP context.

The HHASA$_{RL}$ algorithm unfolds in four primary stages, delineated below:

1. **Initialization Procedure:** Initiation involves setting up internal variables and generating a feasible random solution ($\boldsymbol{s}$), achieved by randomizing customer order, forming vehicle routes according to load, and strategically incorporating charging station stops for battery recharging.

2. **Iterative Loop with Perturbations:** The solution $\boldsymbol{s}$ is refined through a loop applying perturbations or local adjustments until the fitness function access limit is reached ($acc \leq M_{Acc}$). The acc variable monitors the number of evaluations, ensuring it stays within the predefined maximum.

3. **Local Search Block:** At this stage, I_{Iter} perturbations are executed to refine $\boldsymbol{s}$ and minimize tour distances. The reward vector is then reset, and the fitness of the best solution generated in the local search, fit_s, is compared with the fitness of the global best solution, fit_B. If the route distance improves, the global solution is updated. Otherwise, h_{up} is increased by 1. The variable h_{up} determines whether the temperature should continue cooling or if it requires reheating. This block process is elaborated in Section 3.2.6.

4. **Temperature Adjustment:** The algorithm modifies the temperature based on h_{up}'s relation to $limit$. If h_{up} is below $limit$, indicating ongoing fitness enhancement, the temperature is reduced using $T = \alpha \cdot T$. Conversely, if h_{up} equals $limit$, signifying a lack of improvement in the solution, the temperature undergoes reheating. The amount added to the current temperature is determined by the variable β in Equation 3.3 to increase the probability of accepting worse solutions to escape from local minima through the Metropolis relation.

   The β value, modulated by the variable acc representing the current number of accesses to the objective function, is calculated using the linear decrement formula presented in Equation 3.3 between the points $(x_{\text{ini}}, y_{\text{ini}})$ and $(x_{\text{end}}, y_{\text{end}})$.

$$m = (y_{end} - y_{ini})/(x_{end} - x_{ini}) \tag{3.3a}$$

$$\beta = m \cdot \left(\frac{acc}{M_{Acc}} \cdot 100 \right) + y_{ini} \tag{3.3b}$$

   where x represents the current percentages of accesses to the objective function, with x_{ini} starting at the beginning of the algorithm, corresponding to a 0 %. x_{end} represents the final percentage by which the temperature can be heated if the fitness does not improve in $limit$ local searches.

   On the other hand, the values of y represent the dynamic temperatures added to heat the system in the case of no improvement in fitness. y_{ini} denotes the initial temperature increased for reheating, while y_{end} is the final temperature added.

Local Search Block

The flowchart depicted in Figure 3.3 outlines the local search process in the proposed algorithm. This local search spans I_{Iter} iterations, maintaining a constant temperature

throughout the cycle.

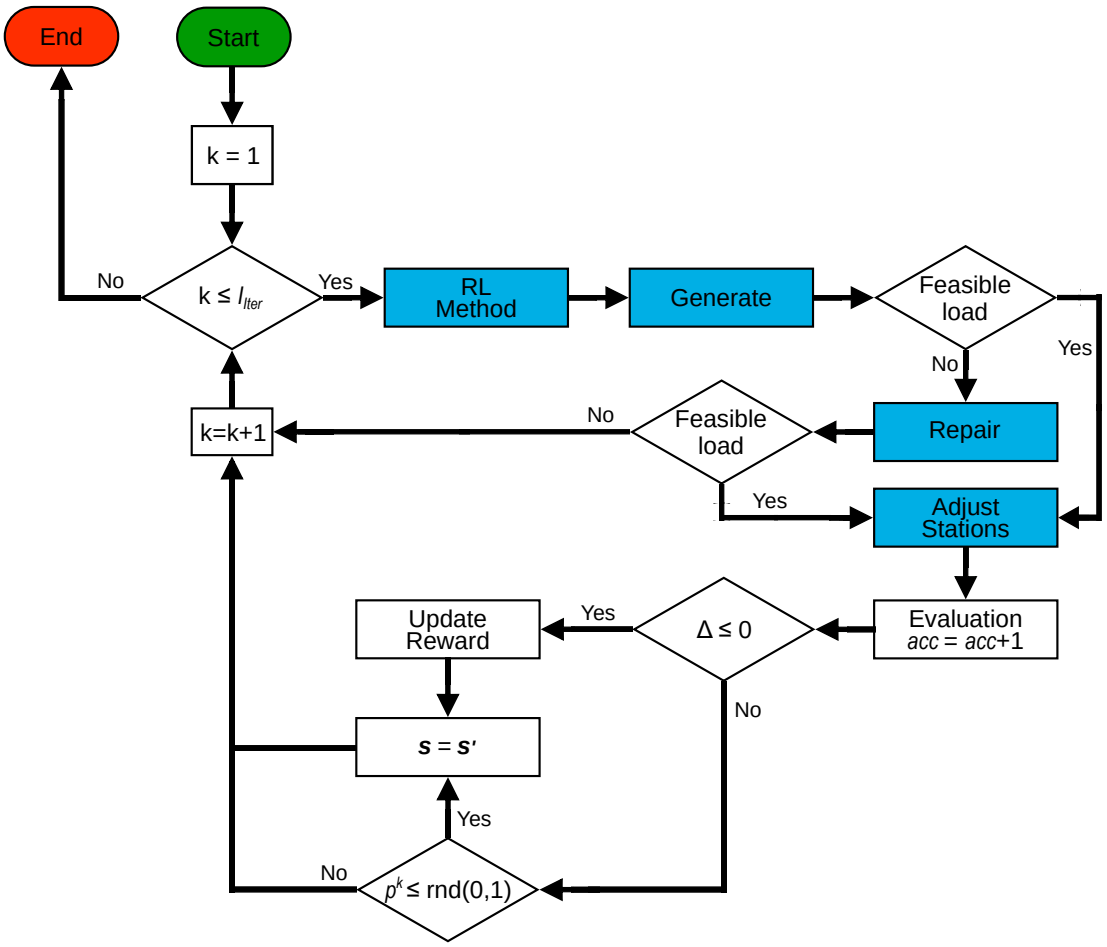

Figure 3.3: Local search flowchart of HHASA$_{RL}$

The local search consists of the following key blocks:

1. **RL Method Block:** This block utilizes a MAB reinforcement learning method (as described in Section 3.2.4) to choose an appropriate heuristic. The decision is based on the reward vector specific to the ongoing local search. The pool of heuristics consists of eight commonly used perturbation heuristics, detailed in Section 3.2.5: Swap, Reversion, 2Opt, and Insertion. The heuristics are divided into two groups of four each. The first four have a subindex $r1$, while the second four have a subindex $r2$. The subindices correspond to a percentage, determining the range of closeness between two customers relative to the total number of customers (n_c) in each problem instance. This indicates that the heuristic randomly chooses customer c_2 based on the closeness of the specified percentage interval of its subindex to customer c_1.

2. **Generate Block:** This block involves constructing the new solution $\boldsymbol{s'}$ using the chosen heuristic. The pseudo-code for this block is presented in Algorithm 5. In this heuristic, customers c_1 and c_2 are modified in the solution $\boldsymbol{s}$. To avoid repetition

of customer c_1, a random vector consisting of all customers, known as ***cust***, is created. Customer c_1 is then assigned and removed from the first element of ***cust*** to facilitate the algorithm process. Once all customers in the current vector have been considered, ***cust*** is regenerated with a new random order to ensure a continuous supply of unique clients.

Algorithm 5 Pseudo-code of *Generate block*

Inputs: $\boldsymbol{s}$, *heuristic*, n_c, ***cust***
if $\sim$ isempty(***cust***) **then**
  cust $\leftarrow$ permutation(n_c)
end if
$c_1 \leftarrow cust(1)$
Remove c_1 from ***cust***
Select c_2
$\mathbf{s}' \leftarrow$ Apply the *heuristic* to c_1 and c_2
$\mathbf{s}' \leftarrow$ Eliminate stations that are next to each other
Return: $\mathbf{s}'$, ***cust***

3. **Repair Block:** After generating a new solution, the load capacity constraint for $\boldsymbol{s'}$ is checked. If the constraint is unsatisfied, this block is activated to adjust the generated route and ensure that EV loads remain feasible. The pseudo-code is outlined in Algorithm 6.

   The algorithm stores the last customers who exceed the EV load capacity in a vector called ***repair***. The block then evaluates other routes to determine the feasibility of adding these customers to each route, ensuring that the EV load limit is not exceeded.

   During load repairs, two possibilities can arise. Firstly, if other EVs have enough capacity to accommodate these loads, customers are added to the route next to the customer with the minimum distance. On the other hand, if there is no available space in other EVs for additional loads, the new solution $\boldsymbol{s'}$ cannot be repaired. In this scenario, the variable k is incremented, and the process starts again, beginning with heuristic selection in the *RL Method* block. This decision prevents the unregulated creation of new routes that could lead to suboptimal convergence.

4. **Adjust Station Block:** If $\boldsymbol{s'}$ is feasible, or if the load is successfully repaired, the Adjust Station block is applied. This block is elaborated in detail in Algorithm 7 and offers the flexibility to relocate or eliminate a charging station in a route based on probabilities using the roulette wheel selection method. The probabilities for relocation and elimination actions are denoted as p_r and p_e, respectively. It is essential to emphasize that charging stations are added only to comply with power restrictions and ensure that EVs do not run out of battery during their journey.

   Afterwards, the objective function is evaluated to obtain the total distance traveled by the vehicles. Δ is then calculated to decide whether to reward the selected heuristic for iteration k by updating the best solution or to use the Metropolis

Algorithm 6 Pseudo-code of *Repair* block

Inputs: $\mathbf{s}'$
for (v $\leftarrow$ 1 to num_{routes}) **do**
  q_T(v) $\leftarrow$ Check load of the total route(v)
  if ($q_T(v) > Max_C$) **then**
    repair $\leftarrow$ Last customers exceeding Max_C
  end if
end for
$\mathbf{s}'$ $\leftarrow$ Move ***repair*** next to the customer with the minimum distance of the feasible routes to add the load
Return: $\mathbf{s}'$

relation to accept movements with worse fitness. This local search process continues to iterate until iteration k reaches the maximum specified by I_{Iter}.

Algorithm 7 Pseudo-code of *AdjustStation* block

Inputs: $\mathbf{s}'$
for (v $\leftarrow$ 1 to num_{routes}) **do**
  e_T(v) $\leftarrow$ Check the total energy of the route(v)
  if ($e_T(v) > Max_Q$) **then**
    $\mathbf{s}'$ $\leftarrow$ Add station where needed
  else
    if ($rand > 0.9$) **then**
      ii $\leftarrow$ Roulette Wheel Selection (Relocate, Eliminate)
      $\mathbf{s}'$ $\leftarrow$ Apply(ii)
    end if
  end if
end for
Return: $\mathbf{s}'$

3.3 Experimental Framework

This section explains the experimental setup, detailing the benchmark used, the algorithms selected for the comparative analysis, and the statistical and non-parametric tests applied to evaluate the performance and effectiveness of the proposed algorithm.

3.3.1 Benchmark Description

The recent public benchmark proposed for the IEEE WCCI2020 competition on computational intelligence conference for CEVRP [117] is used to test the performance of the proposed approach. This benchmark consists of 17 instances, including seven small instances with up to 100 clients and ten large instances with up to 1000 clients. The detailed information of each instance is summarized in Table 3.1.

The table provides data on the number of customers (n_c), charging stations (n_s), the minimum number of EVs required (Min_{Routes}), the maximum load capacity (Max_C), the maximum battery charge (Max_Q), and the energy consumption rate (h). The main objective is to minimize the total distance traveled by vehicles, with a single depot from which all EVs depart and return at the end of the route. It is worth noting that a solution may consist of multiple EVs to achieve this objective.

Table 3.1: Details of the CEVRP benchmark set

Name	**Customers** (n_c)	**Stations** (n_s)	Min_{Routes}	Max_C	Max_Q	h
E22	21	8	4	6000	94	1.2
E23	22	9	3	4500	190	1.2
E30	29	6	4	4500	178	1.2
E33	32	6	4	8000	209	1.2
E51	50	5	5	160	105	1.2
E76	75	7	7	220	98	1.2
E101	75	9	8	200	103	1.2
X143	142	4	7	1190	2243	1.0
X214	213	9	11	944	987	1.0
X352	351	35	40	436	649	1.0
X459	458	20	26	1106	929	1.0
X573	572	6	30	210	1691	1.0
X685	684	25	75	408	911	1.0
X749	748	30	98	396	790	1.0
X819	818	25	171	358	926	1.0
X916	915	9	207	33	1591	1.0
X1001	1000	9	43	131	1684	1.0

Baseline Algorithms and Compared Methods

For the comparative analysis, this study incorporates the top three algorithms from the IEEE WCCI2020 CEVRP competition: VNS, SA, and GA. Additionally, it integrates a methodology proposed by Woller et al., known as the Greedy Randomized Adaptive Search Procedure (GRASP) [118]. Moreover, the study compares the findings with those presented by Jia et al. in 2021, who introduced the Bilevel Ant Colony Optimization (BACO) algorithm. Notably, BACO has shown the best state-of-the-art results [119].

Furthermore, three variations of the proposed algorithm are evaluated and compared using simple methods for solving the MAB problem, named HHASA$_{\epsilon-G}$, HHASA$_{UCB_1}$ and HHASA$_{TS}$. An additional version, HHASA, substitutes the RL component with a heuristic random selection to gauge the impact of simple RL algorithms in the HH.

3.3.2 Experimental Setup

To ensure fair comparisons, the proposed methodology aligns with the evaluation criteria of the competition. These evaluation criteria consist of executing 20 independent runs with random seeds and adhering to a stopping criterion of $25,000 \cdot n_c$ maximum evaluations to the objective function (M_{Acc}), where n_c represents the instance size of the problem.

Within the set of internal parameters for HHASARL, α is assigned with a value of 0.99, $limit$ is set to 20, I_{iter} is defined as $40 \cdot n_c$, and p_r and p_e are allocated 60% and 40%, respectively. The parameters used to obtain the β value in the reheating stage are 0% and 90% for x_{ini} and x_{end}, and 1 and 0.05 for y_{ini} and y_{end}, respectively. For heuristics, a value of 10% is selected for the subindex $r1$ and 100% for the subindex $r2$. All these parameters were empirically determined based on preliminary testing and observations of algorithm behavior. Experiments were conducted using Matlab 9.4 on an Intel Core i5 CPU @ 2.7 GHz with 16 GB of RAM.

Given the unavailability of accessible source code for the comparative algorithms to evaluate the efficacy of the proposed method, the results reported in the literature are used directly. These results include the Minimum (MIN), Average (AVG), and Standard Deviation (STD) values over 20 runs. In addition, to assess the statistical differences among the performance of the algorithms, Friedman's non-parametric test for multiple comparisons [120, 121] is used, along with Holm's post-hoc test for 1-to-n comparisons [122].

3.4 Results and Discussion

This section provides experimental results of the different aspects used to evaluate the efficiency of the HH proposal. First, a comparison is made with the statistical results of the independent runs of the proposals with the state-of-the-art. Then the non-parametric analysis is shown to rank the algorithms and determine if there is a significant difference in their average. Subsequently, a visual comparison of the selection of heuristics among the MAB RL methods is presented. Next, a comparison of the difference between the average of the solutions against the best fitness found is reported. Finally, a visualization of the solution generated for four instances is displayed.

3.4.1 Comparison of the Statistical Results

The statistical results obtained by applying all instances of the CEVRP benchmark to the algorithms mentioned in the previous section are shown in Tables 3.2 and 3.3. These tables present the MIN, AVG, and STD values of the solutions obtained by the algorithms in 20 independent runs. Bold and asterisk-marked values indicate the minimum average distances, while values presented in bold alone denote results surpassing the minimum AVG obtained by the state-of-the-art.

According to the short instances in Table 3.2, the following observations can be obtained. According to the statistical test, the four variants of the proposed HH only show worse average results than BACO in instances E51 and E76. Other than that, HHASA$_{RL}$ and HHASA have equivalent performance with the compared algorithms and are superior

for E33 and E101. Meanwhile, the HHASA$_{UCB1}$ algorithm achieves the lowest distance values for the objective function in the seven small instances. HHASA$_{\epsilon-G}$ obtains the best fitness in six cases with E101 missing, while HHASA$_{TS}$ and HHASA$_{TS}$ proposals found five. In general, results reveal that the HHASA$_{UCB1}$ algorithm is highly effective in finding the lowest fitness. However, it is challenging to determine which algorithm is better and more robust in these types of instances since HHASA$_{UCB1}$, HHASA$_{TS}$, and BACO present better AVG results in five instances.

Table 3.2: Results of the proposed algorithm applied to small instances of the benchmark

Instances	Values	HHASA$_{TS}$	HHASA$_{UCB_1}$	HHASA$_{\epsilon-G}$	HHASA	BACO	VNS	SA	GA	GRASP
E22	MIN	384.67	384.67	384.67	384.67	384.67	384.67	384.67	384.67	389.82
	AVG	**384.67***	**384.67***	**384.67***	**384.67***	**384.67***	**384.67***	**384.67***	**384.67***	389.89
	STD	0	0	0	0	0	0	0	0	0.41
E23	MIN	571.94	571.94	571.94	571.94	571.94	571.94	571.94	571.94	571.94
	AVG	**571.94***	**571.94***	**571.94***	572.51	**571.94***	**571.94***	**571.94***	**571.94***	572.36
	STD	0	0	0	2.54	0	0	0	0	0.56
E30	MIN	509.47	509.47	509.47	509.47	509.47	509.47	509.47	509.47	512.19
	AVG	**509.47***	**509.47***	**509.47***	**509.47***	**509.47***	**509.47***	**509.47***	**509.47***	512.67
	STD	0	0	0	0	0	0	0	0	0.31
E33	MIN	840.14	840.14	840.14	840.14	840.57	840.14	840.57	844.25	841.08
	AVG	840.70	**840.41***	840.82	841.10	842.30	840.43	854.07	845.62	845.06
	STD	1.40	0.57	1.28	2.95	1.42	1.18	12.80	0.92	1.56
E51	MIN	529.90	529.90	529.90	529.90	529.90	529.90	533.66	529.90	536.09
	AVG	536.98	535.13	534.16	535.09	**529.90***	543.26	533.66	542.08	546.21
	STD	7.27	7.25	7.95	7.30	0	3.52	0	8.57	5.32
E76	MIN	692.74	692.64	692.64	694.54	692.64	692.64	701.03	697.27	701.63
	AVG	694.96	695.65	695.14	694.94	**692.85***	697.89	712.17	717.30	711.36
	STD	1.63	2.47	2.84	1.02	0.81	3.09	5.78	9.58	5.27
E101	MIN	837.10	835.63	836.17	837.10	840.25	839.29	845.84	852.69	847.47
	AVG	**843.10***	**843.31**	**844.77**	**843.17**	845.95	853.34	852.48	872.69	856.86
	STD	3.90	4.04	5.61	3.79	4.58	4.73	3.44	9.58	6.90

The results of comparing the algorithms on large instances are presented in Table 3.3. According to the findings, all four variants of the proposed HH demonstrate a lower AVG value than the state-of-the-art results for the largest instances, which are X573, X685, X749, X819, X916, and X1001. Moreover, the proposed HHASA$_{TS}$ outperforms the instance X214, showcasing the best average fitness in six out of ten cases with a large number of customers and establishing itself as the most effective variant within the proposed HHs.

Regarding the minimum values found for the objective function, the HHASA$_{TS}$ algorithm updated the best-known solutions at five instances out of ten, namely X214, X685, X819, X916, and X1001. The HHASA$_{UCB1}$ algorithm also updated the fitness at X573 with a marginal difference of 0.90 compared to the best distance found by HHASA$_{TS}$, while the HHASA$_{\epsilon-G}$ updated the best fitness for the X459 instance and the HHASA updated the X749.

In summary, the results underscore the effectiveness of the HHASA$_{TS}$ approach in achieving the best AVG values over 20 independent runs for large customer instances, demonstrating its capability to update minimum best-known solutions.

Table 3.3: Results of the proposed algorithm applied to large instances of the benchmark

Instances	Values	**HHASA$_{TS}$**	**HHASA$_{UCB_1}$**	**HHASA$_{\epsilon-G}$**	**HHASA**	**BACO**	**VNS**	**SA**	**GA**	**GRASP**
X143	MIN	15910.86	15912.77	15899.86	15921.68	15901.23	16028.05	16610.37	16488.60	16460.80
	AVG	16214.37	16231.33	16173.06	16271.78	**16031.46***	16459.31	17188.90	16911.50	16823.00
	STD	215.77	173.73	198.91	250.09	262.47	242.59	170.44	282.30	157.00
X214	MIN	11090.28	11097.63	11098.34	11120.28	11133.14	11323.56	11404.44	11762.07	11575.60
	AVG	**11206.60***	11260.83	11247.30	11251.80	11219.70	11482.20	11680.35	12007.06	11740.70
	STD	84.58	88.73	99.53	73.03	46.25	76.14	116.47	156.69	80.41
X352	MIN	26622.42	26549.88	26486.05	26606.06	26478.34	27064.88	27222.96	28008.09	27521.20
	AVG	26750.60	26760.35	26760.58	26812.89	**26593.18***	27217.77	27498.03	28336.07	27775.30
	STD	102.55	116.44	135.77	90.44	72.86	86.20	155.62	205.29	111.99
X459	MIN	24794.35	24769.67	24752.03	24815.37	24763.93	25370.80	27222.96	26048.21	25929.20
	AVG	25041.10	25036.67	24979.89	25060.02	**24916.60***	25582.27	25809.47	26345.12	26263.30
	STD	237.58	114.68	151.54	121.58	94.08	106.89	157.97	185.14	134.66
X573	MIN	51436.90	51436.00	51485.68	51545.10	53822.87	52181.51	51929.24	54189.62	52584.50
	AVG	**51776.70**	**51764.24**	**51771.50**	**51748.42***	54567.15	52548.09	52793.66	55327.62	52990.90
	STD	166.86	152.69	158.01	119.57	231.05	278.85	577.24	548.05	246.79
X685	MIN	69955.95	70348.53	70323.62	70413.81	70834.88	71345.40	72549.90	73925.56	72481.60
	AVG	**70401.25***	**70719.10**	**70684.34**	**70791.10**	71440.57	71770.57	73124.98	74508.03	72792.70
	STD	218.98	291.53	174.26	222.85	281.78	197.08	320.07	409.43	189.53
X749	MIN	79779.87	79829.23	79850.73	79732.99	80299.76	81002.01	81392.78	84034.73	82187.30
	AVG	**80135.67***	**80256.36**	**80318.42**	**80397.82**	80694.54	81327.39	81848.13	84759.79	82733.40
	STD	219.50	303.30	399.47	432.11	223.91	176.19	275.26	376.10	213.21
X819	MIN	161924.79	162350.42	162387.34	162523.88	164720.80	164289.95	165069.77	170965.68	166500.00
	AVG	**162530.67***	**162819.78**	**162883.17**	**163031.19**	165565.79	164926.41	165895.78	172410.12	166970.00
	STD	289.41	258.35	300.11	389.12	401.02	318.62	403.70	568.58	211.84
X916	MIN	336717.71	337200.96	337520.94	338007.56	342993.01	341649.91	342796.88	357391.57	345777.00
	AVG	**337641.92***	**338349.57**	**338639.53**	**338688.50**	344999.95	342460.70	343533.85	360269.94	347269.00
	STD	461.47	454.28	544.69	328.64	905.72	510.66	556.98	229.19	654.93
X1001	MIN	75469.29	75864.07	75782.95	75850.15	76297.09	77476.36	78053.86	78832.90	77636.20
	AVG	**75931.28***	**76131.56**	**76245.73**	**76234.51**	77434.33	77920.52	NA	79163.34	78111.20
	STD	304.10	212.24	226.30	271.18	719.86	234.73	306.27	NA	315.31

3.4.2 Non-Parametric Analysis

The results of the non-parametric analysis, conducted through the Friedman test for multiple comparisons and the Post Hoc Holm's test for 1-to-n comparisons, considering the 17 instances of the benchmark, are presented in Table 3.4. The p-values of Friedman's test, with values lower than 0.05, are highlighted in bold, suggesting the rejection of the null hypothesis of equal performance. Notably, the HHASA$_{TS}$ algorithm attains the best ranking according to the Friedman test.

It is worth mentioning that the three HH proposals that use MAB RL methods have a better ranking than the HHASA with its random heuristic selection, indicating that the RL methods improve performance. Additionally, the p_{Holm} value of HHASA is less than 0.05, which implies that its performance is significantly worse than the control algorithm, HHASA$_{TS}$.

The following non-parametric analysis compares three HH proposals that contain the RL block and five state-of-the-art algorithms in Table 3.5. This table provides two comparisons; the first three columns consider all instances, while the remaining columns focus on 11 large instances from E101 to X1001.

In this analysis, it is evident that, for both comparisons, the top three ranking positions are secured by the HH proposals introduced in this work, with HHASATS emerging as the highest-ranked. Additionally, employing HHASATS as a control in the p_{Holm} analysis

Table 3.4: Average Friedman's rankings and Holm's p values (0.05) of the four proposed HHs for the CEVRP benchmark.

Algorithm	Ranking	p_{Holm}
HHASA$_{TS}$	1.8824	
HHASA$_{UCB1}$	2.4706	0.287886
HHASA$_{\epsilon-G}$	2.5294	0.287886
HHASA	3.1176	**0.015828**

reveals a significant difference in performance compared to the VNS, SA, GRASP, and GA algorithms. Notably, while there is no statistically significant distinction with the BACO algorithm, the HHASA$_{TS}$ algorithm exhibits superior performance in the average results and overall ranking.

Table 3.5: Average Friedman's rankings and Holm's p values (0.05) of the comparison with the state-of-the-art for the CEVRP benchmark.

Algorithm	Ranking $_{all}$	$p_{Holm\ all}$	Ranking $_{\geq E101}$	$p_{Holm\ \geq E101}$
HHASA$_{TS}$	2.4118		1.7273	
HHASA$_{UCB1}$	2.8824	0.882417	2.5455	0.676703
HHASA$_{\epsilon-G}$	3.0588	0.882417	2.7273	0.676703
BACO	3.4118	0.701859	3.5455	0.245168
VNS	4.6471	**0.031207**	4.8182	**0.012333**
SA	5.6471	**0.000589**	6.0909	**0.000147**
GRASP	6.8824	**0.000001**	6.6364	**0.000016**
GA	7.0588	**0**	7.9091	**0**

3.4.3 Analysis of the Selection of Heuristics of the Hyper-Heuristic Proposals

Figures 3.4 and 3.5 present plots detailing each local search within a single run for instances E101 and X916, respectively. The x-axis in both figures reflects the progression of iterations or local searches, while the y-axis in the first row signifies the frequency with which each heuristic was selected during the local search process. The second row on the y-axis presents the reward vector for the eight heuristics across all local searches. This reward vector illustrates how often each heuristic contributed to the improvement of the global solution when s' exhibited a fitness lower than s. Essentially, this vector serves as a quantitative measure of the effectiveness of each heuristic in enhancing the overall solution quality. The peaks and variations in the reward vector demonstrate the dynamics of heuristic selections during the local search process.

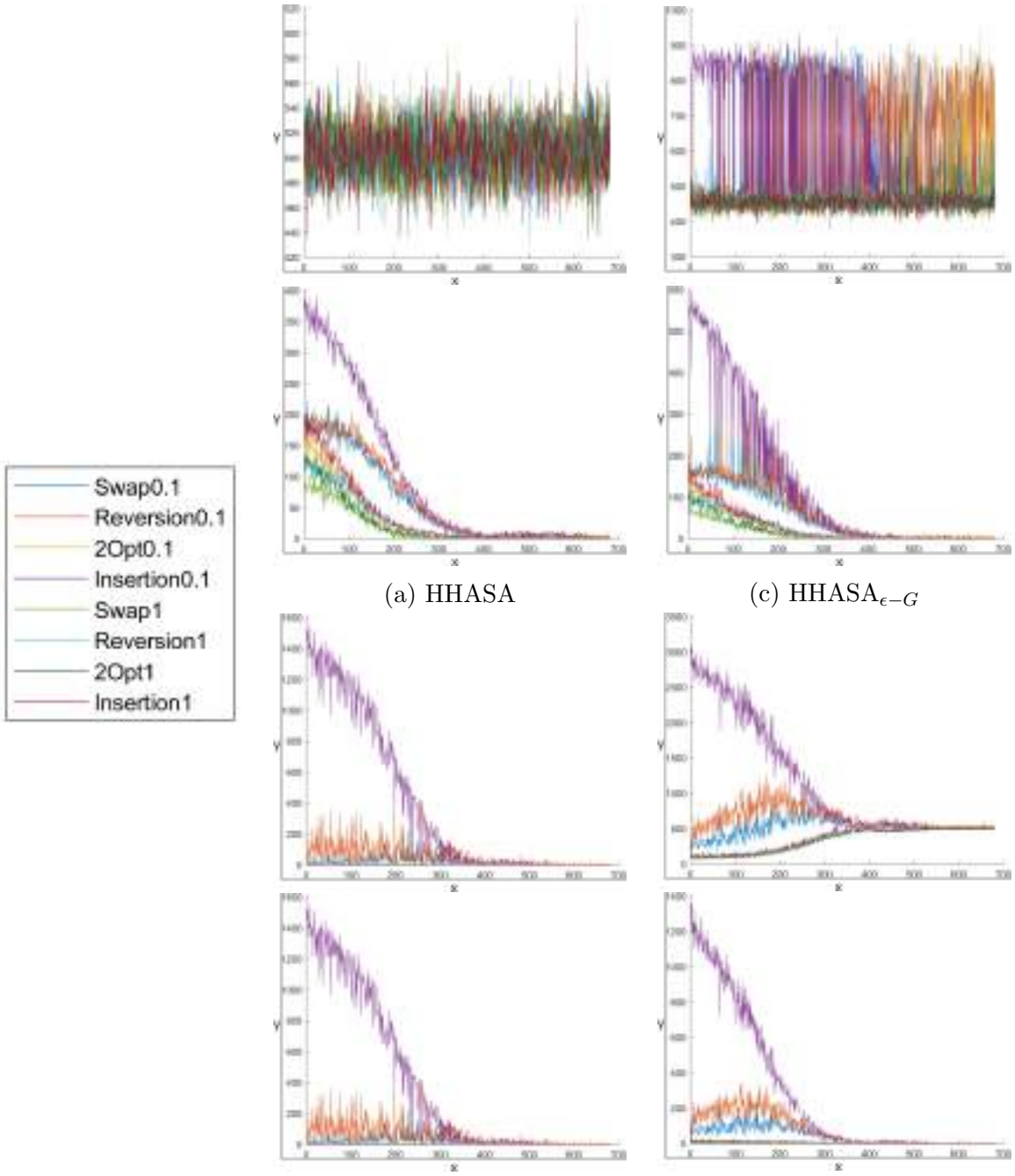

(a) HHASA (c) HHASA$_{\epsilon-G}$

(b) HHASA$_{TS}$ (d) HHASA$_{UCB1}$

Figure 3.4: Graphs of the vectors of the selected heuristics and the rewards of all the local searches of the four proposals of this work for the E101 instance.

Figures 3.4a and 3.5a show the HHASA proposal, and as expected, the heuristic selection vector does not give preference to any of them because it is random. Consequently, the reward figures showcase the performance of each heuristic when they have an equal chance of being chosen.

Similarly, Figures 3.4c and 3.5c present the vectors of the HHASA$_{\epsilon-G}$ algorithm. De-

spite the similarity to the proposal without the RL method, notable differences exist, especially in the vector of selected heuristics. Peaks in this vector are more pronounced due to the nature of the ϵ-G algorithm, which chooses the heuristic with the highest reward in that local search.

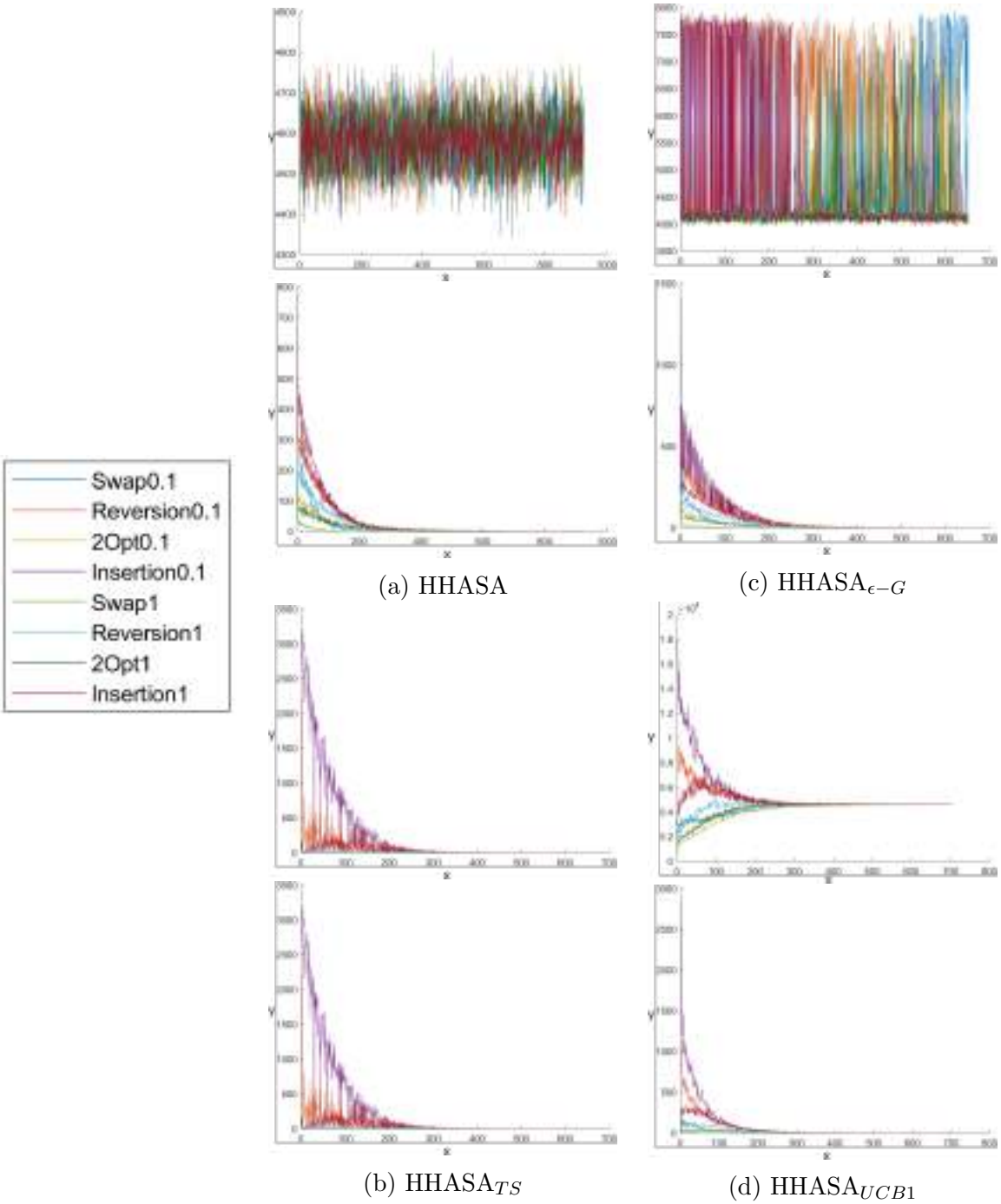

(a) HHASA (c) HHASA$_{\epsilon-G}$

(b) HHASA$_{TS}$ (d) HHASA$_{UCB1}$

Figure 3.5: Graphs of the vectors of the selected heuristics and the rewards of all the local searches of the four proposals of this work for the X916 instance.

The HHASA$_{TS}$ plots are depicted in Figures 3.4b and 3.5b. The Beta distribution used

in the TS process evolves from a flat linear shape to a more realistic probability model of the mean reward as more data is collected. Actions with fewer trials have a higher range of possible values, contributing to wider dispersion. Consequently, a heuristic with a low estimated mean reward tried less frequently may yield a higher sample value, indicating its potential selection at that instant of the local search. In both cases, the $Insertion1$ heuristic is selected more frequently in the first half of the search process. However, in the second half of the search process, the heuristic selection graph begins to behave more like the random mode because the number of times a reward is obtained decreases.

Finally, in Figures 3.4d and 3.5d, the vectors of the proposed HHASA$_{UCB1}$ are presented graphically. The UCB1 method exhibits a lower regret level than the ϵ-G and TS methods, enabling the quick identification of the optimal selection and testing of other heuristics only when uncertainty is high. The graphs show that in the beginning, $Insertion1$ is selected as the optimal heuristic at the end of the first local searches with fewer selections on the other heuristics. However, as the local searches progress, the uncertainty of $Insertion1$ increases, and more probability is assigned to the other heuristics to be selected.

3.4.4 Comparison of Additional Energy Used

The table 3.6 illustrates the additional energy consumed by the solutions of the two most efficient HH proposals and the BACO algorithm. This extra energy is derived from the variance between the AVG values obtained by each algorithm and the smallest distance found for the benchmark instances, as detailed in Tables 3.2 and 3.3. The energy consumption is calculated by multiplying the difference between the average and the best fitness, representing the average and shortest route lengths, respectively, by the energy consumption constant h (specified in Table 3.1). While the difference is not particularly noticeable for small instances, it becomes more significant as the number of clients increases, as observed in the X573 instance. Notably, the HHASA$_{TS}$ algorithm exhibits the lowest total energy difference in this comparison.

Table 3.6: Difference in energy consumption between the average distance values and the minimum distance found so far.

Instances	HHASA$_{TS}$	HHASA$_{UCB1}$	BACO
E22	0	0	0
E23	0	0	0
E30	0	0	0
E33	0.67	0.32	2.59
E51	8.50	6.28	0.00
E76	2.78	3.61	0.25
E101	8.96	9.22	12.38
X143	313.14	330.10	130.23
X214	116.32	170.55	129.42
X351	272.26	282.01	114.84
X459	289.07	284.64	164.57
X573	340.70	328.24	3131.15
X685	445.30	763.15	1484.62
X749	402.68	523.37	961.55
X819	605.88	894.99	3641.00
X916	924.21	1631.86	8282.24
X1001	461.99	662.27	1965.04
Total	4192.47	5890.61	20019.89

3.4.5 Graphical Analysis of the Solution

A graphical representation (Figure 3.6) intended to provide a visual understanding of the solutions generated by the HHASA$_{TS}$ algorithm for selected instances of the CEVRP benchmark. The chosen instances for visualization, namely E51, E101, X685, and X1001, are strategically selected to offer a comprehensive representation of different complexity levels within the benchmark. Notably, these instances exhibit varying n_c sizes, ranging from 50 to 1000, providing a nuanced perspective on the performance across a spectrum of problem intricacies.

For instances E51 and E101, as depicted in Figures 3.6a and 3.6b respectively, the number of routes is visually appreciable. Figure 3.6b illustrates the eight routes identified in the best solution, highlighting examples where a charging station is left unused, and one route utilizes two charging stations.

In contrast, in Figures 3.6c and 3.6d, representing instances X685 and X1001 with larger problem sizes, it may be challenging to visualize the intricacies of individual routes due to the extensive routing distances. However, these instances are included to underscore the inherent complexity in benchmark problems of varying scales. The figures offer a visual representation of the challenging nature of the instances, enabling a qualitative understanding of the complexity without the necessity for detailed route visualization.

Furthermore, it is important to note that the proposed HH strategically places charging stations along the route, anticipating the depletion of EV batteries and ensuring timely and efficient replenishment to prevent the EVs from excessively deviating from the route

to the remaining customers.

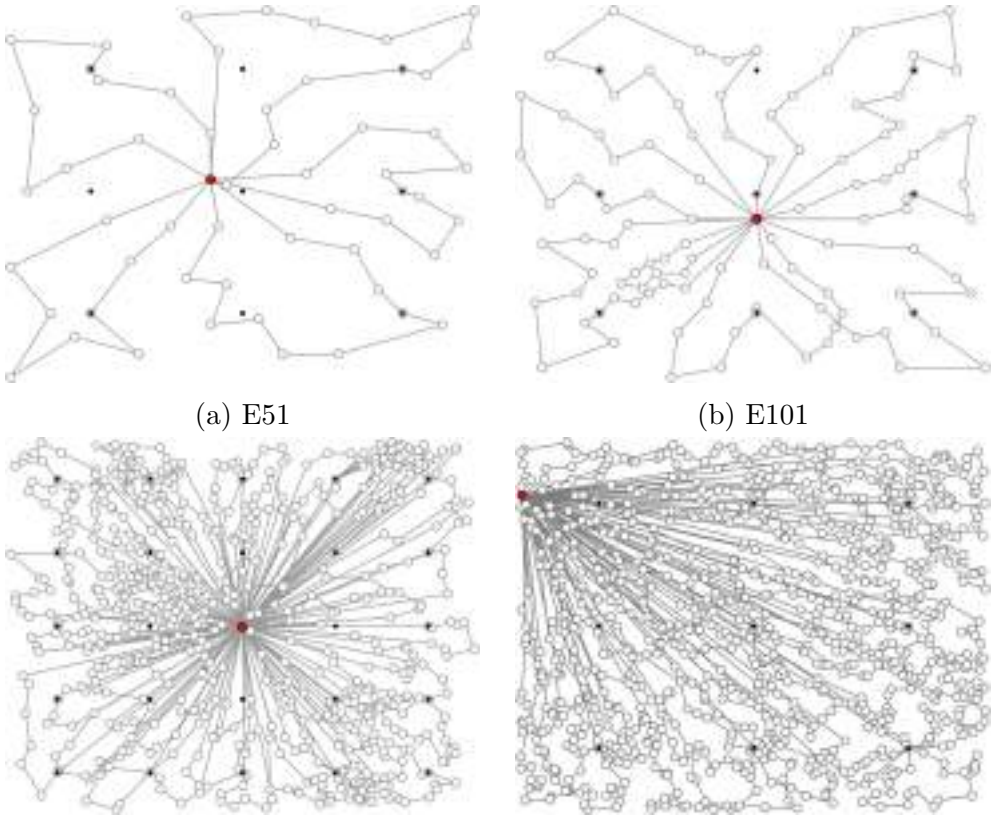

(a) E51 (b) E101

(c) X685 (d) X1001

Figure 3.6: Solutions generated by HHASA$_{TS}$ for instances E51, E101, X685, and X1001. The symbols ●, ○, and • represent the depot, customers, and charging stations, respectively.

3.5 Conclusions

LML has had a significant economic, social, and environmental impact in urban areas, owing to the escalating number of vehicles engaged in goods transportation. This study aimed to formulate a methodology for optimizing freight vehicle routes by promoting the use of EVs to increase efficiency and reduce the times and/or costs of LML. Consequently, an efficient algorithm named HHASA$_{RL}$ is introduced to address the optimization challenges of high-dimensional CEVRP, overcoming the limitations of existing state-of-the-art methods.

The proposed approach hybridizes the well-established Metropolis criterion from the self-adaptive SA metaheuristic as a movement acceptance mechanism and the RL algorithm as a heuristic selection mechanism. Experimental results showcase the superior performance of HHASARL on the IEEE WCCI2020 competition benchmark, outperforming all algorithms in the state-of-the-art employing the same dataset. Notably, the algorithm discovers multiple new best-known solutions for high-dimensional instances. The three proposals of HHASA$_{RL}$ algorithms have a more efficient and better performance than the

compared algorithms for large instances. Among these, HHASA$_{TS}$ stands out as the top-performing algorithm, as indicated by average results and non-parametric tests, utilizing the TS method to address the MAB problem.

4

A New Model for Stationary Parcel Locker Location Problem under Realistic Constraints

4.1 Introduction

4.1.1 Challenges in Last-Mile Operations

As mentioned in the introduction in Chapter 1, urban environments, with their dense populations and intricate infrastructure, pose distinct challenges to conventional delivery systems. Traffic congestion, increased carbon emissions, and the strain on logistical networks are just a few hurdles that demand innovative solutions [11]. The Last-Mile Logistic (LML), representing the final leg of a product's journey from warehouse to customer, is often the most resource-intensive and environmentally impactful phase.

A novel solution is gaining traction to address the challenges associated with home deliveries, such as missed deliveries, long wait times, and traffic problems [123, 124]. This solution involves using Stationary Parcel Lockers (SPLs) that provide customers with a convenient self-service process to pick up their packages at any time [125]. SPLs are strategically placed in areas, such as shopping centers, transportation hubs, and residential zones, allowing customers to pick up their packages flexibly [126]. Figure 4.1 shows a typical SPL setup.

Current SPL methodologies have a notable gap as they fail to consider a model with realistic constraints. These constraints may include stochastic demand distributions, limited capacity of lockers, dynamic costs and collection periods, and the prediction of customer acceptance choices. Addressing these limitations is paramount for developing more effective SPL systems. Accurately incorporating realistic constraints for parcel delivery can improve customer satisfaction and optimize LML operations for Logistics Service

Providers(LSPs) and society in urban areas [127].

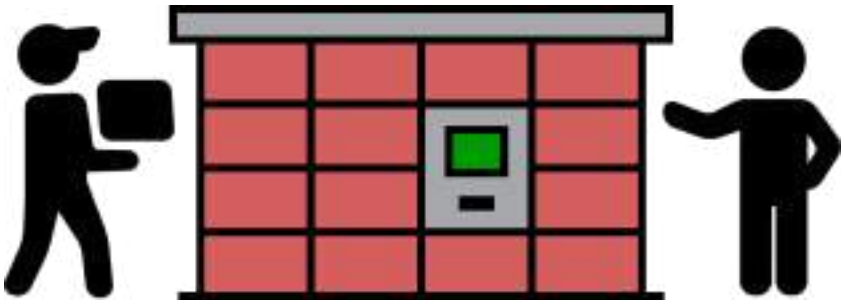

Figure 4.1: A static parcel locker paradigm.

4.1.2 Objectives and Contributions

This chapter explores the Constrained Locker Location Problem under the Threshold Luce Model (CLLPTLM) as a robust and realistic model for SPL allocation in LML operations. By employing a modified Genetic Algorithm (GA), this research aims to optimize the placement of lockers, accounting for stochastic customer demand, dynamic pick-up periods, and facility costs. The validation of this approach through synthetic and real-world datasets underscores its feasibility and adaptability to diverse scenarios.

Building on previous research [87], the CLLPTLM introduces additional constraints, including flexible pick-up times and locker capacity limitations. These constraints enhance customer satisfaction by allowing convenient package retrieval within specified time frames while ensuring efficient locker usage. The primary objective is to maximize profit for Logistic Service Providers (LSPs) by balancing revenue and service costs.

The subsequent sections present a detailed exploration of this innovative approach to optimizing LML. After that, Section 4.2 details the proposed methodology, outlining its key components and features. Section 4.3 provides a detailed account of the experimental setup, elucidating the parameters and considerations involved. Moving forward, Section 4.4 presents the results obtained from three synthetic and one real dataset, offering insights into the performance and applicability of the proposed method. Finally, Section 4.5 consolidates conclusions drawn from the study.

4.2 Methodology

In this section, we present a detailed formulation of the problem named the Constrained Locker Location Problem under the Threshold Luce Model (CLLPTLM). This model aims to optimize the placement of parcel lockers, taking into account various constraints, such as maximum pick-up periods, limited capacities at locker locations, and the Threshold Luce Model (TLM) to predict customer choices. Furthermore, a detailed description of an adapted GA used in this chapter to determine optimal facility locations is provided.

4.2.1 Model Formulation

The Locker Location Problem under the Threshold Luce model (LLPTL) is a combinatorial optimization challenge introduced by Lin et al. [91]. In essence, this problem arises as companies seek to implement a locker service for efficient order delivery while maximizing profits, taking both revenue and the installation cost of the facilities under consideration. The primary objective is to identify the optimal combination of locker locations from a set of feasible options to fulfill daily customer demand. This involves minimizing total lost demand and facility costs, all subject to various constraints.

The LLPTL employs TLM to determine the likelihood of a customer using an available locker facility. Each locker has a unique intrinsic attraction, which varies depending on the customer. The terms "open" and "closed" are used to indicate the status of lockers within a set of SPLs represented by $\boldsymbol{J}$. "Open" lockers are currently available, while "closed" lockers are not. The model also considers an "outside" option, representing the possibility that customers may choose alternatives outside the facilities of the company.

The authors [91] reformulated the TLM into a mixed-integer quadratic conic program, enhancing convexity, a desired property in optimization. This reformulation has made the LLPTL model implementable and has effectively addressed the limitations of traditional modeling frameworks. As a result, it has led to improved company profits. In this study, we extend the research of Lin et al. [91] to enhance the realism of the problem formulation. To achieve this, we have incorporated constraints such as a maximum package pick-up period and limited capacity at SPL locations. Additionally, the model considers installation costs and the number of cabins/towers associated with each parcel locker facility.

For clarity, we provide a comprehensive list of notations used in the mathematical formulation proposed for the CLLPTLM in Table 4.1.

Table 4.1: Notations for the CLLPTLM model

Sets:	
$\boldsymbol{I}$	Set of customers
$\boldsymbol{J}$	Set of candidate locker facilities
$\boldsymbol{H}$	Set of days
C_i	Non-dominated set for customer i, $\forall\ i \in \boldsymbol{I}$
Ω_{hij}	Set of lockers that are dominated by locker j for customer zone i on day h, $\forall\ h \in \boldsymbol{H}$,$i \in \boldsymbol{I}$, $j \in \boldsymbol{J}$
Parameters:	
a_0	Attraction of the outside option
a_{hij}	Attraction of option j for customer i on day h, $a_{hij} > 0$, $\forall\ h \in \boldsymbol{H}$, $i \in \boldsymbol{I}$, $j \in \boldsymbol{J}$
d_{hi}	Demand for customer i on day h, $\forall\ h \in \boldsymbol{H}$, $i \in \boldsymbol{I}$
t_{hi}	Pick-up period for customer i on day h, $\forall\ h \in \boldsymbol{H}$, $i \in \boldsymbol{I}$
f_j	Cost of locker facility j, $\forall\ j \in \boldsymbol{J}$
g_j	Cost of cabinets for facility j, $\forall\ j \in \boldsymbol{J}$
γ	Dominance threshold in Threshold Luce Model
b	Cost of demand
Max_P	Maximum number of packages in each cabinet
Max_C	Maximum number of cabinets in each facility
p	Percentage of number of customers served per day
Variables:	
n_c	Number of customers
n_l	Number of lockers
x_j	1, if locker j is open; 0, otherwise, $\forall\ j \in \boldsymbol{J}$
y_{hij}	1, if the open locker j is in the non-dominated set for customer i on day h; 0, otherwise, $\forall\ h \in \boldsymbol{H}$, $i \in \boldsymbol{I}$, $j \in \boldsymbol{J}$
w_j	Number of cabinets in locker j, $\forall\ j \in \boldsymbol{J}$
u_{hj}	Number of packages in locker j on day h, $\forall\ h \in \boldsymbol{H}$, $j \in \boldsymbol{J}$.
c_{hi}	1, if customer i is served on day h; 0, otherwise, $\forall\ h \in \boldsymbol{H}$, $i \in \boldsymbol{I}$

The mathematical formulation of the CLLPTLM optimization problem is expressed in Equation 4.1, where the objective is to maximize profit by minimizing the total cost of lost demand, installation costs, and cabinet costs per day. The objective function, constraints, and variable definitions are outlined to provide a clear understanding of the optimization problem.

$$\min_{w,x,y} \quad f(\mathbf{w},\mathbf{x},\mathbf{y}) = \sum_{h\in\boldsymbol{H}} \left(\sum_{i\in\boldsymbol{I}} \frac{bd_{hi}}{\sum_{j\in\boldsymbol{J}} \pi_{hij} y_{hij} + 1} + \sum_{j\in\boldsymbol{J}} f_j x_j + \sum_{j\in\boldsymbol{J}} g_j w_j \right) \tag{4.1a}$$

$$s.t. \quad y_{hij} \leq x_j, \quad \forall h \in \boldsymbol{H}, i \in \boldsymbol{I}, j \in \boldsymbol{J} \tag{4.1b}$$

$$y_{hij} + y_{hik} \leq 1, \quad \forall k \in \Omega_{hij}, \forall h \in \boldsymbol{H}, i \in \boldsymbol{I}, j \in \boldsymbol{J} \tag{4.1c}$$

$$\sum_{i\in\boldsymbol{I}} c_{hi} = pn_c, \quad \forall h \in \boldsymbol{H}, i \in \boldsymbol{I} \tag{4.1d}$$

$$0 \leq u_{hj} \leq w_j Max_P, \quad \forall j \in \boldsymbol{J} \tag{4.1e}$$

$$w_j \in \{0, Max_C\}, \quad \forall j \in \boldsymbol{J} \tag{4.1f}$$

$$x_j \in \{0,1\}, \quad \forall j \in \boldsymbol{J} \tag{4.1g}$$

$$y_{hij} \in \{0,1\}, \quad \forall h \in \boldsymbol{H}, i \in \boldsymbol{I}, j \in \boldsymbol{J} \tag{4.1h}$$

where $\pi_{hij} = a_{hij}/a_0$, and $\Omega_{hij} = \{k \in \boldsymbol{J} \mid a_{hij} > (1+\gamma)a_{hik}\}$; Ω_{hij} represents the set of lockers dominated by locker j for customer i. This minimization reflects the sum per day of the cost of the lost demand, the cost of the installations, and the cost of the cabinets in each facility.

The constraint of Equation 4.1b states that locker j cannot be part of the non-dominated set unless locker j is open. Moreover, Equation 4.1c imposes a restriction allowing only one of the variables y_{hij} and y_{hik} to have a value of 1 if locker i dominates locker j on day h. The desired percentage of customers to be served each day is determined by Equation 4.1d. To guarantee that the number of allocated packages for installation j does not exceed its capacity, we introduce the capacity constraint expressed in Equation 4.1e. Finally, the sets w_j, x_j, and y_{hij} are defined by Equations 4.1f, 4.1g, and 4.1h, respectively.

Furthermore, Figure 4.2 illustrates an example of the SPLs problem under the CLLPTLM, showcasing the available delivery facilities and the optimized solution using the model. The figure demonstrates the optimal allocation of four open lockers to efficiently satisfy customer demand. In Figure 4.2a, seven potential delivery facilities, represented by squares $(j_1, j_2, \ldots, j_7)$, serve eight customers $(i_1, i_2, \ldots, i_8)$. Figure 4.2b displays the result of minimizing the objective function of the CLLPTLM.

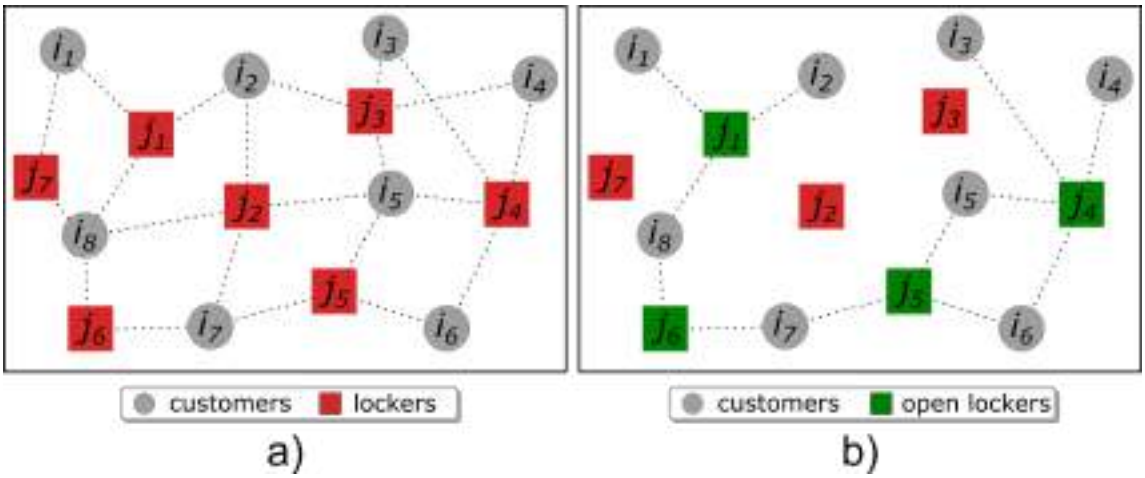

Figure 4.2: Example of the fixed lockers problem under the CLLPTLM model. a) fixed parcel lockers problem. b) solution using the CLLPTLM.

4.2.2 Proposed Method

The challenge faced by the company, involving the selection of locker facilities within a predefined set of feasible locations to minimize the objective function of the CLLPTLM (Equation 4.1), is addressed through the implementation of an adapted GA. This subsection outlines the proposed methodology to solve the combinatorial optimization problem, summarized in the flowchart depicted in Figure 4.3.

General Flowchart and Encoding Scheme

The flowchart comprises three main blocks. The initial block involves data input, defining the sets, parameters, and variables necessary for the CLLPTLM, as explained in Subsection 4.2.1. The second block illustrates the adapted GA, and the third block represents the optimal solution obtained through the algorithm. The encoding scheme utilized by the algorithm is also presented in Figure 4.3.

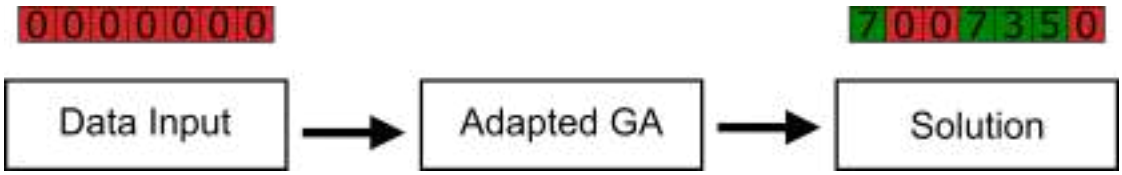

Figure 4.3: General flowchart and encoding of the locker set.

The example in Figure 4.3 mirrors the scenario depicted in Figure 4.2, with a set of candidate SPLs ($\boldsymbol{J}$) and eight customers ($\boldsymbol{I}$). The data input phase involves presenting all feasible lockers. Subsequently, the adapted GA iterates to derive an optimal solution. The outcome reveals four open lockers (j_1, j_4, j_5, j_6) with capacities of "7," "7," "3," and "5" cabinets, respectively. Conversely, the remaining three lockers (j_2, j_3, j_7) remain closed to enhance the profit generated by the LML service through SPLs.

Adapted Genetic Algorithm

The GA is a robust optimization technique that uses natural selection and genetic principles to solve complex optimization problems. This method is particularly effective for exploring large solution spaces and identifying optimal or near-optimal solutions due to its inherent randomization [128]. The adaptation of the GA to address the CLLPTLM involves initiating a population of solutions represented as chromosomes. Each chromosome encodes a potential solution to the SPL set, and the GA iteratively evolves this population through genetic operations: selection, crossover, and mutation [129].

The flowchart of the adapted GA, presented in Figure 4.4, begins with the generation of an initial random population comprising 50 potential solutions. These solutions, represented as integer numbers in the range of $[0, Max_C]^{n_l}$ (where n_l is the number of lockers), undergo fitness evaluation based on the objective function defined in Equation 4.1. Subsequently, the GA employs the tournament selection method, with $k = 3$, to choose two parents with the highest fitness.

The crossover and mutation operations follow. The crossover operation involves combining information from two parents (s^1 and s^2) to produce an offspring (s^c), utilizing the Blend crossover operator (BLX-α) as defined in Equation 4.2. Here, $\alpha = 0.8$.

$$s_i^c = (1 - \sigma_i)\, s_i^1 + \sigma_i s_i^2 \tag{4.2}$$

For this problem, α is set with a value of 0.8 and $\sigma_i = (1 + 2\alpha)\, u_i - \alpha$, where u_i is a random number between 0 and 1.

The mutation operation introduces random changes in the offspring, maintaining diversity in the population. The swap operator randomly exchanges the position of two elements within the offspring solution (s^c) with a probability of 0.2.

Considering the context of CLLPTLM, which involves discrete and natural variables to represent locker locations, the adapted evolutionary algorithm ensures valid solutions by rounding values resulting from crossover and mutation to the nearest integer. Additionally, bounds within the discrete interval of $[0, Max_C]$ are applied.

The fitness of the offspring is then calculated for comparison with one of the parents. If the offspring outperforms the second parent obtained through the selection operator, it replaces the parent and enters the population. The algorithm iterates until the stopping criterion is met, defined by a predetermined maximum number of iterations.

4.3 Experimental Framework

This section provides a comprehensive overview of the two datasets employed in this study: synthetic and real-world datasets. Additionally, the experimental setup for the conducted experiments is described.

The synthetic dataset is generated to address the absence of established benchmarks for the SPLs problem, considering both locker capacity and the dynamic nature of the collection period. This dataset is essential for testing the proposed methodology. The generation process involves several parameters, including the number of customers (n_c), potential locations for stationary parcel lockers (n_l), and the maximum number of compartments each customer can request (Max_d). Additionally, it incorporates information

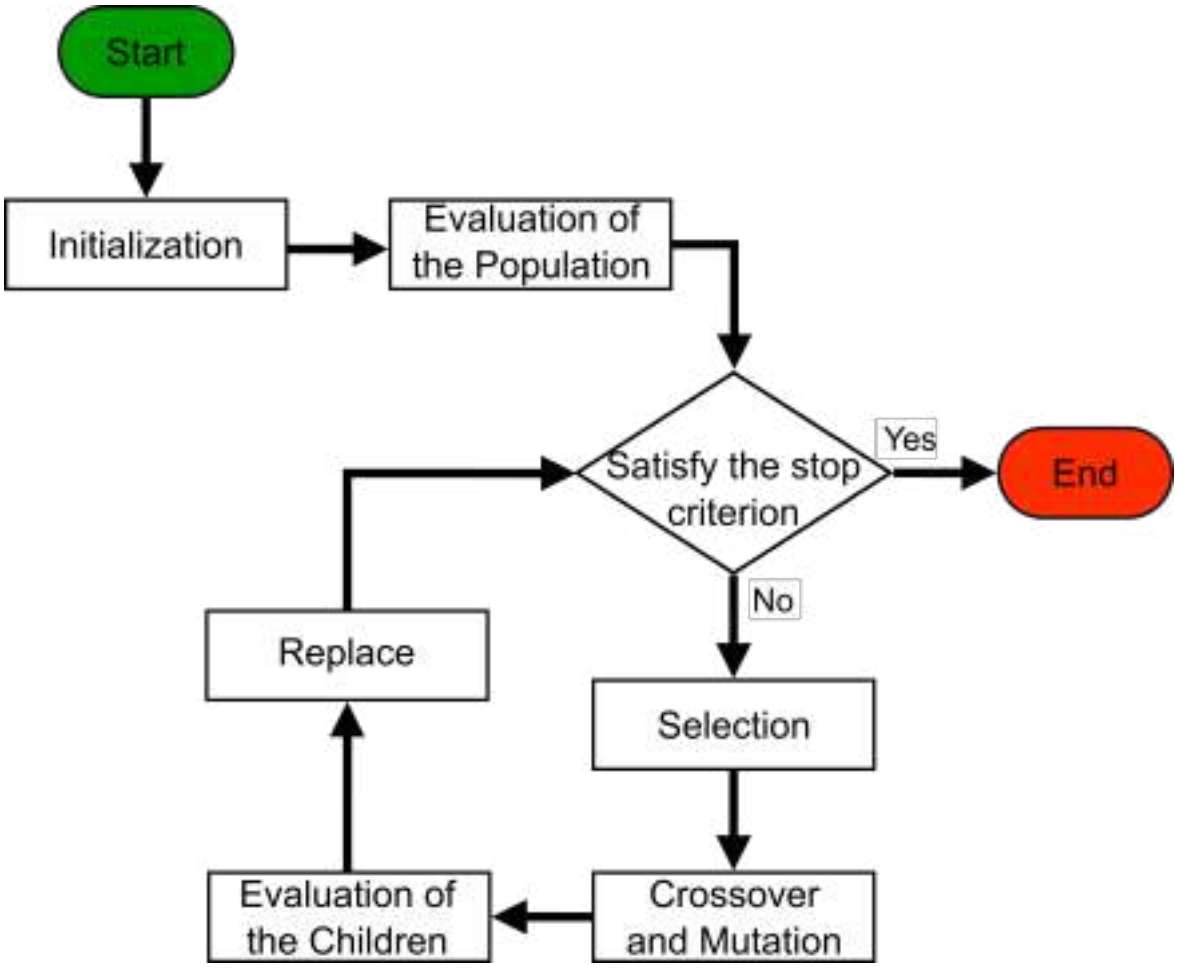

Figure 4.4: Flowchart of the adapted GA.

on the maximum number of days customers have to retrieve their packages from the locker after delivery (Max_t).

The following is a description of the instance generator subsection, which explains how the instance for the synthetic dataset will be generated.

4.3.1 Instance Generator for the Synthetic Dataset

In order to conduct a thorough assessment and validation of the proposed methodology, the creation of comprehensive datasets is paramount. This subsection explores the detailed process of generating synthetic instances, a fundamental component of this study. Synthetic datasets play a crucial role in overcoming the absence of established benchmarks for the SPLs problem, particularly when considering locker capacity and the dynamic nature of the collection period. The following details outline the meticulous steps involved in generating geographic positions, modeling customer orders, and configuring parcel lockers, all contributing to the robust construction of the synthetic dataset. This dataset serves as a critical testing ground for evaluating the efficacy and adaptability of the proposed methodology.

Geographic Positions

The generation of potential locker locations ($\boldsymbol{L}$) and customer positions ($\boldsymbol{Z}$) is a critical aspect of the synthetic dataset creation. In this phase:

- **Parcel Locker Locations ($\boldsymbol{L}$):** Potential locker locations are randomly generated within a two-dimensional Cartesian coordinate system, encompassing the range from $[0, 100]^2$.
- **Customer Positions ($\boldsymbol{Z}$):** Customer positions are strategically determined using four distinct distributions within a two-dimensional Cartesian coordinate system, encompassing the range from $[0, 100]^2$ for 30 days:
  1. *Distribution 1*: A random uniform distribution (Figure 4.5a).
  2. *Distribution 2*: A standard Gaussian distribution (Figure 4.5b).
  3. *Distribution 3*: A shifted Gaussian distribution (Figure 4.5c).
  4. *Distribution 4*: A mixed distribution composed of two Gaussian distributions (Figure 4.5d).

This configuration of four distributions ensures wide spatial coverage, introduces randomness based on the Gaussian distribution, incorporates spatial displacement for increased variability, and enhances diversity through a mix of two Gaussian distributions.

Distances between customer i and locker j on day h are calculated using the Manhattan Metric: $M_{hij} = (|Z_{hi1} - L_{j1}| + |Z_{hi2} - L_{j2}|), \forall\ h \in \boldsymbol{H},\ i \in \boldsymbol{I},\ j \in \boldsymbol{J}$.

Orders

Synthetic customer demand is modeled through the generation of compartment requests (d) and collection time periods (t) over a 30-day period. The ordering process includes:

- **Customer Demand (d):** The number of compartments required for each customer is drawn from a uniform distribution within the defined range $[1, Max_d]$ for 30 days.
- **Collection Time Period (t):** Each customer's collection time period is established using a uniform distribution within $[1, Max_t]$. This ensures that customers are allotted a reasonable time frame to retrieve their orders, with no customer exceeding Max_t days.

Parcel Lockers

The characteristics of the SPLs, representing key parameters for the synthetic dataset, are predetermined in this phase:

- Maximum Compartments per Cabinet (Max_P): The permissible number of compartments/packages for each cabinet or tower is specified.
- Maximum Cabinets in Each Installation (Max_C): The predefined limit for the number of cabinets in each locker installation is set.

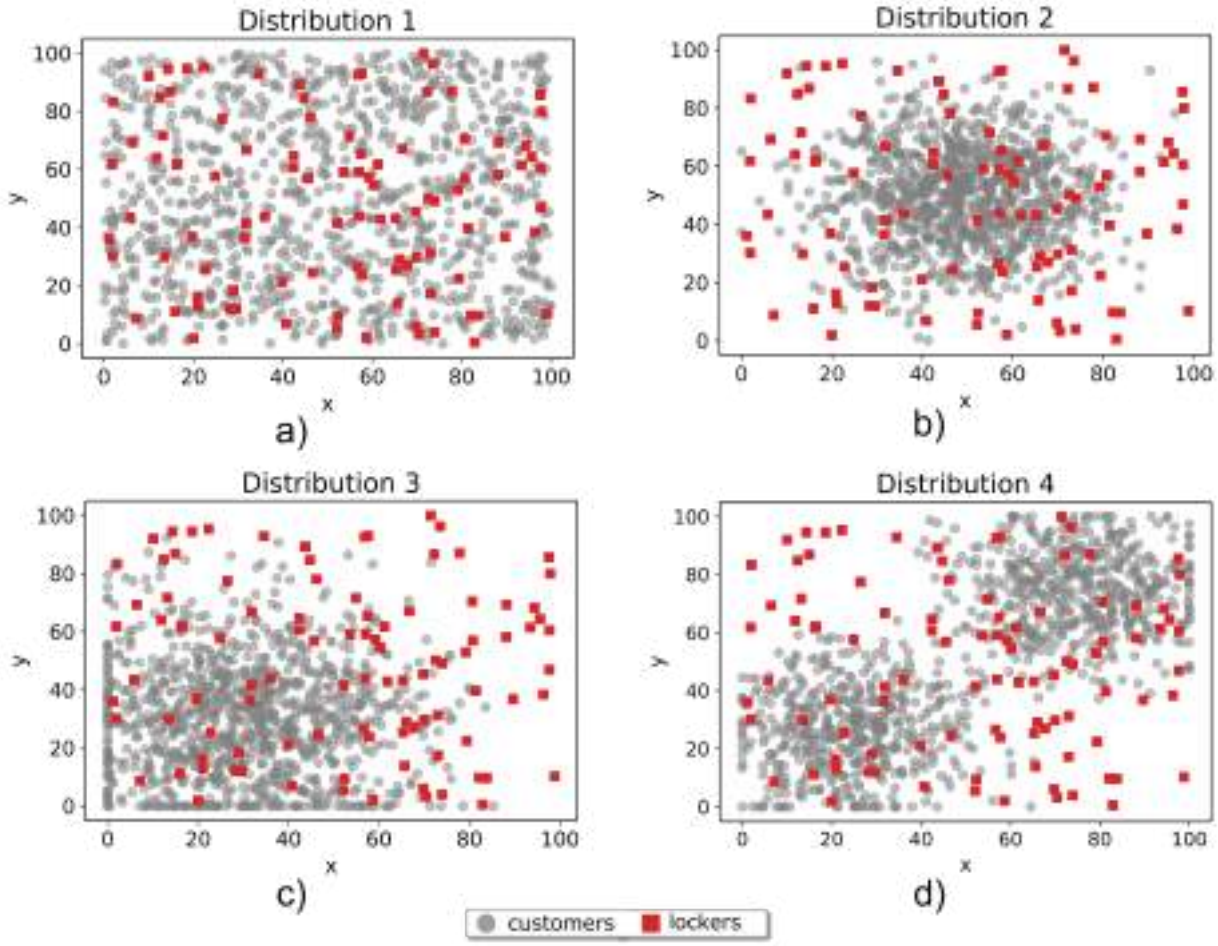

Figure 4.5: Distribution of the position of the customers: a) uniform distribution; b) standard Gaussian distribution; c) shifted Gaussian distribution; d) mixture of two Gaussian distributions.

- Daily Cost Parameters:

  1. Facility Cost (f_j): The daily cost of operating the locker facility.
  2. Cabinet/Tower Cost (g_j): The daily cost associated with each cabinet or tower at a given locker location.

By establishing these parameters, we create a realistic and diverse synthetic dataset, capturing the spatial, demand, and facility aspects essential for evaluating the proposed methodology.

4.3.2 Experimental Setup

Each experiment involves 20 independent executions with random seeds to assess the robustness, stability, and consistency of the proposed methodology, given the inherent randomness of the GA. The algorithm's stopping criterion is set to a maximum of $n_l * 40$

iterations. Experiments are conducted in Python on an Intel Core i5 @ 2.7 GHz CPU with 16 GB of RAM.

Two datasets are used for evaluation:

1. **Synthetic Dataset:** This dataset comprises three instances: small (B1), medium (B2), and large (B3) generated by the instance generator described in Subsection 4.3.1. Each instance represents a different scale, with varying numbers of daily customers and predefined locker facilities.

   - B1: 100 customers per day and 10 predefined locker facilities.
   - B2: 500 customers per day and 50 predefined locker facilities.
   - B3: 1,000 customers per day and 100 predefined locker facilities.

2. **Real-World Dataset:** Collected from a logistics company based in Dublin, this dataset represents a large-scale instance with 1,000 daily customers and 150 predefined locker facilities. Due to confidentiality concerns, specific details such as coordinates and demand data are withheld to safeguard sensitive business information. The customer count is genuine; however, location data is only available for 60% of the customer population. The remaining 40% locations have been generated based on the spatial distribution of "known" customers.

   The geographical distribution of lockers is based on considerations from the literature [130, 85], taking into account factors like proximity to public spaces, parking lots, supermarkets, restaurants, and eco-friendly collection methods.

   The customer demand, denoted as the number of compartments (d), relies on the data extracted from customer orders processed by the logistics company over 30 days. The company classifies (d) into three sizes: small, medium, and large. Small demand requires one compartment; medium, two; and large, three.

   In order to obtain the precise walking times for calculating the M_{hij} matrix, the Valhalla routing engine is used [131]. It retrieves real-time data from OpenStreetMap to determine the time it will take for customer i to pick up their package at locker j on day h.

Both datasets utilize SPLs that have a standard size with uniform dimensions of 366 cm (length) x 61 cm (width) x 183 cm (height) [132]. Each cabinet/tower has 14 compartments (defined as Max_P), each measuring 4 cm x 4 cm x 12 cm. The reference for this setup is Amazon, the largest e-commerce company in the U.S.A., which allows a tolerance period of 3 days (denoted as Max_t) for order pick-up after delivery. Additionally, customers are permitted to request a maximum of 3 compartments for their order (referred to as Max_d).

The parameters of the CLLPTLM are defined as follows. The attraction a_{hij} between the customer i for the locker j on day h is calculated in Equation 4.3:

$$a_{hij} = e^{-\beta M_{hij}}, \quad \forall h \in \boldsymbol{H}, i \in \boldsymbol{I}, j \in \boldsymbol{J} \tag{4.3}$$

Here, M denotes the time-distance matrix (depending on the dataset), and β is a parameter that determines customers' sensitivity to this distance. For simplicity, β is set

to the value of 1. This exponential decay function of utility is commonly employed to address location-related problems [133].

For the outside option (a_0), the same equation presented by Lin et al. [91] is adopted, which is shown in Equation 4.4:

$$a_0 = \xi e^{-1}, \quad \forall i \in \boldsymbol{I} \tag{4.4}$$

Here, ξ is a specific parameter that controls the strength of attraction. A higher value indicates that the outside option is more attractive. In this work, ξ is set to 0.5. This value has been chosen so that there is a 50% chance that customers will not choose any of the company's facilities to collect their packages. This helps to ensure that customer preferences are neutral among all available options.

The CLLPTLM incorporates three parameters defined as follows: a dominance threshold $\gamma = 1$, and uniform costs for all lockers, where $f_j = 10$ represents the operating cost, and $g_j = 1$ denotes the daily cost of each cabinet. To conduct a comprehensive study, we explore varying values for the percentage of customers served per day ($p = [1, 0.8, 0.5]$), the maximum number of cabinets per establishment ($Max_C = [5, 7, 10]$), and the demand cost ($b = [1, 0.75, 0.5]$). These sensitivity analyses involve adjusting parameters to assess their impact on the CLLPTLM.

The comprehensive experimental framework ensures a thorough evaluation of the proposed methodology under diverse conditions and datasets, providing valuable insights into its performance and applicability.

For both datasets, the analysis will encompass the following aspects:

1. **Computational Results:** The average fitness and the number of SPL locations are key indicators of the methodology's effectiveness. We will investigate how changes in parameters influence these metrics, providing insights into the algorithm's performance and the optimal placement of parcel lockers.

2. **Convergence Analysis:** The convergence analysis involves studying the algorithm's stability and efficiency. By assessing convergence curves, we aim to understand the iteration dynamics and identify scenarios where the algorithm consistently converges to optimal solutions.

3. **Cost Analysis:** Analyzing the costs associated with SPL locations is crucial for evaluating the economic implications of the proposed methodology. We will explore monthly demand revenue, average monthly costs related to SPL locations (installation and number of cabinets), and the resulting profits.

4. **Demand Cost Sensitivity Analysis:** This analysis explores the sensitivity of the proposed model to variations in demand cost. By considering different scenarios of demand cost ($b = [1, 0.75, 0.5]$), we aim to understand how changes in this parameter impact the profitability of the logistics company.

The comprehensive experimental framework ensures an exhaustive evaluation of the proposed methodology under diverse conditions and datasets. The systematic exploration of parameter variations provides a robust understanding of the adaptability and performance of the CLLPTLM.

4.4 Results and Discussion

This section delves into the experimental outcomes of the proposed method, centering on the optimal selection of parcel lockers from a set of feasible locations, utilizing two distinct datasets for analysis.

4.4.1 Synthetic Dataset Results

The results for the artificial B3 instance are visually presented in Figure 4.6 under the configuration of $p = 1$ and $Max_C = 7$. Gray circles represent customers, red squares depict candidate SPLs, and green squares signify the optimal lockers to open/install. As anticipated, the four distributions showcase distinct SPL locations, aligning with variations in customer density across different areas of the map.

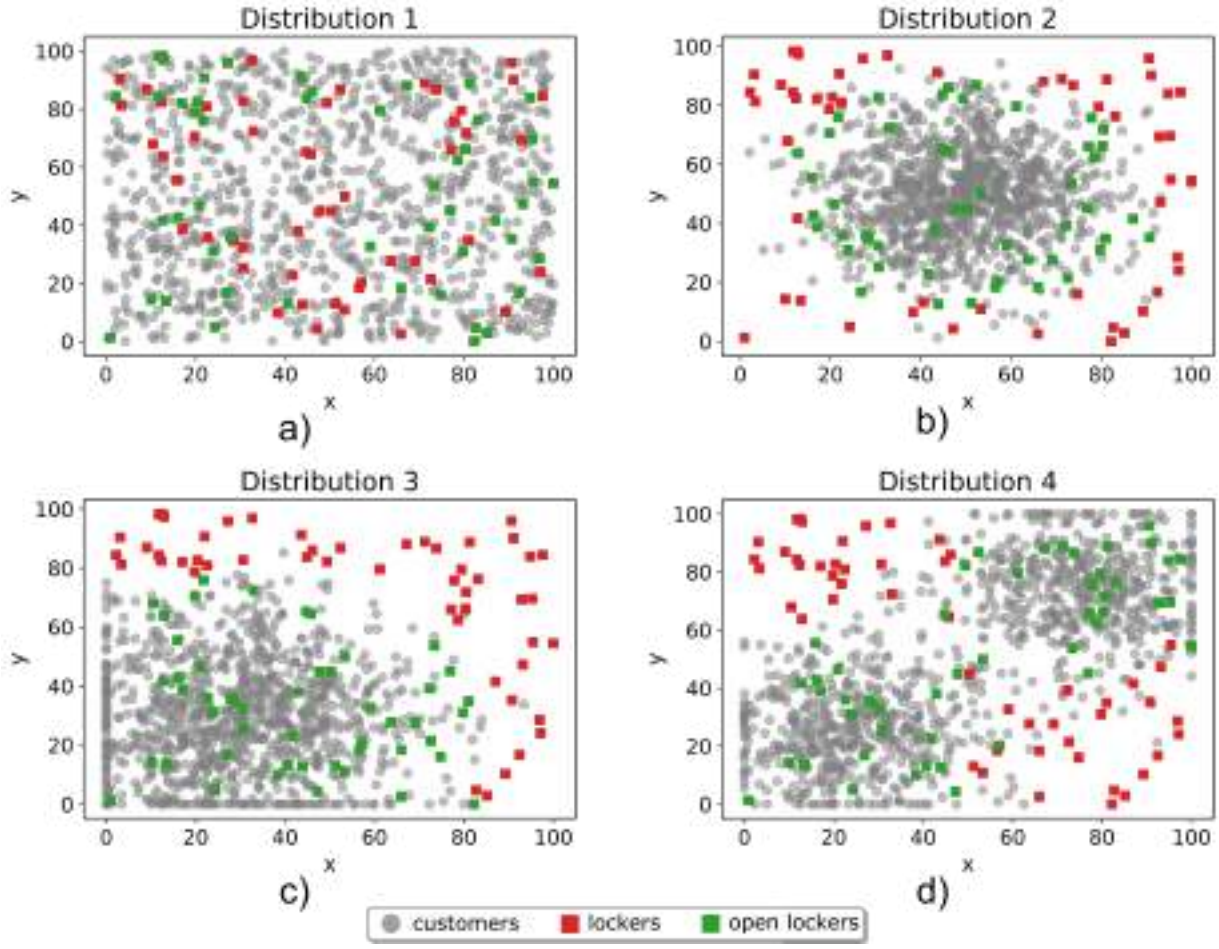

Figure 4.6: Geographical locations of the SPLs with the solutions obtained for the instance B3 with $p = 1$ and $Max_C = 7$.

Computational Results for Synthetic Dataset

The results for all configurations (p, Max_C) for the three instances (B1, B2, B3) regarding the synthetic dataset are shown in Tables 4.2, 4.3 and 4.4, respectively. The tables display the average number of SPL locations and the average fitness of the objective function after executing all iterations. As the number of facilities remains the same in the three instances for the 20 runs, the standard deviation has been omitted for conciseness.

These results demonstrate that the proposed GA approach employed to tackle the CLLPTLM problem is robust and stable. It is evident that for all four distributions, as the maximum number of available cabinets in each location increases, there is a concurrent decrease in the average fitness and the requisite number of installations needed to cover the percentage of demand specified by the LSPs.

Table 4.2: Computational results of the B1 instance under all combinations (p, Max_C).

B1 instance										
Distribution	Max Cabins	Percentage								
		100%			80%			50%		
		#Lockers	Fitness		#Lockers	Fitness		#Lockers	Fitness	
		AVG	AVG	STD	AVG	AVG	STD	AVG	AVG	STD
1	5	7	9092	0.0	6	8654	0.0	4	7855	0.0
	7	5	8488	0.0	5	8332	0.0	3	7528	0.0
	10	4	8179	0.0	3	7780	0.0	2	7253	0.0
2	5	7	9131	0.0	6	8662	0.0	4	7799	0.0
	7	5	8510	0.0	5	8325	0.0	3	7467	0.0
	10	4	8175	0.0	3	7744	0.0	2	7188	0.0
3	5	7	9153	0.0	6	8675	0.0	4	7818	0.0
	7	5	8534	0.0	5	8344	0.0	3	7480	0.0
	10	4	8197	0.0	3	7751	0.0	2	7210	0.0
4	5	7	9165	0.0	6	8677	0.0	4	7827	0.0
	7	5	8547	0.0	5	8360	0.0	3	7484	0.0
	10	4	8228	0.0	3	7753	0.0	2	7207	0.0

The medium-scale B2 instance shows slight variations in solution quality, with non-zero standard deviations indicating more variability. Distribution 4 with $p = 1$ and $p = 0.8$ consistently produces good results, while some configurations have low standard deviations, suggesting stable and consistent solutions. On the contrary, higher standard deviations in certain configurations suggest increased variability, indicating that specific parameter combinations generate more predictable and stable results than others.

Comparatively, the large-scale B3 instance displays slightly higher standard deviation values, hinting at increased variability as the number of lockers to evaluate grows. However, the observed low standard deviation in fitness values suggests that this variability does not significantly impact the algorithm's overall performance. In other words, the proposed methodology showcases adaptability and robustness, promising for logistics companies as it dynamically adjusts SPL locations to changing demand and customer behaviors while maintaining efficiency.

Table 4.3: Computational results of the B2 instance under all combinations (p, Max_C).

B2 instance										
Distribution	Max Cabins	Percentage								
		100%			80%			50%		
		#Lockers	Fitness		#Lockers	Fitness		#Lockers	Fitness	
		AVG	AVG	STD	AVG	AVG	STD	AVG	AVG	STD
1	5	35	44578	99.63	30	42749	130.78	20	38546	139.45
	7	25	41797	247.33	21	40332	138.31	14	36855	109.08
	10	17	39780	343.0	15	38514	90.83	10	35700	98.19
2	5	35	44967	33.58	30	43000	36.92	20	38635	67.24
	7	25	41759	61.87	21	40255	37.5	15	36843	61.07
	10	17	39237	0.0	15	38054	0.0	10	35556	20.96
3	5	3	44999	13.69	30	43010	0.0	20	38653	105.35
	7	25	41706	13.41	21	40232	0.0	15	36981	39.66
	10	17	39364	247.85	15	38263	19.09	10	35701	49.99
4	5	35	45140	0.0	30	43140	0.0	20	38698	24.83
	7	25	41887	0.0	21	40330	0.0	15	36906	23.58
	10	17	39379	0.0	15	38179	0.0	10	35517	0.0

Table 4.4: Computational results of the B3 instance under all combinations (p, Max_C).

B3 instance										
Distribution	Max Cabins	Percentage								
		100%			80%			50%		
		#Lockers	Fitness		#Lockers	Fitness		#Lockers	Fitness	
		AVG	AVG	STD	AVG	AVG	STD	AVG	AVG	STD
1	5	69	87290	163.56	61	84758	235.11	40	76802	264.24
	7	49	82114	275.15	44	80057	253.57	29	73683	175.48
	10	34	78533	758.27	31	76752	256.38	20	71247	115.27
2	5	69	89691	181.99	59	86469	41.48	40	77331	136.68
	7	49	83335	16.07	44	81008	15.27	29	73818	90.98
	10	34	78659	2.08	31	76824	4.49	20	71038	16.51
3	5	69	89261	42.54	59	85995	68.04	40	76725	91.74
	7	49	82519	20.8	44	80137	12.88	29	73075	96.96
	10	34	77407	6.94	31	75654	85.11	20	70583	73.67
4	5	69	88234	37.06	60	85133	75.88	40	77048	41.45
	7	49	81401	9.92	44	79428	59.79	29	73300	56.52
	10	34	77052	429.3	31	75583	44.84	20	70470	0.0

Convergence Analysis for Synthetic Dataset

The convergence curves for the B3 instance, considering $p = 0.8$ and $Max_C = 5$ in 20 executions, are illustrated in Figure 4.7. The graphs show the fitness values obtained during the iterative process, revealing convergence within 1,000 iterations out of the designated 4,000. This convergence is consistent across multiple executions, underscoring the algorithm's effectiveness in solving the SPL problem for the diverse distributions.

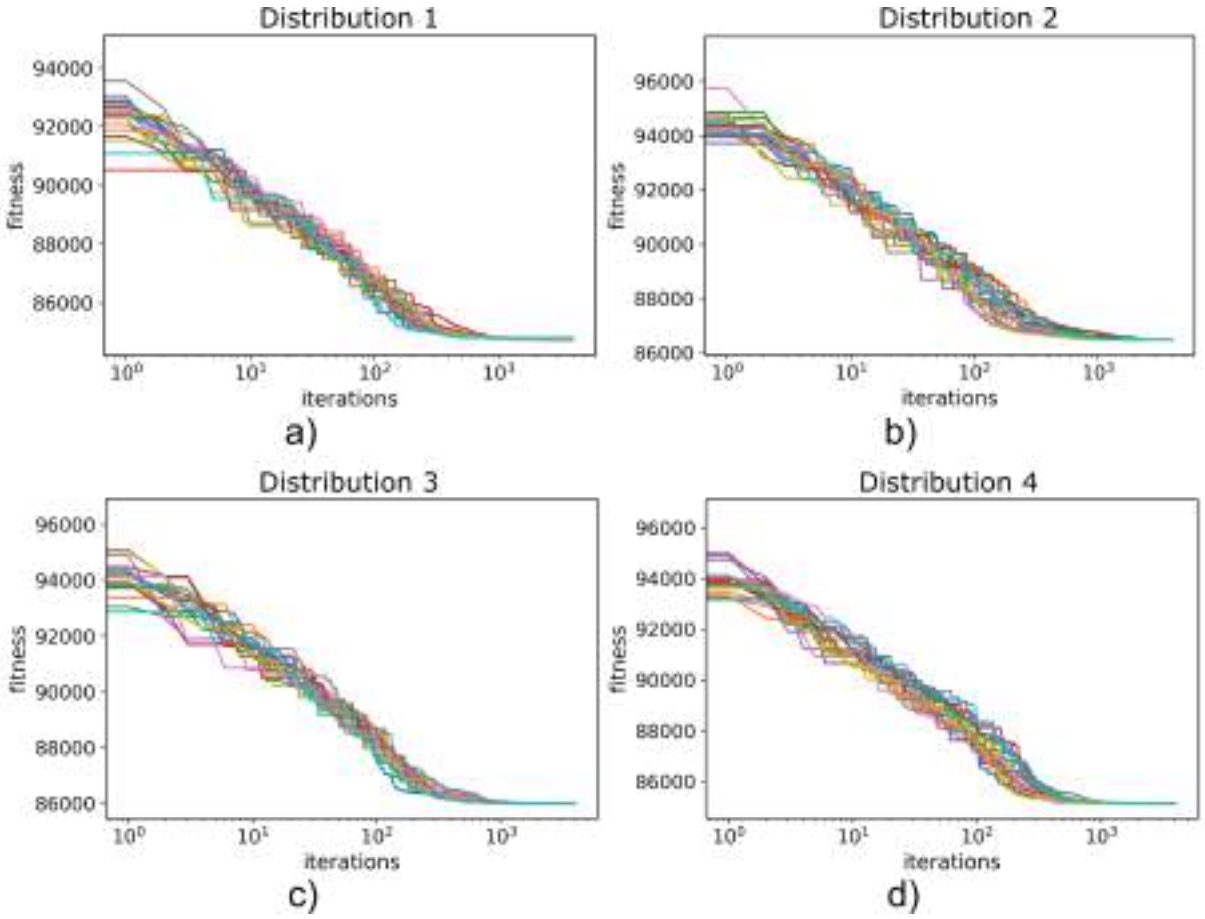

Figure 4.7: Convergence curve for the B3 instance with $p = 0.8$ and $Max_C = 5$: a) uniform distribution; b) standard Gaussian distribution; c) shifted Gaussian distribution; d) mixture of two Gaussian distributions.

Cost Analysis for Synthetic Dataset

The findings of the cost analysis are presented in Tables 4.5, 4.6, and 4.7. These tables showcase the outcomes of the proposed methodology implementation in all configurations (p, Max_C) for the three instances, respectively. The tables display the monthly demand revenue, the average monthly costs related to SPL locations (installation and cabinets), and LSP profits.

Profit values, expressed as a percentage (pct) of the revenue, are calculated by subtracting costs from the monthly revenue. The objective of comparing these tables is to discern the percentage of customers served per day that yields the maximum monetary profit for the company across varying maximum numbers of cabinets per facility. The most profitable percentage values are highlighted in bold. For the B1 instance (4.5), the configuration with the highest profitability for all four distributions is (0.8, 10). This outcome may be due to the low number of installed lockers and very few customers.

However, for the B2 (4.6) and B3 (4.7) instances, the configuration with the highest profitability for all distributions is (1, 10), regardless of the scenario. For the majority of the results for the three instances, the costs are consistent (with variations indicated

by the standard deviation) across different configurations, suggesting that the cost results are relatively robust and can be reliably estimated.

Table 4.5: Cost results for the B1 instance under all combinations (p, Max_C).

B1 instance														
Distribution	Max Cabins	Demand	Percentage											
			100%				80%				50%			
			Costs		Profit		Costs		Profit		Costs		Profit	
			AVG	STD	value	pct	AVG	STD	value	pct	AVG	STD	value	pct
1	5	5980	3150.0	0.0	2830.0	47.32	2700.0	0.0	2084.0	43.56	1800.0	0.0	1190.0	39.79
	7	5980	2550.0	0.0	3430.0	57.35	2430.0	0.0	2354.0	49.20	1530.0	0.0	1460.0	48.82
	10	5980	2280.0	0.0	3700.0	61.87	1800.0	0.0	2984.0	**62.37**	1200.0	0.0	1790.0	59.86
2	5	5980	3150.0	0.0	2830.0	47.32	2700.0	0.0	2084.0	43.56	1800.0	0.0	1190.0	39.79
	7	5980	2550.0	0.0	3430.0	57.35	2400.0	0.0	2384.0	49.83	1530.0	0.0	1460.0	48.82
	10	5980	2280.0	0.0	3700.0	61.87	1800.0	0.0	2984.0	**62.37**	1200.0	0.0	1790.0	59.86
3	5	5980	3150.0	0.0	2830.0	47.32	2700.0	0.0	2084.0	43.56	1800.0	0.0	1190.0	39.79
	7	5980	2550.0	0.0	3430.0	57.35	2400.0	0.0	2384.0	49.83	1530.0	0.0	1460.0	48.82
	10	5980	2280.0	0.0	3700.0	61.87	1800.0	0.0	2984.0	**62.37**	1200.0	0.0	1790.0	59.86
4	5	5980	3150.0	0.0	2830.0	47.32	2700.0	0.0	2084.0	43.56	1800.0	0.0	1190.0	39.79
	7	5980	2550.0	0.0	3430.0	57.35	2400.0	0.0	2384.0	49.83	1530.0	0.0	1460.0	48.82
	10	5980	2280.0	0.0	3700.0	61.87	1800.0	0.0	2984.0	**62.37**	1200.0	0.0	1790.0	59.86

Table 4.6: Cost results for the B2 instance under all combinations (p, Max_C).

B2 instance														
Distribution	Max Cabins	Demand	Percentage											
			100%				80%				50%			
			Costs		Profit		Costs		Profit		Costs		Profit	
			AVG	STD	value	pct	AVG	STD	value	pct	AVG	STD	value	pct
1	5	30022	15690.0	0.0	14332.0	47.73	13477.5	98.07	10540.10	43.88	8970.0	0.0	6041.0	40.24
	7	30022	12660.0	0.0	17362.0	57.83	10710.0	0.0	13307.60	55.40	7140.0	0.0	7871.0	52.43
	10	30022	10236.0	108.0	19786.0	**65.90**	9000.0	0.0	15017.60	62.52	5964.0	20.34	9047.0	60.26
2	5	30022	15690.0	0.0	14332.0	47.73	13432.5	160.68	10585.10	44.07	9000.0	0.0	6011.0	40.04
	7	30022	12660.0	0.0	17362.0	57.83	10710.0	0.0	13307.60	55.40	7560.0	0.0	7451.0	49.63
	10	30022	10200.0	0.0	19822.0	**66.02**	9000.0	0.0	15017.60	62.52	6000.0	0.0	9011.0	60.02
3	5	30022	15690.0	0.0	14332.0	47.73	13500.0	0.0	10517.60	43.79	9000.0	0.0	6011.0	40.04
	7	30022	12660.0	0.0	17362.0	57.83	10710.0	0.0	13307.60	55.40	7560.0	0.0	7451.0	49.63
	10	30022	10218.0	78.46	19804.0	**65.96**	9000.0	0.0	15017.60	62.52	6000.0	0.0	9011.0	60.02
4	5	30022	15690.0	0.0	14332.0	47.73	13500.0	0.0	10517.60	43.79	9000.0	0.0	6011.0	40.04
	7	30022	12660.0	0.0	17362.0	57.83	10710.0	0.0	13307.60	55.40	7560.0	0.0	7451.0	49.63
	10	30022	10254.0	128.54	19768.0	**65.84**	9000.0	0.0	15017.60	62.52	6000.0	0.0	9011.0	60.02

Demand Cost Sensitivity Analysis for Synthetic Dataset

Figure 4.8 illustrates the demand cost sensitivity analysis for various configurations of the B3 instance, considering different (b, p, Max_C) configurations across four distributions. This analysis aims to analyze the influence of variations in demand cost on profitability, encompassing three distinct cost values: $b = [1, 0.75, 0.5]$. Figure 4.8 consists of three sets of bars in blue, red, and green, each denoting a distinct demand cost scenario with values of 1, 0.75, and 0.5 euros, respectively. These bars represent the maximum number of cabinets that can be installed ($Max_C = [5, 7, 10]$) for the four distributions on the x-axis.

As a result, there are nine bars in each distribution, with each set of three bars corresponding to a specific maximum number of cabinets. Each bar is divided into three

Table 4.7: Cost results for the B3 instance under all combinations (p, Max_C).

B3 instance														
Distribution	Max Cabins	Demand	Percentage											
			100%				80%				50%			
			Costs		Profit		Costs		Profit		Costs		Profit	
			AVG	STD	value	pct	AVG	STD	value	pct	AVG	STD	value	pct
1	5	60155	31050.0	0.0	29105.0	48.38	27360.0	180.0	20764.0	43.14	17998.5	6.53	12079.0	40.15
	7	60155	24990.0	0.0	35165.0	58.45	22440.0	0.0	25684.0	53.37	14730.0	0.0	15347.5	51.02
	10	60155	20478.0	156.0	39677.0	**65.95**	18510.0	0.0	29614.0	61.53	12000.0	0.0	18077.5	60.10
2	5	60155	30990.0	0.0	29165.0	48.48	26595.0	135.0	21529.0	44.73	18000.0	0.0	12077.5	40.15
	7	60155	24960.0	0.0	35195.0	58.50	22440.0	0.0	25684.0	53.37	14757.0	9.0	15320.5	50.93
	10	60155	20400.0	0.0	39755.0	**66.08**	18540.0	0.0	29584.0	61.47	12000.0	0.0	18077.5	60.10
3	5	60155	30991.5	6.53	29163.5	48.48	26617.5	160.68	21506.5	44.68	18000.0	0.0	12077.5	40.15
	7	60155	24960.0	0.0	35195.0	58.50	22440.0	0.0	25684.0	53.37	14754.0	12.0	15323.5	50.94
	10	60155	20400.0	0.0	39755.0	**66.08**	18540.0	0.0	29584.0	61.47	12000.0	0.0	18077.5	60.10
4	5	60155	30990.0	0.0	29165.0	48.48	27000.0	0.0	21124.0	43.89	18000.0	0.0	12077.5	40.15
	7	60155	24960.0	0.0	35195.0	58.50	22440.0	0.0	25684.0	53.37	14766.0	18.0	15311.5	50.90
	10	60155	20449.5	117.83	39705.5	**66.00**	18540.0	0.0	29584.0	61.47	12000.0	0.0	18077.5	60.10

portions, representing the percentage of clients served by the company per day. The darkest portion represents 100% client service, the next shade represents 80%, and the lightest section represents only 50% of customers served.

When analyzing the profitability of a business, higher percentages indicate greater profitability, whereas negative values signify economic losses. Considering the fixed costs (f_j and g_j) associated with the lockers in use, a value of $b = 0.5$ would not yield a positive profit. As expected, the configuration (1, 1, 10) generates the highest profit across all four distributions. However, the differences in profit percentages for $b = 0.75$ slightly decrease the overall profit. Therefore, depending on the company's desired objectives, the company may consider using this value.

4.4.2 Real-World Dataset Results

The visual results for the real-world dataset are presented in Figure 4.9 under the configuration of $p = 1$ and $Max_C = [5, 7, 10]$. These results provide a tangible representation of the proposed methodology's performance when applied to actual data. It's important to mention that the data location has undergone normalization to safeguard the privacy of the company's customers, ensuring that their locations remain undisclosed.

In the figure, gray circles represent the customers, while the red squares represent the set of SPL candidates. The green squares indicate the optimal lockers to be opened. Across all three examples, as expected, the distribution of SPL locations gravitates towards areas with higher customer density.

Computational Results for Real-World Data

The computational results from a logistics company based in Dublin, obtained by evaluating all combinations of the parameters (p, Max_C), are presented in Table 4.8. These results are derived from real data and show the average number of SPL locations and the average fitness of the objective function resulting from 20 runs. Unlike the synthetic dataset results, the standard deviation has been omitted because the number of installations remains the same.

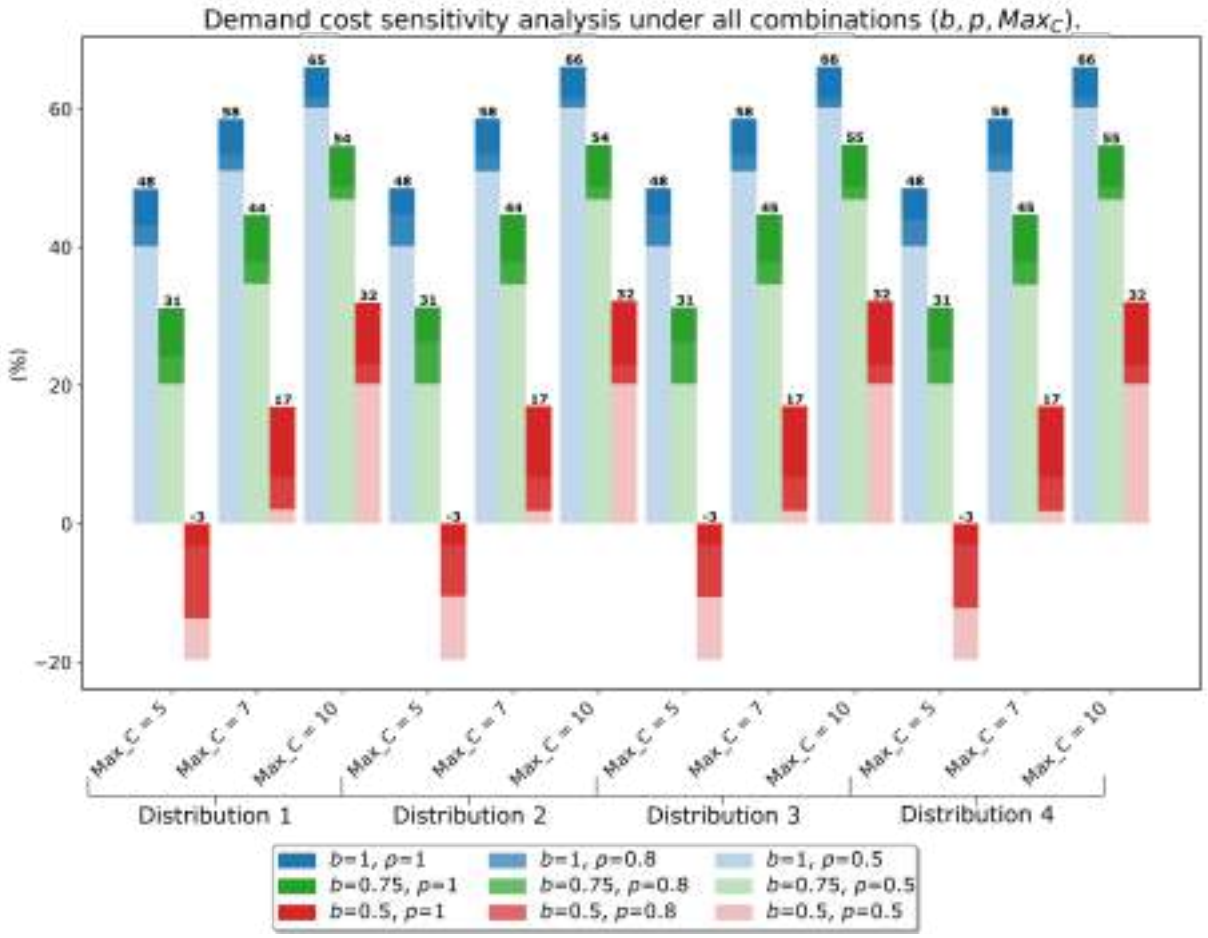

Figure 4.8: Demand Cost Sensitivity Analysis of the B3 instance for the four distributions.

The quality of the solutions obtained shows a slight variation due to the increased dimensionality of the lockers to be evaluated. Nevertheless, as in the previous cases, upon analyzing the fitness values, it is evident that the standard deviation is relatively low.

Table 4.8: Computational results of the real-world dataset under all combinations (p, Max_C).

Real data									
Max Cabins	Percentage								
	100%			80%			50%		
	#Lockers	Fitness		#Lockers	Fitness		#Lockers	Fitness	
	AVG	AVG	STD	AVG	AVG	STD	AVG	AVG	STD
5	64	715852	106.33	58	696948	77.14	37	641129	144.36
7	46	646137	179.85	42	637432	248.46	27	607486	342.62
10	32	599882	345.34	29	597145	414.54	19	585940	367.32

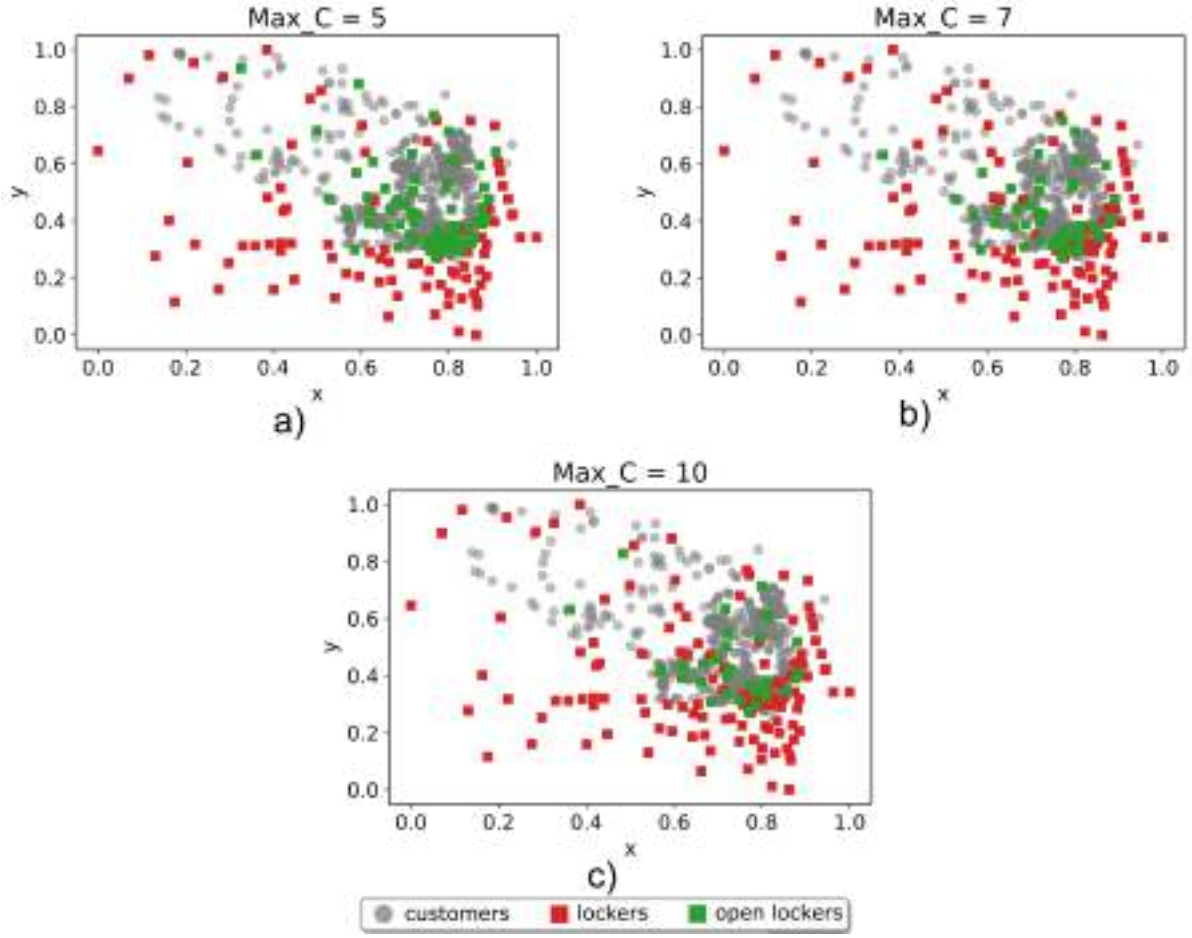

Figure 4.9: Geographical locations of the SPLs with the solutions obtained for the real-world dataset with $p = 1$. a) $Max_C = 5$. b) $Max_C = 7$. c) $Max_C = 10$.

Convergence Analysis for Real-World Data

Convergence curves in Figure 4.10 illustrate the efficiency and reliability of the algorithm when applied to the real data provided by the Dublin logistics company using $p = 0.8$ for 20 runs. The convergence curves in the three configurations $Max_C = [5, 7, 10]$ (Figure 4.10a, 4.10b, and 4.10c, respectively) indicate that the algorithm achieves convergence within 1,000 iterations out of the 6,000 iterations designated as the stopping criterion.

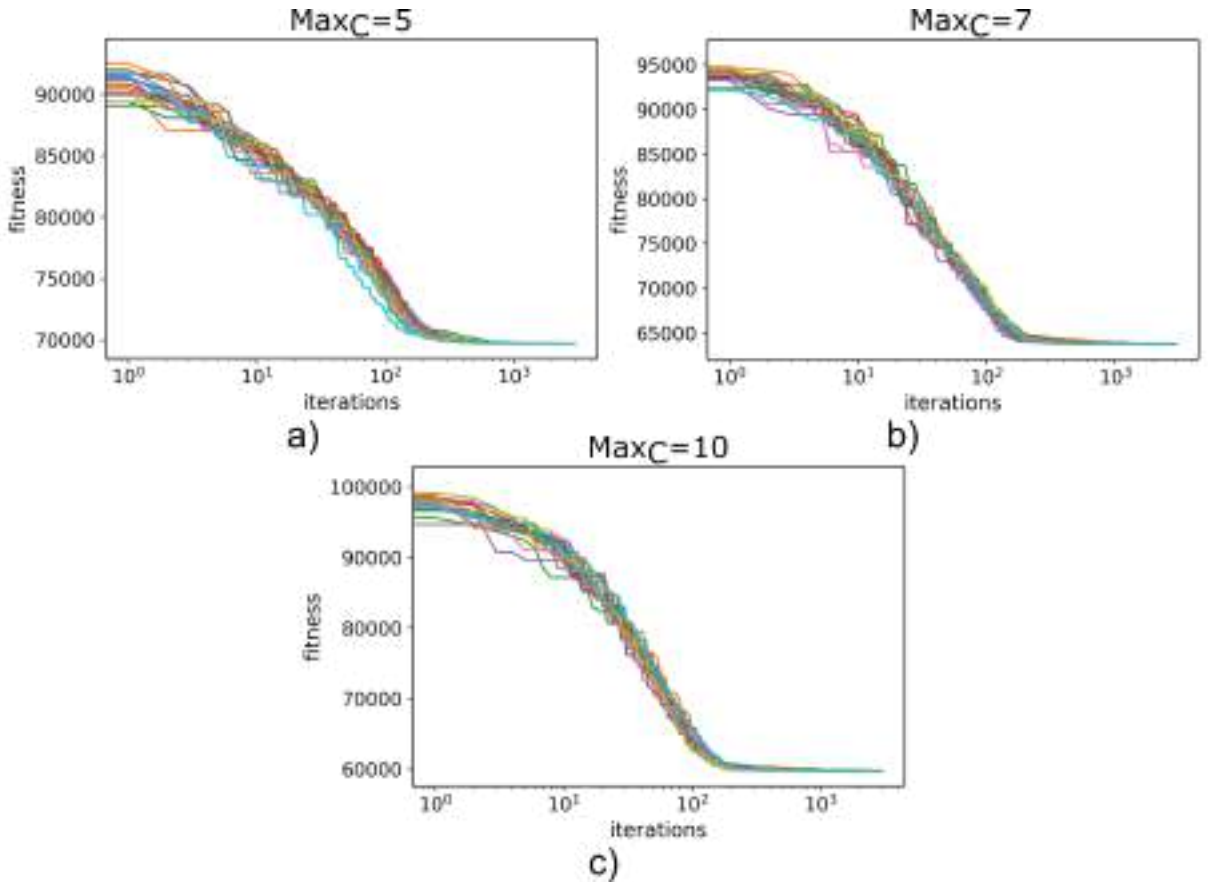

Figure 4.10: Convergence curve for the real-world dataset with $p = 0.8$ and a) $Max_C = 5$, b) $Max_C = 7$, c) $Max_C = 10$.

Cost Analysis for Real-World Data

The cost analysis is showcased in Table 4.9, displaying the outcomes derived from the application of the proposed model across all configurations of (p, Max_C). The table presents monthly revenues generated from demand, the average monthly costs linked to SPL locations, and the company's profit. The most profitable percentage is highlighted in bold, as is also seen in the results obtained from the synthetic data. In this case, the optimal configuration for profitability is (1, 10).

Table 4.9: Cost results for the real-world dataset under all combinations (p, Max_C).

Real data													
Max Cabins	Demand	Percentage											
		100%				80%				50%			
		Costs		Profit		Costs		Profit		Costs		Profit	
		AVG	STD	value	pct	AVG	STD	value	pct	AVG	STD	value	pct
5	55386	28740.0	0.0	26646.0	48.10	26100.0	0.0	18208.8	41.09	16650.0	0.0	11043.0	39.87
7	55386	23173.5	183.09	32212.5	58.16	21253.5	144.95	23055.3	52.03	13722.0	19.89	13971.0	50.44
10	55386	19114.5	98.71	36271.5	**65.48**	17518.5	180.11	26790.3	60.46	11355.0	126.74	16338.0	58.99

Sensitivity Analysis for Real-World Data

The sensitivity analysis of demand costs for the Dublin logistics company is shown in Figure 4.11. The results are obtained by evaluating various combinations of parameters encompassing b, p, and Max_C. Three cost scenarios of $b = [1, 0.75, 0.5]$ are presented in the figure, each distinguished by a distinct color (blue, red, and green, respectively). The figure highlights the impact of different demand cost values on the logistics company. It is worth noting that the results are similar regarding the respective results of the synthetic datasets.

Each bar is subdivided into three segments, denoting the percentage of customers served daily by the company. The darkest segment illustrates the outcomes of serving 100% of the customers, the subsequent lighter shade portrays the results of an 80% service rate, and the lightest segment represents the outcomes of serving only 50% of the customers.

As anticipated, the (1, 1, 10) configuration, mirroring the synthetic dataset, emerges as the most lucrative. These findings furnish valuable insights for a logistics company to evaluate how changes in demand and costs can affect their overall profitability.

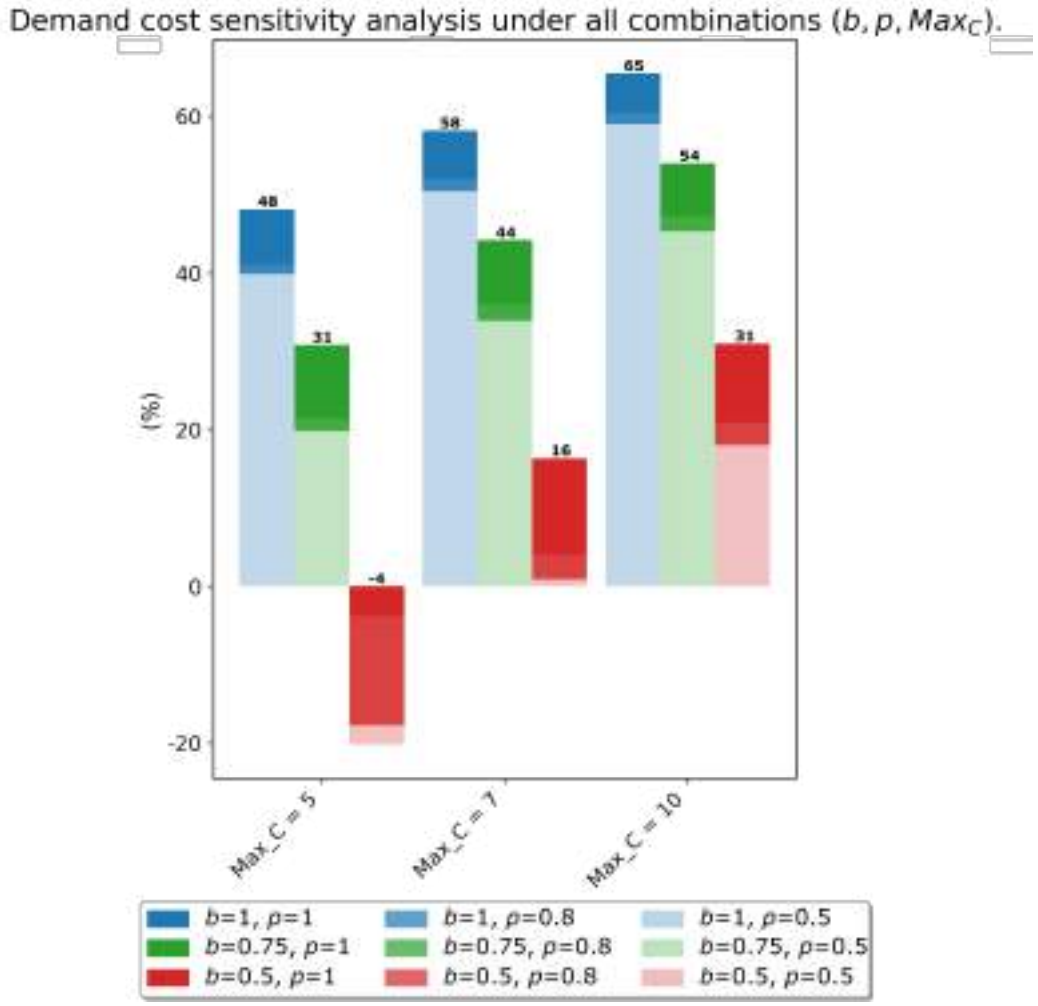

Figure 4.11: Demand Cost Sensitivity Analysis of the real-world dataset.

4.5 Conclusions

This work delves into the crucial challenges inherent in LML operations within urban areas. With the growing demand for delivery logistics and its influence on economic, social, and environmental sustainability, it has become essential to identify efficient and sustainable solutions. SPLs emerge as a potent and sustainable remedy for LML. Their implementation reduces traffic congestion, improves delivery efficiency, and minimizes CO_2 emissions while benefiting consumers and the community. A strategic integration of logistics solutions can contribute to a more efficient and sustainable logistics system in urban environments. The work, grounded in the presented methodology, contributes significantly to the practical implementation of such logistics solutions, offering the following key insights:

- **Extension of the Optimization Model Formulation:** We have formulated a more realistic LLPTL model extension called Constrained Locker Location Problem under the Threshold Luce Model (CLLPTLM). This model addresses the allocation of SPLs in LML operations, encompassing critical factors such as stochastic customer demand, dynamic collection periods, capacity constraints at SPL locations, and associated facility costs.

- **Utilization of an Adapted GA:** We have proposed an adapted GA to solve the locker allocation problem. This algorithm has proven its efficiency in finding optimal or near-optimal solutions in large and complex solution spaces. The adapted GA algorithm is designed to minimize the sum of lost demand and the total cost of the facilities, ensuring the selection of an optimal combination of lockers.

- **Validation on Synthetic and Real-World Datasets:** Validation of the model and approach extends to synthetic datasets with diverse sizes and characteristics, affirming its robustness and applicability in varied scenarios. Furthermore, successful application to real-world LML data underscores the model's practicality and capacity to address real-world challenges.

To summarize, this work provides a valuable tool for managing and planning LML operations. The proposed solution has a strong foundation and is suitable for real-world environments. This approach is scalable and adaptable to various conditions, making it a significant contribution in addressing LML challenges, leading towards a more efficient and sustainable logistics system.

5

A Robust Hyper-Heuristic Approach for Vehicle Segmentation

5.1 Introduction

5.1.1 Challenges in Last-Mile Operations

Given the rising number of vehicles, efficient traffic management in urban areas is crucial. Image-Based Vehicle Traffic Monitoring offers real-time traffic analysis tools to alleviate congestion, but integrating it with existing systems is challenging. Advanced methodologies leveraging image-based data are essential to enhance traffic management [134].

In this urban context, the challenges of Last-Mile Logistics (LML) are magnified by intricate city landscapes and the surge in delivery demands driven by e-commerce, as mentioned in Chapter 1. Traffic congestion aggravates delays and inflates operational costs. Under these circumstances, effective vehicle segmentation becomes critical, serving as a linchpin for boosting the efficiency of LML [135]. By optimizing delivery routes and timetables, vehicle segmentation to estimate road occupancy is fundamental in diminishing congestion's adverse effects and enhancing operational productivity, thereby supporting a more sustainable and efficient urban transport ecosystem [136].

However, current methodologies exhibit gaps in the precision and adaptability of vehicle segmentation, especially in adjusting to various environmental conditions and incorporating real-time data. Improving the accuracy and robustness of vehicle segmentation techniques is imperative to fully exploit the potential of image-based vehicle traffic monitoring to reduce urban congestion and improve the efficiency of LML [137].

5.1.2 Objectives and Contributions

This chapter presents a novel algorithm, Hyper-heuristic Genetic Algorithm based on Thompson Sampling with Diversity (HHGATSD), tailored to address the vehicle segmentation challenges in the LML context. The method proposed incorporates sophisticated optimization techniques to dynamically segment vehicles in traffic camera video frames, enabling accurate and adaptive road occupancy estimation.

The main objective of this research is to devise and validate a robust Hyper-heuristic (HH) algorithm that improves vehicle segmentation in urban delivery environments, taking into account the variability of environmental conditions and the requirement for real-time traffic management, thus improving logistics coordination and efficiency. This contribution has significant value to the logistics field, offering a powerful tool for LML operations.

Section 5.2 details the methodology encompassing the components and operational mechanics of HHGATSD. Subsequently, Section 5.3 describes the experimental setup, demonstrating the algorithm's application to a representative set of segmentation problem instances and its comparative analysis against existing methods. The experimental results, discussed in Section 5.4, highlight the algorithm's performance and implications for LML optimization. Finally, Section 5.5 summarizes the findings.

5.2 Methodology

This section presents a comprehensive methodology for multilevel image segmentation, focusing on the Minimum Cross-Entropy Thresholding (MCET) technique. The MCET is implemented within the proposed HHGATSD, detailed in Section 5.2.2. This iterative process of minimizing the statistical cross-entropy criterion refines threshold values, enhancing image segmentation quality, promoting homogeneity, and reducing uncertainty.

5.2.1 Multilevel Image Segmentation

Multilevel image segmentation, a crucial step in various image processing applications, focuses on categorizing pixels with similar attributes, such as intensity, to identify objects within the background. This process transforms the image representation into a more analytically manageable format for subsequent processing stages [138].

Selecting appropriate thresholds poses a challenge in multilevel image segmentation, and various manual and automated criteria are employed to address this. The proposal of this chapter tackles this challenge by utilizing cross-entropy minimization as a segmentation criterion [139].

The thresholding technique is a commonly used and straightforward method in image processing. It involves dividing the image histogram into different regions based on specific threshold values. The resulting segmented image called $\boldsymbol{I_{th}}$, is generated using these threshold values according to the rules specified in Equation 5.1 [140].

$$I_{th}(x,y) = \begin{cases} th_1, & \text{if } I_{Gr}(x,y) \leq th_1 \\ th_i, & \text{if } th_{i-1} < I_{Gr}(x,y) < th_i, \\ th_{nt}, & \text{if } I_{Gr}(x,y) > th_{nt} \end{cases} \tag{5.1}$$

where, $\boldsymbol{I_{Gr}}$ denotes the original grayscale image, nt represents the total number of thresholds, and th_i ($\forall\ i = 2, 3, \ldots, nt-1$) are optimal threshold values used for image segmentation.

Addressing the challenge of determining optimal thresholds is accomplished by formulating the problem as the minimization of the statistical cross-entropy criterion. This criterion serves as the objective function within an optimization algorithm, guiding the search for optimal threshold values. The cross-entropy criterion quantifies the homogeneity of histogram information between the original image and its segmentation.

Minimum Cross-Entropy Thresholding

In 1968, Kullback et al. introduced cross-entropy as a metric to determine the difference between two probability distributions. It involves finding the optimal threshold value for given probability distributions $\boldsymbol{P} = p_1, p_2, \ldots, p_n$ and $\boldsymbol{Q} = q_1, q_2, \ldots, q_n$, by minimizing a theoretical data distance [141]. The cross-entropy formula is expressed in Equation 5.2.

$$CE(\boldsymbol{P}, \boldsymbol{Q}) = \sum_{i=1}^{n} p_i \log \frac{p_i}{q_i} \tag{5.2}$$

The MCET technique determines the optimal threshold by minimizing the statistical criterion of cross-entropy between the input grayscale image and the histogram $h(i)$, where $i = 1, 2, \ldots, L$, and L is the number of gray intensities present in the image. The image, using a single threshold (th) for binary thresholding outlined in Equation 5.3, segments image $\boldsymbol{I_{Gr}}$ into an $\boldsymbol{I_{th}}$ image with two areas: foreground and background [142].

$$I_{th}(x,y) = \begin{cases} \mu(1, th), & \text{if} \quad I_{Gr}(x,y) < th \\ \mu(th, L+1), & \text{if} \quad I_{Gr}(x,y) \geq th \end{cases} \tag{5.3}$$

where μ is defined in Equation 5.4.

$$\mu(a,b) = \sum_{i=a}^{b-1} ih(i) \Bigg/ \sum_{i=a}^{b-1} h(i) \tag{5.4}$$

The MCET is calculated by rewriting Equation 5.3 to obtain the entropy value by evaluating the objective function presented in Equation 5.5. This function, denoted as $f_{MCET}(th)$, combines information from the histogram, image, and optimal threshold th to measure the divergence between the original and the segmented image.

$$\begin{aligned} f_{MCET}(th) = \Bigg(& \sum_{i=1}^{th-1} ih(i) \log \left(\frac{i}{\mu(1, th)} \right) \\ & + \sum_{i=th}^{L} ih(i) \log \left(\frac{i}{\mu(th, L+1)} \right) \Bigg) \end{aligned} \tag{5.5}$$

The bilevel segmentation equation mentioned earlier can be extended to a multilevel approach using a vector called $\boldsymbol{th} = [th_1, th_2 \ldots, th_{nt}]$. This vector contains nt threshold

values. However, using more threshold values increases the computational cost. Yin [143] proposed a faster recursive programming technique to obtain the optimal threshold for digital image segmentation. Therefore, the formula presented as Equation 5.5 can be expressed as Equation 5.6.

$$f_{MCET}(th) = \Bigg(\sum_{i=1}^{L} ih(i)log(i) - \sum_{i=1}^{th-1} ih(i)log(\mu(1, th)) - \sum_{i=th}^{L} ih(i)log(\mu(th, L+1)) \Bigg) \tag{5.6}$$

The bilevel approach in Equation 5.6 is extended to make the multilevel approach using the vector $\boldsymbol{th}$, which contains nt threshold values, shown in Equation 5.7.

$$f_{MCET}(\boldsymbol{th}) = \sum_{i=1}^{L} ih(i)log(i) - \sum_{i=1}^{nt} H_i \tag{5.7}$$

where nt is the total number of thresholds and H_i is determined as (5.8).

$$\begin{aligned} H_1 &= \sum_{i=1}^{th_1-1} ih(i)log(\mu(1, th_1)) \\ H_k &= \sum_{i=th_{k-1}}^{th_k-1} ih(i)log(\mu(th_{k-1}, th_k)), \;\; 1 < k < nt \\ H_{nt} &= \sum_{i=th_{nt}}^{L} ih(i)log(\mu(th_{nt}, L+1)) \end{aligned} \tag{5.8}$$

In addressing the challenge of multilevel image segmentation, the paper employs the MCET criterion as a pivotal segmentation tool. This choice is based on a detailed mathematical model of the problem, where the task of pixel classification is transformed into a well-defined optimization problem. The formulation is designed to capture the intricacies and complexities of multilevel image segmentation.

The mathematical foundation provided by MCET facilitates the translation of the problem into an optimization objective function, seeking to minimize the statistical cross-entropy criterion. This criterion, as detailed before, operates as a robust measure of the divergence between the original grayscale image and its segmented counterpart. The approach models the mathematical complexities inherent in multilevel image segmentation to identify optimal threshold values that not only meet the stringent requirements of the task but also contribute to solving practical engineering problems in image processing.

5.2.2 Hyper-heuristic Genetic Algorithm based on Thompson Sampling with Diversity

This section introduces the proposed novel approach called the HHGATSD. The algorithm is based on the HH approach using Thompson Sampling, which dynamically selects crossover and mutation operators. Crucially, HHGATSD stands out as a unique algorithm by seamlessly integrating this operator selection strategy into a comprehensive GA framework. This integration significantly enhances its efficacy in solving optimization problems.

HHGATSD incorporates two key stages, strategically designed to balance the need for exploring and exploiting solutions. The diversity stage uses the Normalized True Diversity (D_{TD}) metric to measure population diversity dynamically throughout the evolutionary process. The cloning stage, on the other hand, generates clones of the worst-performing individuals and is guided by a finely tuned α parameter that enhances exploration. These innovative components collectively make the algorithm robust, scalable, and efficient.

The flowchart depicted in Figure 5.1 visually illustrates the structural resemblances shared by the HHGATSD and the conventional GA outlined in [144]. However, it includes the two additional stages mentioned before aimed at enhancing overall performance and the capacity to discover high-quality solutions. The figure also highlights specific blocks within the flowchart, symbolized by a rectangle with dotted lines, which are integral components influenced by the Multi-Armed Bandit (MAB) theory.

Steps of the Algorithm

1. **Initialization:** The process starts by setting the parameters and randomly generating particles uniformly for the initial population of candidate solutions. The diversity of the particle distribution is determined and quantified using the Normalization with Maximum Diversity so Far (NMDF) method [145]. Following initialization, each individual's fitness is evaluated based on the objective function.

2. **Fitness Evaluation:** Following the generation of the initial population, each candidate solution undergoes evaluation using the objective function. The best solution is identified based on the smallest fitness value within the population, marking the beginning of the iterative process.

3. **Parent Selection:** This stage is responsible for choosing individuals from the current population to act as parents for the next generation [146]. The Roulette Wheel Selection strategy, widely employed in the GAs, assigns a selection probability, denoted as ps, to each individual in the population based on its fitness function value. This approach follows a proportional selection strategy akin to a roulette wheel mechanism [147]. The selection probability of an individual for the next generation is determined by the ratio of its fitness value to the total fitness values across the entire population. For a population $P = a_1, a_2, \ldots, a_N$ with each element ai having the fitness value $f(a_i)$, the probability $ps(a_i)$ for selecting a_i is computed based on Equation 5.9.

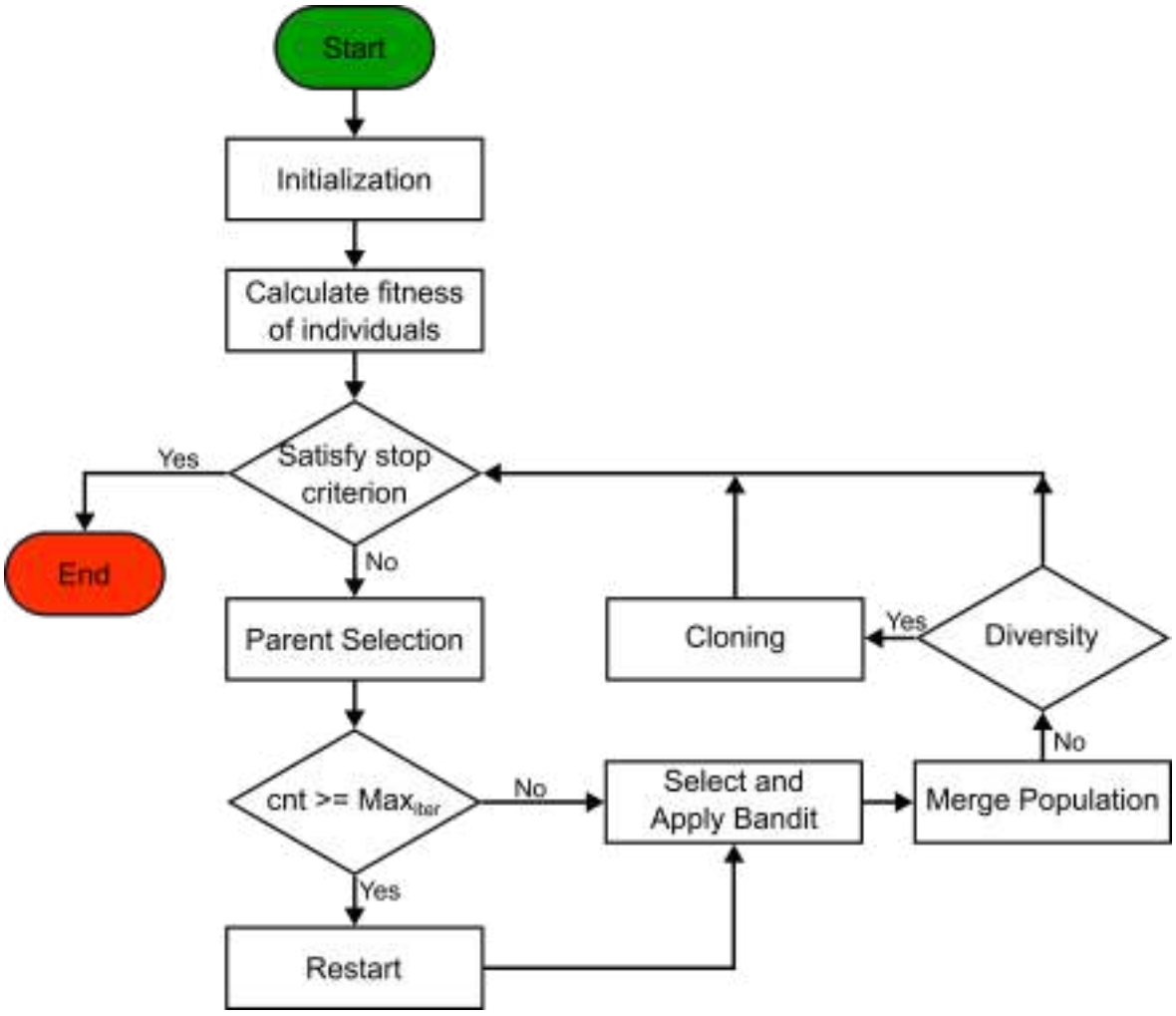

Figure 5.1: Flowchart of the proposed HHGATSD.

$$P(a_i) = \frac{f(a_i)}{\sum_{j=1}^{N} f(a_j)}, \quad \text{where } j = 1, 2, \ldots, N \tag{5.9}$$

However, it's important to note that this strategy does not guarantee that the best individuals will be selected.

4. **Operator Selection:** It is the first additional stage of the HH. Instead of using fixed crossover and mutation operators, the operator selection is treated as a MAB problem [148]. To tackle this problem, Thompson sampling is utilized, which outperforms other algorithms [28]. It dynamically selects the most promising operators by performing stochastic sampling based on the estimated reward of each operator. The algorithm performs stochastic sampling based on the estimated reward of each operator, effectively choosing the optimal operator with an appropriate probability for the highest cumulative reward over Max_{Iter} iterations. The outcome of this process is the action that contains the combination of heuristics for the crossover

and mutation to be applied. This parent selection and operator selection process is repeated N times. The pseudocode of this process is presented in Algorithm 8.

Algorithm 8 Pseudocode of TS

Inputs: $\boldsymbol{R}$, $\boldsymbol{P}$, cnt
if $(cnt \leq Max_{Iter})$ **then**
  Reinitialize $\boldsymbol{R}$, $\boldsymbol{P}$ and cnt
else
  $cnt \leftarrow cnt + 1$
end if
for (i $\leftarrow$ 1 to $num_{actions}$) **do**
  $\theta_i \leftarrow Beta(R_i + 1, P_i + 1)$ sample from Beta distribution
end for
$acion \leftarrow$ Select the action with the $argmax(\boldsymbol{\theta})$
Return $acion$

5. **Merge Population:** After applying the operators to the current population, a set of N new individuals is generated from these operations. The fitness of the new solutions is evaluated using the objective function. The generational replacement and sorting strategy are then employed to select the new population with the smallest values [149].

6. **Diversity:** During this stage, the D_{TD} calculation takes place, serving as a metric to gauge the diversity within the population. This metric represents the average standard deviation of the position of each individual, and its computation is based on Equation 5.10, as detailed in the work of Oliva et al. [150]. Throughout each iteration, the Diversity stage assesses the D_{TD} value and verifies whether it falls below 0.2. Simultaneously, it checks whether the number of accesses to the objective function is less than half of the maximum permissible accesses (Max_{Acc}). Upon satisfying these conditions, the Cloning stage is executed.

$$D_{TD} = \frac{\frac{1}{N}\sqrt{\sum_{k=1}^{N}(\overline{x_k^2} - (\overline{x_k})^2)}}{NMDF} \tag{5.10}$$

$$\overline{x_k^2} = \frac{1}{D}\sum_{i=1}^{D} x_{i,k}^2 \tag{5.11}$$

where $i = 1, 2, \ldots, D$ and $k = 1, 2, \ldots, N$, and D is the dimension of the problem and N is the number of particles in the population.

7. **Cloning:** During this phase, as described in Equation 5.12, the goal is to create copies of the $0.3N$ individuals with the lowest fitness in the population. Subsequently, these clones undergo evaluation, and the most promising ones replace their

corresponding original individuals in the population. This process helps to enhance diversity and exploration in the search space of the proposed HH.

$$x_{i,k} = x_{i,k} + \xi \tag{5.12}$$

where ξ represents a randomly generated number falling within the range of -α to α, with α as a positive parameter controlling the search domain. For this approach, the value assigned to α is 10.

8. **Stop Criterion:** The algorithm evaluates if it has reached the maximum allowed objective function accesses (Max_{Acc}). If the stop condition is not met, the algorithm returns to the Parent Selection step (Step 3) to repeat the evolutionary cycle. This stop criterion is crucial for managing computational resources and preventing the algorithm from running indefinitely, ensuring the termination of the cycle within a reasonable time frame.

The set of operators that form the pool of LLHs utilized by the HHGATSD algorithm, to be applied to the parents selected in Step 4, is detailed below. This strategy encompasses four distinct crossover operators:

- UNDX - Unimodal Normal Distribution Crossover [151]
- PCX - Parent Centric Recombination [152]
- BLX - Blend Crossover [153]
- Single Point Crossover [154]

Additionally, four mutation operators are taken into consideration:

- Michalewicz's Mutation [155]
- DE Mutation [156]
- Random Mutation [157]
- OBL - Opposition-Based Learning [158]

Two internal parameters significantly affect the performance of the HHGATSD algorithm. The first parameter, called $Iter$, is used in Step 4 and sets the maximum cumulative reward for each iteration. Its main function is to reset the reward ($\boldsymbol{R}$) and penalty ($\boldsymbol{P}$) vectors, which are essential components of the Thompson Sampling algorithm. By resetting the algorithm, it adapts to the changing dynamics of the environment and ensures the effective exploration of the search space. Therefore, the variable $Iter$ plays a crucial role in the algorithm. The second parameter, α, is used in Step 5 and acts as a positive control parameter during the cloning phase. This parameter determines the magnitude of random adjustments applied to solutions during the cloning phase.

5.3 Experimental Framework

5.3.1 Datasets

For the evaluation of the HHGATSD's effectiveness, three distinct datasets are utilized:

1. **IEEE CEC2017 Benchmark:** This dataset is commonly used as a reference point to evaluate the effectiveness of optimization algorithms. It comprises 30 carefully selected functions, specifically formulated to address optimization problems with real and constrained parameters [159]. Renowned for its intricacy, particularly in 30 and 50 dimensions, this benchmark stands as a rigorous testing ground for evaluating optimization algorithms. The dataset's inclusion of functions tailored to pose challenges in real-parameter optimization underscores its significance in assessing algorithmic performance under diverse and demanding conditions.

2. **Berkeley Segmentation Dataset (BSDS500):** Comprising a set of 500 images, this dataset is extensively employed as a benchmark for assessing contour detection algorithms [160]. Its design is specifically tailored for the evaluation of natural edge detection and surpasses the mere identification of object contours. The dataset includes a comprehensive assessment of object interior boundaries and background boundaries. This approach provides a holistic perspective on the algorithm's performance, aiming to evaluate its efficacy in capturing diverse aspects of natural scenes, rather than solely focusing on object outlines. Consequently, the dataset facilitates a more nuanced and rigorous evaluation of the algorithm's overall performance.

3. **Traffic Camera Video Frames:** This dataset comprises 612 frames captured from a stationary road traffic surveillance camera, providing a real-world scenario for the comprehensive assessment of algorithms. The dataset offers a diverse and dynamic environment, allowing for the evaluation of algorithmic performance under real-world conditions. The frames serve as a practical and challenging benchmark, simulating the complexities of traffic scenarios. This dataset contributes to a robust evaluation, enabling the analysis of the algorithm's adaptability and effectiveness in addressing the challenges posed by actual road traffic scenarios.

The first evaluation phase involves a comprehensive verification and comparison of the effectiveness of the proposed HHGATSD algorithm with other commonly used MH algorithms on the challenging IEEE CEC2017 benchmark for 30 and 50 dimensions. Table 5.1 presents the functions, their features, and optimal or minimum values. The set contains 29 benchmark functions, excluding f_2, due to the unstable behavior of it [161]. It includes four sets of functions: unimodal functions (f_1), multimodal functions ($f_3 - f_9$), hybrid functions ($f_{10} - f_{19}$), and composition functions ($f_{20} - f_{30}$).

Table 5.1: Summary of the CEC2017 Benchmark Functions

Type	No.	Functions	$F_i^* = F_i(x^*)$
Unimodal	1	Shifted and Rotated Bent Cigar Function	100
Multimodal	3	Shifted and Rotated Rosenbrock's Function	300
	4	Shifted and Rotated Rastrigin's Function	400
	5	Shifted and Rotated Expanded Scaffer's F6 Function	500
	6	Shifted and Rotated Lunacek Bi_Rastrigin Function	600
	7	Shifted and Rotated Non-Continuous Rastrigin's Function	700
	8	Shifted and Rotated Levy Function	800
	9	Shifted and Rotated Schwefel's Function	900
Hybrid	10	Hybrid Function 1 (N=3)	1000
	11	Hybrid Function 2 (N=3)	1100
	12	Hybrid Function 3 (N=3)	1200
	13	Hybrid Function 4 (N=4)	1300
	14	Hybrid Function 5 (N=4)	1400
	15	Hybrid Function 6 (N=4)	1500
	16	Hybrid Function 7 (N=5)	1600
	17	Hybrid Function 8 (N=5)	1700
	18	Hybrid Function 9 (N=5)	1800
	19	Hybrid Function 10 (N=6)	1900
Composition	20	Composition Function 1 (N=3)	2000
	21	Composition Function 2 (N=3)	2100
	22	Composition Function 3 (N=4)	2200
	23	Composition Function 4 (N=4)	2300
	24	Composition Function 5 (N=5)	2400
	25	Composition Function 6 (N=5)	2500
	26	Composition Function 7 (N=6)	2600
	27	Composition Function 8 (N=6)	2700
	28	Composition Function 9 (N=3)	2800
	29	Composition Function 10 (N=3)	2900
	30	Composition Function 11 (N=3)	3000
Search range: $[-100, 100]^D$			

During the second evaluation phase, the HHGATSD algorithm is applied to the image segmentation problem using two datasets. The initial dataset, frequently referenced in image processing literature, comprises 500 natural images showcasing varying intensity complexities. From this benchmark, ten random images are selected to create the second evaluation set to asses the proposed HH. Figure 5.2 displays the benchmark images used in this study, accompanied by their respective histograms. Accessible through the provided link[1], these images play a pivotal role in our evaluation. They represent a diverse array of real-world scenarios, enabling a thorough examination of the proposed method's robustness and adaptability across different levels of image complexity.

[1] www.eecs.berkeley.edu/Research/Projects/CS/vision/grouping/resources.html

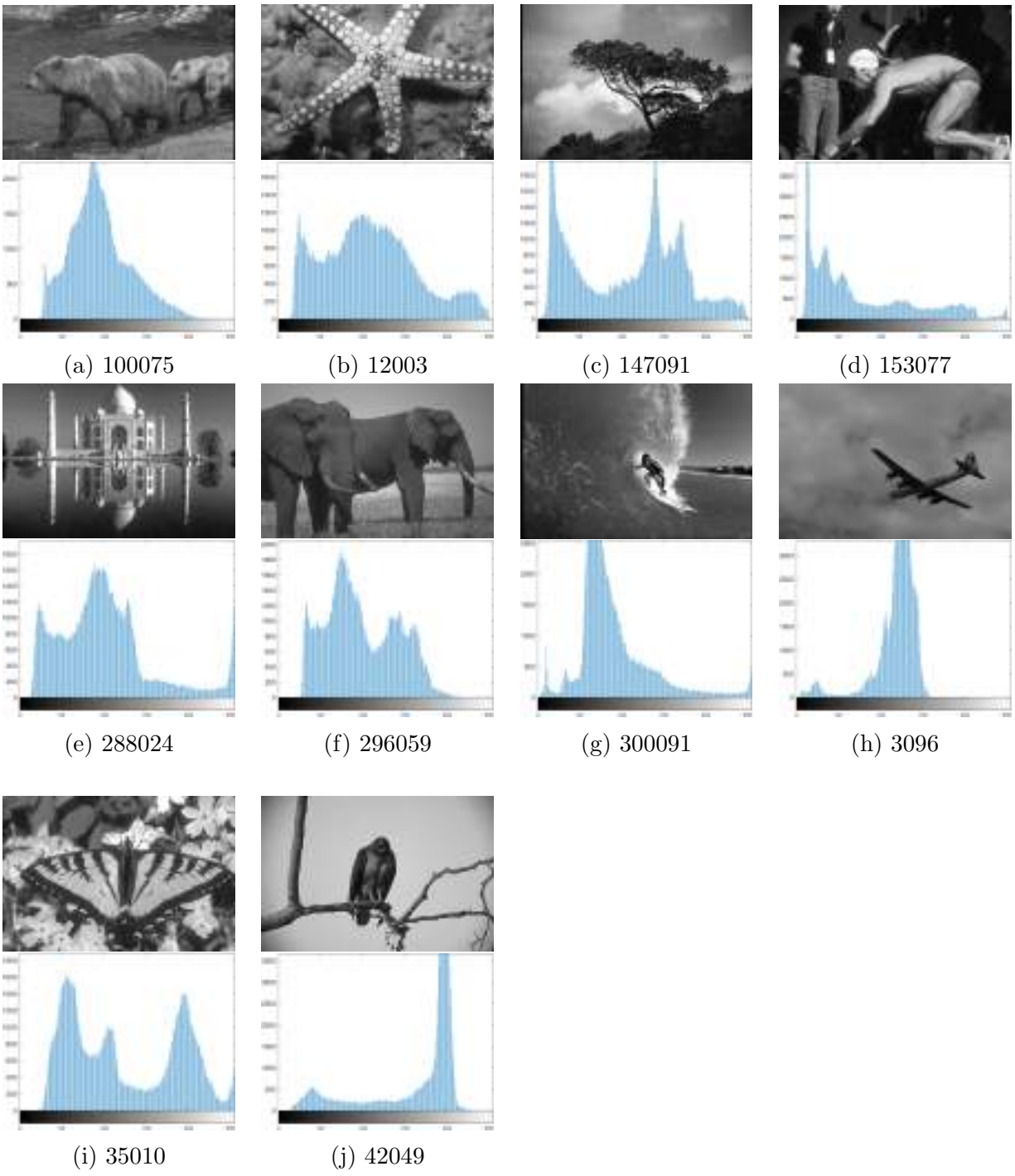

(a) 100075 (b) 12003 (c) 147091 (d) 153077

(e) 288024 (f) 296059 (g) 300091 (h) 3096

(i) 35010 (j) 42049

Figure 5.2: Set of benchmark images and their corresponding histograms depicting the distribution of pixel intensities. The histograms offer insights into the frequency of intensity values in each image, providing additional information about the image features.

The second dataset employed for the image segmentation problem is sourced from a stationary road traffic surveillance camera, accessible at the following link[2]. Figure 5.3 showcases eight randomly chosen frames out of a total of 612, serving as sample images to constitute the third evaluation set for assessing the HHGATSD algorithm.

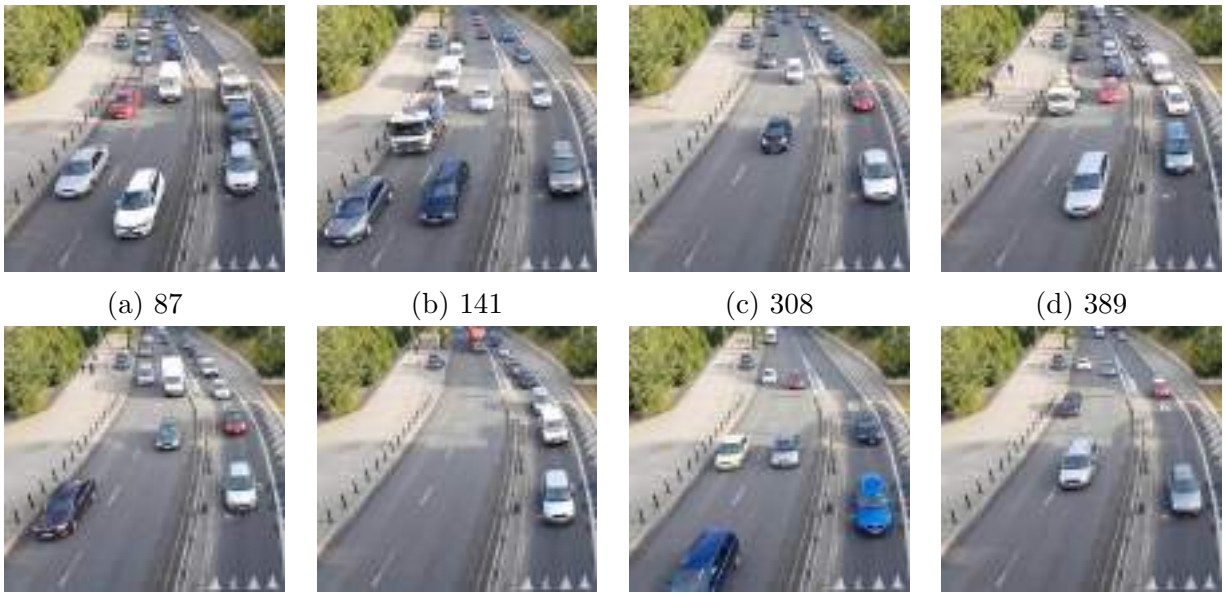

(a) 87 (b) 141 (c) 308 (d) 389

(e) 416 (f) 441 (g) 507 (h) 534

Figure 5.3: Examples of frames captured from the road traffic surveillance camera.

5.3.2 Experimental Setup

To conduct a comprehensive performance comparison of the HHGATSD algorithm for the first phase of evaluation on the IEEE CEC2017 Benchmark (Figure 5.1) and for the second phase on the BSDS500 (Figure 5.2), a comparative analysis is performed, pitting the HHGATSD against well-established MH optimizers. The lineup included GA, Particle Swarm Optimization (PSO) [162], Differential Evolution (DE) [156], Bernstain-Search Differential Evolution Algorithm (BSD) [163], Grey Wolf Optimizer (GWO) [164], Harris Hawks Optimization (HHO) [165], Self-adaptive Differential Evolution (JADE) [166] and Biogeography-based Learning Particle Swarm Optimization (BLPSO) [167]. The internal parameters of each MH optimizer underwent meticulous configuration based on its original references to ensure optimal performance.

In each iteration of the experiment, 30 independent executions are carried out, each initialized with random seeds, ensuring a comprehensive assessment of the robustness, stability, and consistency of the proposed HHGATSD algorithm. For the experiments on the IEEE CEC2017 benchmark, uniform termination criteria are implemented for all algorithms, covering both 30 and 50 dimensions (D). The termination conditions are specifically set at 50,000 and 80,000 function accesses for algorithms operating in 30D and 50D, respectively.

[2]www.kaggle.com/foyecey/traffic-road

For the experiments conducted on the BSDS500 dataset, the challenge of multilevel thresholding is addressed by the application of diverse *nt* threshold values (2, 4, 6, 8, and 10) [168]. The MCET approach serves as the designated objective function, with a defined maximum of 100 iterations as the stop criterion for each experiment. This criterion guides the exploration for optimal thresholds, ensuring the effective classification of pixels within the resulting segmented images.

Maintaining uniformity across all test algorithms, the total number of search agents in the population, denoted as N, is consistently set at 50. It is pertinent to note that, for the proposed HH, internal parameters $Iter$ and α are specifically configured to 200 and 5, respectively.

The comparison aims to evaluate and showcase the efficacy of the HHGATSD algorithm in terms of solution quality and convergence speed. The research utilizes performance metrics and non-parametric tests detailed in Sections 5.3.4 and 5.3.5, respectively. The experimental setup specifies the number of executions and termination criteria to ensure result reliability. All experiments are conducted on Matlab version 9.8, running on hardware featuring a 1.60GHz Intel Core i5 CPU with 16GB of RAM.

5.3.3 Methodology for Vehicle Segmentation

A methodology has been proposed to accurately identify and segment vehicles in images from traffic surveillance cameras. This methodology involves using a preprocessing step of multilevel segmentation, which is validated using the proposed HH. The flowchart presented in Figure 5.4 illustrates the output of each crucial step of the methodology.

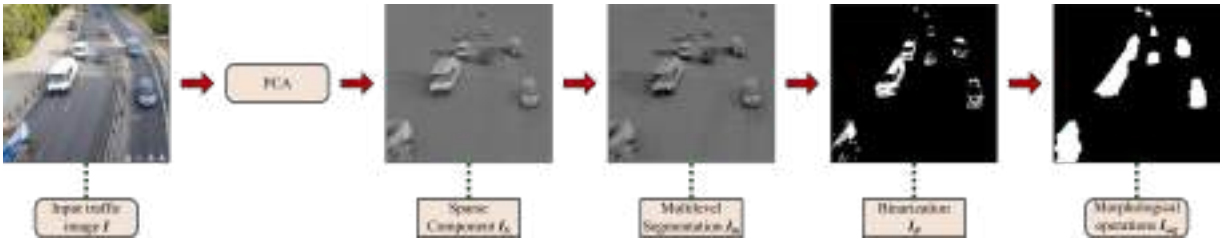

Figure 5.4: Flowchart of the proposed method for vehicle segmentation in a traffic surveillance camera.

The proposed methodology for vehicle segmentation consists of four key steps:

1. **Robust Principal Component Analysis (RPCA):** The process begins with the application of RPCA to a matrix comprising 612 frames extracted from the camera video. RPCA decomposes the information into a low-rank matrix (L), representing structural information, and a high-dimensional sparse matrix (S), capturing noise and unwanted variations. Matrix L corresponds to stationary or background elements, while matrix S identifies moving vehicles and dynamic objects, resulting in the matrix $\boldsymbol{I_S}$ for subsequent analysis. RPCA relies on two crucial parameters: λ and max_{iter}, where λ is normalized based on the size of the input matrix $\boldsymbol{X}$, and

the choice of $\lambda/10$ is set empirically for robustness against outliers. The parameter max_{iter}, indicating the maximum number of iterations, is set to 1000 to ensure convergence while controlling computational resources.

2. **Multilevel Segmentation:** In this step, a segmentation technique is employed on the image $\boldsymbol{I_S}$ using five threshold values (nt). The purpose of this segmentation technique is to partition $\boldsymbol{I_S}$ into distinct regions, each delineating specific attributes associated with vehicles captured in the images.

3. **Binarization:** This step consists of transforming the result $\boldsymbol{I_{th}}$ into a binary mask, $\boldsymbol{I_B}$, considering only the pixels with the highest threshold value (the fifth value obtained through the multilevel segmentation method). This step is essential for the subsequent analysis.

4. **Morphological Operations:** In the final step, morphological operations are applied to refine the binary mask $\boldsymbol{I_B}$. Erosion and morphological closure are employed to enhance region cohesion, utilizing a 2x2 pixel square-shaped structuring element for noise reduction and a 15-pixel radius disk for merging closely spaced regions. The resultant refined binary mask, $\boldsymbol{I_{seg}}$, serves as the groundwork for vehicle feature extraction and tracking, contributing to the accuracy of traffic analysis.

For a thorough understanding of the methodology, Algorithm 9 provides a comprehensive pseudocode, elucidating the sequential steps involved in the proposed approach.

Algorithm 9 Pseudocode of Vehicle Segmentation Methodology

Inputs: $\boldsymbol{X}$
$\lambda \leftarrow 1/\sqrt{\max(\text{size}(\boldsymbol{X}))}$
$max_{iter} \leftarrow 1000$
$nt \leftarrow 5$
$[\boldsymbol{L}, \boldsymbol{S}] \leftarrow \text{RPCA}(\boldsymbol{X}, \lambda/10, max_{iter})$
$i \leftarrow$ index of the image to segment
$\boldsymbol{I_S} \leftarrow \boldsymbol{S_i}$
$\boldsymbol{th} \leftarrow \text{MultilevelMethod}(\boldsymbol{I_S}, nt)$
$\boldsymbol{I_{th}} \leftarrow \text{MultilevelSegmentation}(\boldsymbol{I_S}, \boldsymbol{th})$
for (i $\leftarrow$ 1 to num_{col}) **do**
  for (j $\leftarrow$ 1 to num_{rows}) **do**
    if $Ith(i,j) \geq th_{nt}$ **then**
      $I_B(i,j) \leftarrow 1$
    else
      $I_B(j,k) \leftarrow 0$
    end if
  end for
end for
$\boldsymbol{I_{seg}} \leftarrow \text{MorphologicalOperations}(\boldsymbol{I_B})$
Return $\boldsymbol{I_{seg}}$

For this third analysis, the proposed methodology is assessed for vehicle segmentation in video frames captured by traffic cameras using a set of metrics detailed in Section 5.3.4. The objective is to compare the obtained image mask, resulting from the proposed methodology ($\boldsymbol{I_{seg}}$), with the manually segmented ground-truth reference mask. This comparison aims to verify the accurate classification of pixels representing vehicles in each of the 612 frames in the dataset. The metrics will provide insights into the effectiveness of the proposed methodology in correctly delineating vehicles in the images.

Additionally, another comparison is conducted using the HHGATSD algorithm along with the statistical criterion of MCET from Equation 5.7 as the objective function (MCET-HHGATSD). This approach is employed for multilevel segmentation of the images as part of the segmentation method in Step 2 of the algorithm pseudocode in Algorithm 9, specifically within the MultilevelMethod. This evaluation includes a comparison with the Otsu method [169], the classical K-means algorithm [170], and the Fuzzy IterAg algorithm [171]. The aim is to assess the effectiveness of the proposed methodology and the MCET-HHGATSD against other algorithms commonly utilized in the literature.

5.3.4 Metrics

The comprehensive experimental framework ensures a thorough evaluation of the proposed HHGATSD algorithm and proposed methodology under diverse conditions and datasets, providing valuable insights into its performance and applicability.

Since the algorithm described in this paper operates stochastically, statistical metrics are employed for the result analysis. Two key metrics are consistently utilized throughout all evaluations of the algorithm:

- **Average (AVG):** This metric is represented by Equation 5.13, which serves as a measure of central tendency in the optimizer, providing insights into the typical behavior of the algorithm.

$$AVG = \frac{1}{T_E} \sum_{i=1}^{T_E} s_i \tag{5.13}$$

  Here, s_i represents the individual solutions obtained from the optimizer, and T_E is the total number of evaluations. The symbol μ also denotes the AVG value.

- **Standard Deviation (STD):** STD in Equation 5.14 is used to evaluate the stability of the optimizer. According to Ghamisi et al., a higher STD value indicates that the algorithm is becoming more unstable [172].

$$STD = \sqrt{\sum_{i=1}^{T_E} \frac{s_i - \mu}{T_E}} \tag{5.14}$$

To evaluate the effectiveness of the proposed approach for achieving high-quality multilevel segmentation results on the BSD500, three metrics are used. These metrics act

as quantitative measures for different aspects of segmentation performance and provide valuable insights into the algorithm's ability to delineate and categorize various regions within the images. Below are the explanations of these metrics:

- **Peak Signal to Noise Ratio (PSNR):** PSNR in Equation 5.15a compares the segmented and original images using the root mean square error (RMSE) per pixel represented by Equation 5.15b. A higher PSNR value indicates a higher similarity between the images [173].

$$PSNR = 20\log_{10}\frac{255}{RMSE} \tag{5.15a}$$

$$RMSE = \sqrt{\frac{\sum_{i=1}^{ro}\sum_{j=1}^{co}[I_0^C(i,j) - I_{th}^C(i,j)]}{ro \times co}} \tag{5.15b}$$

- **Structural Similarity Index (SSIM):** SSIM measures the similarity between original and segmented images, identifying internal structures. Higher SSIM values denote better segmentation performances [174].

$$SSIM = \frac{(2\mu_{I_{Gr}}\mu_{I_{th}} + C_1)(2\sigma_{I_{Gr}I_{th}} + C_2)}{(\mu_{I_{Gr}}^2 + \mu_{I_{th}}^2 + C_1)(\sigma_{I_{Gr}}^2 + \sigma_{I_{th}}^2 + C_2)} \tag{5.16}$$

  where $\mu_{I_{Gr}}$ and $\mu_{I_{th}}$ are mean values of the original and segmented images, respectively. $\sigma_{I_{Gr}}$ and $\sigma_{I_{th}}$ represent standard deviations, and $\sigma_{I_{Gr}I_{th}}$ is the covariance of $\boldsymbol{I_{Gr}}$ and $\boldsymbol{I_{th}}$. C_1 and C_2 are stabilization variables, set as $C_1 = C_2 = 0.065$.

- **Feature Similarity Index (FSIM):** FSIM measures the similarity between images in terms of internal features such as edges and corners, with Equation 5.17 [175]. A higher FSIM value indicates better segmentation.

$$FSIM = \frac{\sum_{w\epsilon\Omega} S_L(w)PC_m(w)}{\sum_{w\epsilon\Omega} PC_m(w)} \tag{5.17}$$

  where Ω represents the entire spatial domain of the image and S_L denotes the similarity in components as shown in Equation 5.19. Additionally, PC in Equation 5.18 corresponds to the phase congruence, a dimensionless measure highlighting the importance of local structural elements within the image.

$$PC = \frac{E(\omega)}{(\epsilon + \sum_k A_k(\omega))} \tag{5.18}$$

  $A_k(\omega)$ is the local amplitude on scale n and $E(\omega)$ is the magnitude of the response vector in ω on k. ϵ is a small positive number and $PC_m = max(PC_1(\omega), PC_1(\omega))$.

$$\begin{aligned} \boldsymbol{S_L}(\omega) &= \boldsymbol{S_{PC}}(\omega)\boldsymbol{S_G}(\omega) \\ \boldsymbol{S_{PC}}(\omega) &= \frac{2PC_1(\omega)PC_2(\omega) + T_1}{PC_1^2(\omega) + PC_2^2(\omega) + T_1} \\ \boldsymbol{S_G}(\omega) &= \frac{2G_1(\omega)G_2(\omega) + T_2}{G_1^2(\omega) + G_2^2(\omega) + T_2} \end{aligned} \tag{5.19}$$

Here, T_1 and T_2 are constants and the values chosen are $T_1 = 0.85$ and $T_2 = 160$. From Equation 5.19, G is the gradient magnitude of an image defined by Equation 5.20.

$$G = \sqrt{G_x^2 + G_y^2} \tag{5.20}$$

To evaluate the effectiveness of the proposed methodology to segment vehicles in traffic camera video frames, five metrics are used. These metrics serve to quantify the accuracy and concordance between the segmentation methodology's output mask ($\boldsymbol{I_{seg}}$) and the ground-truth reference mask. These metrics hold particular significance in scenarios where precise identification of the pixels of interest is paramount, as in the case of vehicle segmentation. The following section elaborates on each of these metrics:

- **Dice Coefficient (DSC):** DSC, or F1-score, quantifies the overlap between predicted and ground truth segmentation masks, as expressed in Equation 5.21 [176]. A DSC value of 1 indicates perfect overlap.

$$DSC = \frac{2|A \cap B|}{|A| + |B|} \tag{5.21}$$

- **Jaccard Index (IoU):** IoU measures the similarity between predicted and ground truth masks [177]. This metric is obtained by Equation 5.22, and a higher IoU value means better alignment.

$$IoU = \frac{|A \cap B|}{|A \cup B|} \tag{5.22}$$

- **Precision (P):** Precision evaluates the accuracy of the positive predictions in the generated mask [178]. A higher precision value indicates a more accurate identification of positive pixels, as shown in Equation 5.23.

$$P = \frac{TP}{TP + FP} \tag{5.23}$$

- **Recall (R):** R, or sensitivity, measures the algorithm's ability to identify all positive instances in the mask [179]. The metric R is obtained using Equation 5.24.

$$R = \frac{TP}{TP + FN} \tag{5.24}$$

- **Accuracy (ACC):** ACC provides an overall measure of correctness and is not specific to the positive class, as depicted by Equation 5.25 [179].

$$ACC = \frac{TP + TN}{TP + TN + FP + FN} \tag{5.25}$$

5.3.5 Non-parametric Test

Non-parametric statistical tests are necessary to validate numerical results due to the inherent characteristics of MH algorithms. These tests become particularly relevant when the data fails to meet the assumptions of normality and lacks reliance on specific probability distributions. Hence, they serve as a suitable means to assess the efficacy of the proposed HH and establish its significance in comparison to other algorithms [120].

In this work, the Friedman test is applied to assess whether significant differences exist in the performance of various algorithms across benchmark functions. To refine the precision of the analysis, the implementation of Holm's p-correction method is emphasized [122]. This method assumes a crucial role in controlling the family error rate, especially during multiple pairwise comparisons. Through this, it ensures that the results maintain resilience against random chance influences, thereby establishing a more robust foundation for drawing meaningful conclusions.

The purpose of incorporating these robust statistical techniques into the evaluation is to provide a comprehensive and reliable assessment of the effectiveness of the HHGATSD algorithm in comparison to other methods. This approach allows for the confident identification of algorithms that demonstrate superior performance for both the IEEE CEC2017 Benchmark and the BSDS500.

5.4 Results and Discussion

This section presents the results of three experimental trials that aimed to comprehensively analyze the performance of the HHGATSD algorithm in different scenarios. The main objective is to assess the algorithm's effectiveness in addressing complex high-dimensional optimization problems and to evaluate its adaptability and robustness for real-world challenges, such as multilevel image segmentation. Lastly, the evaluation extends to the methodology in tandem with the MCET-HHGATSD multilevel segmentation approach.

5.4.1 Experiments with IEEE CEC2017 Benchmark

Tables 5.2 and 5.3 showcase the results of experiments conducted on the IEEE CEC2017 benchmark functions in 30 and 50 dimensions, respectively. Each row corresponds to a specific benchmark function, and each column represents an optimization algorithm used in the comparison.

The tables include two key statistics for each algorithm in each benchmark function: AVG and STD of the fitness. The algorithm achieving the best AVG result with the lowest fitness is denoted in bold, and results with the lowest STD values are also highlighted in bold. Additionally, the 'W/T/L' row at the bottom quantifies the number of wins (W), ties (T), and losses (L) for each algorithm in comparison to others across all benchmark functions.

In the realm of 30-dimensional optimization problems, the HHGATSD consistently outperforms other algorithms, as evidenced by lower AVG fitness values and significantly reduced dispersion (Table 5.2). The row denoted as 'W/T/L' underscores HHGATSD's prowess with 18 wins, 0 ties, and 11 losses in average fitness. However, in a comparison

based on the STD metric, it obtained 8 wins, 0 ties, and 21 losses, slightly below the BSDE algorithm.

For 50-dimensional problems, the HHGATSD exhibits enhanced outcomes, as detailed in Table 5.3, sustaining and amplifying its performance relative to other algorithms in both AVG and STD fitness values. The 'W/T/L' row showcases 19 wins, 0 draws, and 11 losses in AVG fitness, along with 13 wins, 0 ties, and 16 losses in STD, aligning closely with the performance of the BSDE algorithm.

Table 5.4 presents the results of non-parametric tests (Friedman and Holm tests) conducted on the IEEE CEC2017 benchmark functions. Notably, the HHGATSD consistently secures the top rank, as highlighted in bold, for both 30 and 50 dimensions. Holm's p-correction values play a crucial role in identifying algorithms that exhibit statistically significant differences in performance compared to their counterparts, thereby providing a robust basis for evaluating their effectiveness. Bolded results in the table signify p-values less than 0.05, indicating substantial differences from the HHGATSD algorithm. These outcomes affirm that the HHGATSD algorithm performs significantly better than the other algorithms tested in the study. It is noteworthy that the only algorithm displaying no significant difference in results is BSDE.

Table 5.4: Average Friedman's Rankings and Holm's p Values (0.05) for the CEC2017 Benchmark Functions in 30 and 50 Dimensions.

Algorithm	30D			50D		
	Ranking	No.	p_{Holm}	Ranking	No.	p_{Holm}
HHGATSD	2.25E+00	**1**		1.87E+00	**1**	
BSDE	3.03E+00	2	2.27E-01	3.58E+00	2	7.96E-03
DE	4.15E+00	3	**3.19E-03**	4.89E+00	6	**3.0E-06**
PSO	4.18E+00	4	**2.68E-03**	4.20E+00	3	**2.96E-04**
GA	4.44E+00	5	**6.64E-04**	4.34E+00	4	**1.27E-04**
JADE	5.34E+00	6	**2.00E-06**	4.63E+00	5	**1.80E-05**
GWO	5.77E+00	7	**0.00E+00**	5.72E+00	7	**0.00E+00**
HHO	6.79E+00	8	**0.00E+00**	6.72E+00	8	**0.00E+00**

Figure 5.5 visually represents the convergence curves of algorithms during a run of 50-dimensional instances, highlighting HHGATSD's efficient convergence across various function categories. The graph is displayed on a logarithmic scale for clarity. Among the algorithms, HHGATSD (represented by a black square with a red dotted line), JADE (magenta triangle with a blue dotted line), BSDE (turquoise triangle with a turquoise dotted line), and GA (green star with a magenta dotted line) show particularly efficient convergence across all categories of benchmark functions.

It is worth noting that HHGATSD consistently performs well when dealing with different types of function categories such as unimodal (F1), multimodal (F4, F7, and F9), hybrid (F14 and F18), and composition (F28 and F30) functions. The convergence curves for the HHGATSD are minimized across all these function categories, indicating its superior performance compared to other algorithms.

Table 5.2: Statistical Results of the CEC2017 Benchmark Functions in 30 Dimensions.

Instance		HHGATSD	GA	PSO	DE	JADE	BSDE	GWO	HHO
F1	AVG	5.48E+03	1.27E+05	**2.31E+03**	1.70E+09	5.03E+03	2.48E+03	1.62E+09	2.84E+07
	STD	1.24E+04	8.44E+04	2.84E+03	1.14E+09	6.06E+03	**1.28E+03**	1.36E+09	6.35E+06
F3	AVG	1.32E+04	1.28E+05	**5.72E+03**	5.19E+04	1.89E+05	6.44E+04	4.73E+04	3.29E+04
	STD	5.00E+03	3.57E+04	**2.84E+03**	1.46E+04	3.07E+04	1.16E+04	1.11E+04	7.00E+03
F4	AVG	5.06E+02	5.12E+02	5.12E+02	6.81E+02	**4.86E+02**	5.10E+02	5.88E+02	5.67E+02
	STD	3.53E+01	2.91E+01	6.13E+01	1.32E+02	1.41E+01	**1.11E+01**	6.41E+01	4.53E+01
F5	AVG	**5.35E+02**	5.82E+02	6.48E+02	5.39E+02	5.94E+02	5.85E+02	6.02E+02	7.55E+02
	STD	1.05E+01	2.26E+01	3.45E+01	1.18E+01	1.59E+01	**1.02E+01**	2.21E+01	3.86E+01
F6	AVG	**6.00E+02**	6.01E+02	6.28E+02	6.01E+02	6.03E+02	6.01E+02	6.07E+02	6.64E+02
	STD	**2.34E-02**	2.82E-02	1.40E+01	9.49E-01	1.29E+00	2.90E-01	2.95E+00	5.68E+00
F7	AVG	8.20E+02	8.09E+02	8.01E+02	**8.00E+02**	8.21E+02	8.20E+02	8.76E+02	1.26E+03
	STD	3.06E+01	2.19E+01	2.37E+01	3.11E+01	1.59E+01	**8.56E+00**	5.38E+01	6.58E+01
F8	AVG	**8.37E+02**	8.83E+02	9.09E+02	8.43E+02	8.92E+02	8.83E+02	8.91E+02	9.67E+02
	STD	1.35E+01	2.42E+01	2.16E+01	1.56E+01	1.60E+01	**1.12E+01**	3.32E+01	2.62E+01
F9	AVG	**9.10E+02**	1.29E+03	2.86E+03	1.06E+03	2.80E+03	1.70E+03	1.70E+03	8.15E+03
	STD	**1.68E+00**	3.44E+02	1.29E+03	1.02E+02	1.18E+03	3.50E+02	6.79E+02	8.53E+02
F10	AVG	**3.17E+03**	4.72E+03	4.37E+03	7.52E+03	5.15E+03	4.62E+03	4.92E+03	5.88E+03
	STD	6.71E+02	6.95E+02	6.75E+02	1.03E+03	**3.07E+02**	4.14E+02	1.45E+03	7.57E+02
F11	AVG	**1.21E+03**	2.48E+03	1.22E+03	1.51E+03	3.76E+03	1.23E+03	1.65E+03	1.29E+03
	STD	4.70E+01	1.32E+03	3.32E+01	3.90E+02	1.26E+03	**2.19E+01**	4.57E+02	4.30E+01
F12	AVG	2.43E+07	3.65E+06	**6.82E+05**	5.62E+07	2.95E+06	7.20E+05	6.32E+07	1.93E+07
	STD	1.69E+07	2.59E+06	4.67E+05	7.60E+07	4.05E+06	**3.67E+05**	6.86E+07	9.66E+06
F13	AVG	**2.79E+03**	4.70E+04	1.22E+04	1.93E+07	2.41E+06	1.25E+04	4.87E+06	7.49E+05
	STD	**1.47E+03**	3.71E+04	1.02E+04	3.98E+07	2.89E+06	4.93E+03	1.68E+07	9.00E+05
F14	AVG	**1.56E+03**	9.54E+05	1.81E+04	1.61E+05	8.58E+05	4.51E+04	2.73E+05	3.82E+05
	STD	**3.29E+02**	9.01E+05	1.70E+04	3.23E+05	9.05E+05	3.69E+04	3.81E+05	5.02E+05
F15	AVG	5.09E+03	1.37E+04	7.64E+03	3.78E+05	1.48E+06	**2.20E+03**	3.56E+05	9.55E+04
	STD	1.96E+03	2.07E+04	7.38E+03	1.14E+06	1.92E+06	**6.73E+02**	9.29E+05	6.07E+04
F16	AVG	**2.06E+03**	2.61E+03	2.54E+03	2.10E+03	2.71E+03	2.31E+03	2.47E+03	3.44E+03
	STD	2.68E+02	2.94E+02	2.75E+02	2.46E+02	2.11E+02	**1.30E+02**	3.50E+02	4.22E+02
F17	AVG	1.88E+03	2.22E+03	2.20E+03	1.83E+03	2.23E+03	**1.87E+03**	2.01E+03	2.60E+03
	STD	7.56E+01	1.97E+02	2.09E+02	9.82E+01	1.52E+02	**7.52E+01**	1.58E+02	3.36E+02
F18	AVG	**1.23E+05**	2.46E+06	2.77E+05	6.35E+05	2.60E+06	1.83E+05	1.17E+06	1.92E+06
	STD	1.54E+05	2.38E+06	2.70E+05	1.13E+06	1.34E+06	**9.71E+04**	1.83E+06	2.42E+06
F19	AVG	**3.32E+03**	1.36E+04	1.02E+04	2.02E+05	7.38E+05	4.58E+03	4.11E+06	6.99E+05
	STD	**2.28E+03**	1.98E+04	9.31E+03	7.22E+05	6.85E+05	2.36E+03	1.06E+07	5.80E+05
F20	AVG	**2.14E+03**	2.55E+03	2.46E+03	2.14E+03	2.56E+03	2.24E+03	2.40E+03	2.76E+03
	STD	**7.12E+01**	2.18E+02	1.35E+02	8.97E+01	1.29E+02	8.95E+01	1.40E+02	2.27E+02
F21	AVG	**2.21E+03**	2.38E+03	2.43E+03	2.35E+03	2.41E+03	2.38E+03	2.39E+03	2.57E+03
	STD	**1.99E-03**	2.18E+01	2.65E+01	1.28E+01	2.02E+01	1.02E+01	3.80E+01	4.71E+01
F22	AVG	**2.28E+03**	4.11E+03	3.46E+03	3.45E+03	5.60E+03	2.33E+03	5.01E+03	6.79E+03
	STD	**2.19E-03**	2.13E+03	1.76E+03	1.99E+03	1.74E+03	3.06E+01	1.71E+03	1.50E+03
F23	AVG	2.84E+03	2.76E+03	2.90E+03	**2.72E+03**	2.76E+03	2.75E+03	2.77E+03	3.21E+03
	STD	1.40E+01	3.13E+01	6.54E+01	2.27E+01	2.27E+01	**1.07E+01**	5.14E+01	1.29E+02
F24	AVG	**2.60E+03**	2.93E+03	3.06E+03	2.89E+03	2.94E+03	2.92E+03	2.94E+03	3.44E+03
	STD	**0.00E+00**	3.42E+01	7.64E+01	2.71E+01	2.45E+01	1.87E+01	6.15E+01	1.38E+02
F25	AVG	2.94E+03	2.90E+03	2.90E+03	3.02E+03	**2.89E+03**	2.90E+03	3.00E+03	2.95E+03
	STD	1.30E+02	1.77E+01	1.39E+01	9.57E+01	**1.01E+01**	1.23E+01	3.84E+01	3.55E+01
F26	AVG	**3.18E+03**	4.86E+03	4.70E+03	4.43E+03	4.63E+03	4.03E+03	4.83E+03	7.32E+03
	STD	9.29E+02	3.64E+02	1.58E+03	**2.28E+02**	2.83E+02	8.30E+02	4.81E+02	1.27E+03
F27	AVG	3.66E+03	3.24E+03	3.27E+03	3.24E+03	**3.22E+03**	3.26E+03	3.26E+03	3.47E+03
	STD	9.28E+01	1.44E+01	4.13E+01	1.96E+01	1.01E+01	**7.02E+00**	2.87E+01	1.10E+02
F28	AVG	**3.24E+03**	3.25E+03	3.29E+03	3.68E+03	3.27E+03	3.28E+03	3.42E+03	3.32E+03
	STD	**1.41E+01**	2.92E+01	3.20E+01	3.15E+02	4.87E+01	1.84E+01	1.27E+02	3.87E+01
F29	AVG	**3.33E+03**	3.83E+03	3.95E+03	3.56E+03	3.79E+03	3.63E+03	3.82E+03	4.81E+03
	STD	1.58E+02	2.14E+02	1.97E+02	1.40E+02	1.20E+02	**7.09E+01**	1.80E+02	4.74E+02
F30	AVG	2.76E+04	1.77E+04	**1.58E+04**	2.58E+05	3.57E+05	2.75E+04	6.35E+06	4.81E+06
	STD	1.88E+04	**6.58E+03**	1.06E+04	3.70E+05	3.34E+05	1.52E+04	5.08E+06	3.96E+06
W/T/L	AVG	**18/0/11**	0/0/29	4/0/25	2/0/27	3/0/26	2/0/27	0/0/29	0/0/29
	STD	8/0/21	1/0/28	1/0/28	1/0/28	2/0/27	**13/0/16**	0/0/0	0/0/0

Table 5.3: Statistical Results of the CEC2017 Benchmark Functions in 50 Dimensions.

Instance		HHGATSD	GA	PSO	DE	JADE	BSDE	GWO	HHO
F1	AVG	2.24E+04	4.98E+05	3.97E+08	7.92E+09	**4.99E+03**	6.21E+03	7.56E+09	9.88E+07
	STD	2.52E+04	2.16E+05	7.20E+08	3.33E+09	5.78E+03	**3.71E+03**	3.31E+09	1.90E+07
F3	AVG	**2.94E+04**	3.01E+05	4.77E+04	1.95E+05	3.51E+05	1.58E+05	9.82E+04	8.75E+04
	STD	**7.67E+03**	5.38E+04	1.28E+04	3.72E+04	4.78E+04	1.94E+04	1.37E+04	1.77E+04
F4	AVG	5.54E+02	5.68E+02	5.81E+02	1.39E+03	**4.89E+02**	5.66E+02	1.11E+03	7.10E+02
	STD	4.53E+01	4.85E+01	7.38E+01	5.56E+02	5.48E+01	**3.82E+01**	4.69E+02	7.02E+01
F5	AVG	**5.92E+02**	6.81E+02	7.45E+02	6.08E+02	6.76E+02	7.00E+02	7.25E+02	8.95E+02
	STD	**1.80E+01**	4.83E+01	3.33E+01	2.20E+01	2.26E+01	2.14E+01	5.80E+01	3.52E+01
F6	AVG	**6.00E+02**	6.01E+02	6.43E+02	6.03E+02	6.03E+02	6.01E+02	6.17E+02	6.74E+02
	STD	**2.70E-02**	3.73E-02	8.06E+00	1.48E+00	1.95E+00	5.20E-01	4.62E+00	5.04E+00
F7	AVG	9.17E+02	9.30E+02	**9.03E+02**	9.76E+02	9.38E+02	9.54E+02	1.08E+03	1.82E+03
	STD	5.17E+01	4.19E+01	3.90E+01	8.13E+01	**2.40E+01**	2.55E+01	8.15E+01	9.55E+01
F8	AVG	**8.99E+02**	9.69E+02	1.07E+03	9.11E+02	9.91E+02	9.95E+02	1.03E+03	1.19E+03
	STD	2.54E+01	2.53E+01	3.65E+01	**1.57E+01**	2.68E+01	2.30E+01	6.37E+01	3.92E+01
F9	AVG	**9.86E+02**	4.81E+03	1.32E+04	2.05E+03	5.39E+03	7.33E+03	6.84E+03	2.62E+04
	STD	**1.02E+02**	3.89E+03	5.35E+03	9.73E+02	3.71E+03	1.33E+03	3.00E+03	2.99E+03
F10	AVG	**5.81E+03**	7.49E+03	6.81E+03	1.39E+04	8.21E+03	7.96E+03	7.09E+03	9.11E+03
	STD	9.20E+02	8.02E+02	7.86E+02	5.26E+02	3.80E+02	**3.06E+02**	9.08E+02	8.03E+02
F11	AVG	1.58E+03	6.72E+03	**1.26E+03**	4.22E+03	2.10E+04	1.41E+03	4.10E+03	1.53E+03
	STD	4.15E+02	5.21E+03	**4.02E+01**	2.00E+03	8.14E+03	4.27E+01	1.81E+03	9.87E+01
F12	AVG	**1.28E+05**	9.19E+06	6.55E+07	1.66E+09	3.55E+06	2.47E+06	7.86E+08	1.00E+08
	STD	**1.21E+05**	4.17E+06	2.18E+08	2.42E+09	4.93E+06	9.38E+05	9.03E+08	3.59E+07
F13	AVG	2.48E+04	3.59E+05	2.30E+06	4.67E+08	1.61E+06	**2.81E+03**	2.14E+08	3.96E+06
	STD	1.70E+04	7.72E+05	7.65E+06	1.15E+09	3.91E+06	**1.31E+03**	2.43E+08	3.49E+06
F14	AVG	**6.97E+03**	2.83E+06	1.16E+05	1.11E+06	3.42E+06	2.97E+05	7.12E+05	1.57E+06
	STD	**4.44E+03**	2.46E+06	9.92E+04	9.49E+05	2.01E+06	1.75E+05	5.60E+05	1.63E+06
F15	AVG	**3.32E+03**	1.17E+05	1.07E+04	1.59E+07	1.43E+06	8.72E+03	9.83E+06	4.84E+05
	STD	**1.39E+03**	1.29E+05	7.98E+03	4.18E+07	1.93E+06	2.97E+03	2.07E+07	2.04E+05
F16	AVG	2.75E+03	3.51E+03	3.00E+03	**2.65E+03**	3.65E+03	2.67E+03	3.11E+03	4.45E+03
	STD	2.78E+02	2.98E+02	5.50E+02	4.42E+02	2.57E+02	**1.74E+02**	5.22E+02	5.31E+02
F17	AVG	2.45E+03	3.17E+03	2.80E+03	**2.43E+03**	3.33E+03	2.63E+03	2.88E+03	3.84E+03
	STD	2.71E+02	3.03E+02	2.47E+02	2.76E+02	1.74E+02	**9.68E+01**	3.48E+02	3.91E+02
F18	AVG	**7.63E+05**	6.64E+06	1.05E+06	1.65E+06	1.13E+07	1.32E+06	5.47E+06	4.61E+06
	STD	**5.49E+05**	6.96E+06	8.02E+05	1.60E+06	8.35E+06	6.18E+05	1.01E+07	4.53E+06
F19	AVG	**5.37E+03**	1.92E+04	1.53E+04	8.66E+06	2.29E+05	1.83E+04	4.58E+06	1.28E+06
	STD	**3.36E+03**	1.17E+04	1.04E+04	2.68E+07	2.65E+05	4.30E+03	9.70E+06	1.20E+06
F20	AVG	**2.41E+03**	3.23E+03	2.93E+03	2.46E+03	3.42E+03	2.66E+03	2.88E+03	3.40E+03
	STD	1.95E+02	3.31E+02	2.88E+02	2.77E+02	1.71E+02	**1.56E+02**	2.71E+02	2.73E+02
F21	AVG	**2.29E+03**	2.47E+03	2.57E+03	2.41E+03	2.50E+03	2.49E+03	2.51E+03	2.87E+03
	STD	3.84E+01	3.83E+01	5.02E+01	2.13E+01	3.51E+01	**1.35E+01**	4.92E+01	8.66E+01
F22	AVG	**2.30E+03**	9.32E+03	8.64E+03	1.40E+04	9.92E+03	9.33E+03	8.88E+03	1.12E+04
	STD	**2.16E+01**	1.52E+03	1.61E+03	3.13E+03	4.26E+02	2.02E+03	1.96E+03	9.93E+02
F23	AVG	3.15E+03	2.96E+03	3.21E+03	**2.90E+03**	2.95E+03	2.97E+03	2.97E+03	3.82E+03
	STD	3.99E+01	4.96E+01	1.09E+02	4.34E+01	3.86E+01	**2.04E+01**	5.95E+01	1.65E+02
F24	AVG	**2.60E+03**	3.15E+03	3.40E+03	3.09E+03	3.14E+03	3.16E+03	3.12E+03	4.20E+03
	STD	**0.00E+00**	6.14E+01	1.01E+02	5.79E+01	4.85E+01	2.57E+01	7.14E+01	2.00E+02
F25	AVG	**3.03E+03**	3.08E+03	3.06E+03	3.89E+03	3.04E+03	3.12E+03	3.63E+03	3.22E+03
	STD	3.07E+01	2.74E+01	2.97E+01	4.90E+02	3.74E+01	**2.11E+01**	4.05E+02	5.64E+01
F26	AVG	**2.80E+03**	6.21E+03	5.95E+03	5.67E+03	5.74E+03	6.47E+03	6.48E+03	1.09E+04
	STD	**0.00E+00**	5.15E+02	2.39E+03	4.96E+02	3.09E+02	4.55E+02	6.11E+02	1.46E+03
F27	AVG	4.11E+03	3.55E+03	3.56E+03	3.58E+03	**3.48E+03**	3.54E+03	3.58E+03	4.38E+03
	STD	2.26E+02	7.66E+01	1.93E+02	8.07E+01	5.44E+01	**4.51E+01**	8.84E+01	5.21E+02
F28	AVG	**3.36E+03**	3.35E+03	3.38E+03	5.36E+03	3.35E+03	3.41E+03	4.21E+03	3.57E+03
	STD	3.98E+01	2.97E+01	4.30E+01	8.23E+02	1.83E+02	**2.68E+01**	3.17E+02	6.99E+01
F29	AVG	4.02E+03	4.27E+03	4.51E+03	3.91E+03	4.28E+03	**3.87E+03**	4.53E+03	5.98E+03
	STD	2.76E+02	3.35E+02	3.54E+02	2.33E+02	2.34E+02	**1.75E+02**	2.51E+02	5.34E+02
F30	AVG	**3.20E+03**	1.14E+06	9.90E+05	3.17E+07	3.18E+06	1.08E+06	1.08E+08	4.03E+07
	STD	**0.00E+00**	3.59E+05	4.69E+05	4.59E+07	2.39E+06	9.73E+04	4.12E+07	8.06E+06
W/T/L	AVG	**19/0/10**	0/0/29	2/0/27	3/0/26	3/0/26	2/0/27	0/0/29	0/0/29
	STD	**13/0/16**	0/0/29	1/0/28	1/0/28	1/0/28	**13/0/16**	0/0/0	0/0/0

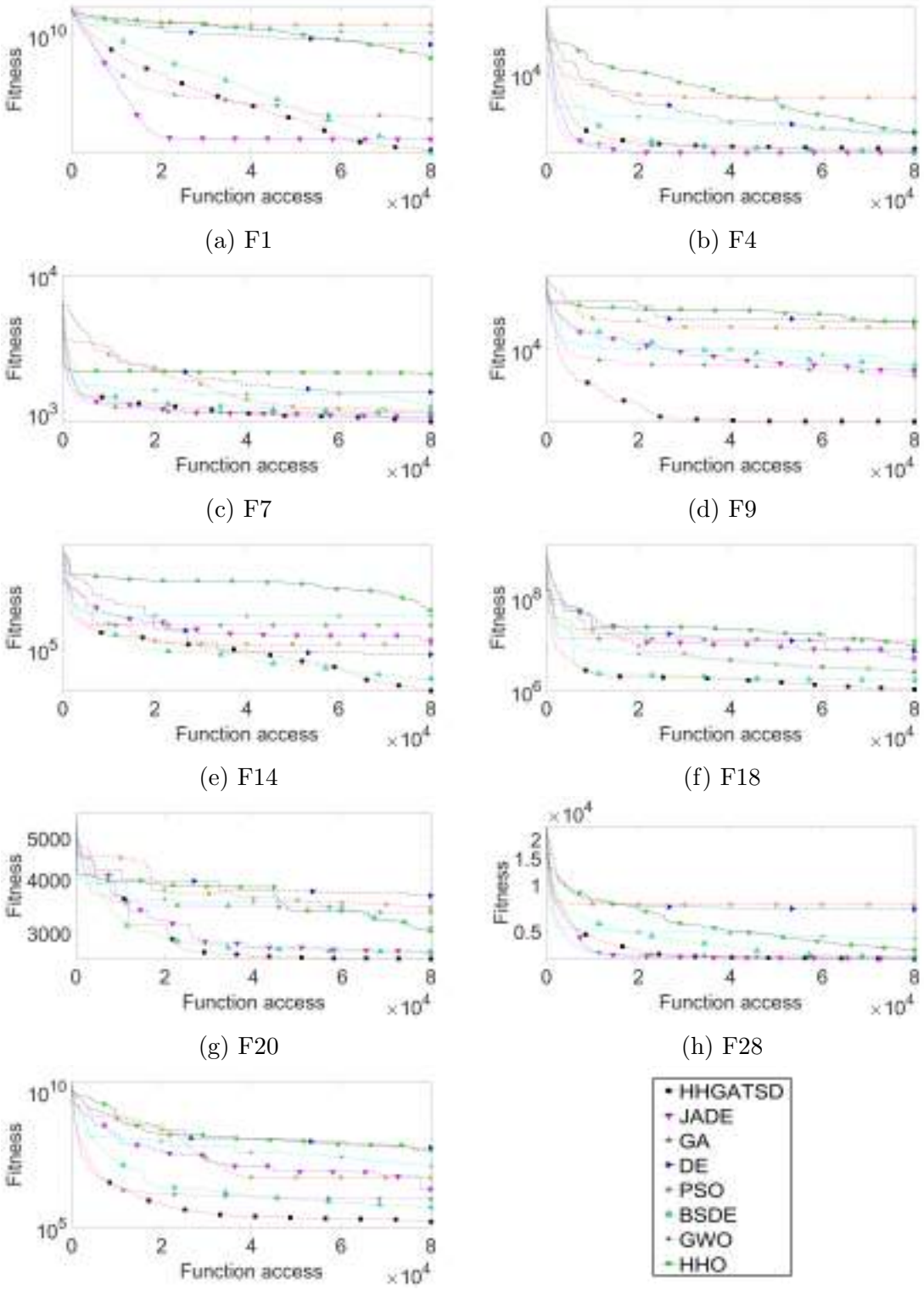

(a) F1 (b) F4

(c) F7 (d) F9

(e) F14 (f) F18

(g) F20 (h) F28

(i) F30 (j) Labels

Figure 5.5: Convergence curves for all algorithms during a specific run of 50-dimensional instances. The curves employ a logarithmic scale for enhanced presentation quality.

5.4.2 Experiments in Multilevel Segmentation

This section summarizes the results of experiments using ten images from BSDS500 and eight frames from a traffic video camera for multilevel thresholding segmentation.

The outcomes presented in Table 5.5 encapsulate the non-parametric evaluation of four criteria, fitness performance and segmentation quality measured by the PSNR, SSIM, and FSIM metrics on BSDS500 images. These metrics serve as quantitative benchmarks, examining algorithmic performance of segmentation accuracy and similarity with the original image.

The results are derived from non-parametric tests conducted on AVG and STD values, extracted from 30 independent runs for each of the five thresholds applied to the images. Algorithms are ranked based on their average Friedman ranking, offering insights into their comparative performance across each metric. Additionally, Holm's p-correction values (p_{Holm}) are incorporated to discern statistical significance, accounting for multiple comparisons during statistical analysis. Top-ranked algorithms are highlighted in bold, and the results showing significant differences from HHGATSD are also indicated in bold.

It's noteworthy that the HHGATSD algorithm consistently ranks first in all metrics, demonstrating its superiority. The BSDE algorithm, while not significantly different from HHGATSD, follows closely in the rankings. Other algorithms exhibit variations in performance, with strengths and weaknesses in fitness and segmentation quality. The detailed rankings and statistical significance provided in the table offer a comprehensive understanding of the comparative performance of these optimization algorithms in the context of image segmentation.

Table 5.5: Average Friedman's Rankings and Holm's p Values (0.05) for the BSDS500.

Algorithm	Fitness			PSNR			SSIM			FSIM		
	Ranking	No.	p_{Holm}	Ranking	No.	p_{Holm}	Ranking	No.	p_{Holm}	Ranking	No.	p_{Holm}
HHGATSD	3.57E+00	**1**		4.35E+00	3	6.55E-01	3.88E+00	3	3.14E-01	4.23E+00	**1**	
BSDE	3.68E+00	2	7.94E-01	4.28E+00	2	7.66E-01	4.27E+00	4	6.24E-02	4.48E+00	4	5.76E-01
DE	4.67E+00	5	1.39E-02	4.52E+00	5	4.12E-01	5.33E+00	7	**2.20E-05**	4.43E+00	3	6.41E-01
PSO	4.75E+00	6	8.15E-03	4.89E+00	8	9.72E-02	5.04E+00	6	**3.23E-04**	4.77E+00	8	2.26E-01
GA	5.76E+00	7	**1.00E-06**	4.63E+00	6	2.80E-01	6.03E+00	8	**0.00E+00**	4.60E+00	7	4.02E-01
JADE	3.82E+00	4	5.76E-01	4.15E+00	**1**		4.38E+00	5	3.36E-02	4.55E+00	6	4.67E-01
GWO	5.90E+00	8	**0.00E+00**	4.75E+00	7	1.80E-01	3.43E+00	**1**		4.52E+00	5	5.14E-01
HHO	3.81E+00	3	5.89E-01	4.42E+00	4	5.39E-01	3.62E+00	2	6.68E-01	4.43E+00	2	6.41E-01

Table 5.6 consolidates the computational outcomes derived from averaging over 30 independent runs across five thresholds applied to images, focusing on the ten images from the BSDS500 dataset and eight frames from the video traffic camera. Notably, in the context of BSDS500, JADE stands out for superior AVG and STD results. Simultaneously, the BSDE algorithm has the fastest computation times for multilevel segmentation of traffic video frames. Despite not clinching the top spot, the proposed HH exhibits competitive performance, demonstrating average computation times ranging from 0.56 to 0.95 seconds.

Table 5.6: Average Computation Times (in seconds) for the BSDS500 and Traffic Video Frames.

Dataset		BSDS500					Traffic video frames				
		2	4	6	8	10	2	4	6	8	10
HHGATSD	AVG	8.13E-01	8.73E-01	8.97E-01	9.25E-01	9.52E-01	5.74E-01	5.62E-01	6.03E-01	5.88E-01	6.01E-01
	STD	8.31E-02	7.63E-02	7.84E-02	7.93E-02	7.93E-02	8.95E-02	6.05E-02	8.58E-02	6.74E-02	6.06E-02
GA	AVG	3.12E-01	3.37E-01	3.64E-01	3.66E-01	3.64E-01	2.39E-01	2.33E-01	2.49E-01	**2.54E-01**	2.60E-01
	STD	2.63E-02	3.10E-02	3.04E-02	3.04E-02	2.74E-02	5.60E-02	2.89E-02	3.12E-02	2.91E-02	3.88E-02
PSO	AVG	3.73E-01	3.62E-01	3.78E-01	3.92E-01	4.14E-01	2.70E-01	2.81E-01	3.02E-01	3.03E-01	3.03E-01
	STD	3.71E-02	2.97E-02	3.24E-02	3.61E-02	3.53E-02	4.42E-02	3.20E-02	3.74E-02	4.60E-02	4.42E-02
DE	AVG	3.26E-01	3.41E-01	3.54E-01	3.71E-01	3.88E-01	2.43E-01	2.49E-01	2.58E-01	2.80E-01	2.84E-01
	STD	3.94E-02	3.06E-02	3.37E-02	3.25E-02	2.82E-02	4.47E-02	3.45E-02	3.09E-02	3.82E-02	5.02E-02
JADE	AVG	**2.07E-01**	**2.15E-01**	**2.35E-01**	**2.45E-01**	**2.48E-01**	3.01E-01	3.11E-01	3.25E-01	3.47E-01	3.41E-01
	STD	**2.11E-02**	**2.11E-02**	**2.12E-02**	**2.42E-02**	**2.38-02**	6.42E-02	3.61E-02	4.03E-02	4.82E-02	3.25E-02
BSDE	AVG	3.15E-01	3.31E-01	3.58E-01	3.84E-01	3.82E-01	**2.06E-01**	2.19E-01	**2.31E-01**	**2.40E-01**	**2.55E-01**
	STD	4.17E-02	3.29E-02	3.50E-02	4.15E-02	3.49E-02	**3.46E-02**	3.21E-02	3.16E-02	2.95E-02	3.49E-02
GWO	AVG	2.78E-01	2.92E-01	3.39E-01	3.73E-01	3.84E-01	2.08E-01	**2.14E-01**	2.44E-01	2.68E-01	2.74E-01
	STD	3.55E-02	2.99E-02	3.29E-02	3.51E-02	4.06E-02	4.19E-02	**2.73E-02**	3.30E-02	3.93E-02	**2.75E-02**
HHO	AVG	6.86E-01	7.32E-01	7.96E-01	8.31E-01	8.59E-01	2.56E-01	2.63E-01	2.78E-01	3.14E-01	3.06E-01
	STD	9.54E-02	8.89E-02	9.18E-02	7.67E-02	1.01E-01	3.79E-02	3.23E-02	**2.86E-02**	4.90E-02	3.32E-02

The proposed HH proves highly effective in thresholding segmentation techniques, yielding segmentations with a notable resemblance to the original image underscored by its remarkable accuracy. However, it exhibits statistically significant differences in fitness only when compared to the GA and GWO algorithms in fitness and the DE, PSO, and GA algorithms in terms of FSIM. In the metric PSNR, the HHGATSD secures a third-place ranking, with the JADE algorithm claiming the top spot. Notably, no significant differences emerge between the algorithms in this criterion. Similarly, in SSIM, the HH occupies the third position, while the GWO algorithm takes the lead without any noteworthy difference compared to the other algorithms, including our proposal. It is crucial to emphasize that, despite subtle variations, there are no statistically significant differences in computational times between the proposed HHGATSD and the compared algorithms, ensuring its practical feasibility for real-world applications.

5.4.3 Experiments with Traffic Video Frames for the Vehicle Segmentation

In this section, we comprehensively analyze the HHGATSD algorithm's performance in vehicle segmentation on traffic video frames. Initially, we delve into hyperparameter combinations ($Iter$ and α) for the multilevel segmentation of a subset of 61 images, aiming to identify the optimal hyperparameter values. Following this, we present visual representations of the significant steps of the methodology for segmenting eight frames. Subsequently, we evaluate and compare the performance of HHGATSD against other well-known segmentation techniques in the literature, considering all 612 images.

Table 5.7 focuses on analyzing combinations of hyperparameters ($Iter$ and α) within the proposed HHGATSD algorithm. This study aims to experimentally identify and validate optimal hyperparameters for the algorithm's performance in multilevel segmentation of traffic video frames, serving as a preprocessing step for vehicle segmentation.

The experiments were conducted on 61 randomly selected images, representing 10% of the total dataset. The tests were done using 2, 4, 6, 8, and 10 thresholds to ensure a

thorough evaluation of the algorithm's performance in vehicle segmentation for traffic video frames. The main objective of the research is to identify the most effective hyperparameter values for vehicle segmentation. The table provides detailed rankings and Holm's p-values obtained from non-parametric Friedman tests. Furthermore, statistical results for AVG and STD in fitness, PSNR, SSIM, and FSIM are presented, with the best AVG highlighted in bold and the highest STD in bold.

Upon analyzing the data, it becomes evident that there are no significant differences among various hyperparameter configurations, indicated by the lack of bold Holm's p-values (all above 0.05). This observation underscores the consistency of the algorithm's performance across different hyperparameter combinations. Notably, the algorithm maintains stability and reliability in its performance, even with variations in internal parameters like $Iter$ and α. The average values across all combinations exhibit no noteworthy distinctions, underscoring the algorithm's versatility and effectiveness in tackling the vehicle segmentation challenge.

The conducted experiments confirm that the chosen hyperparameter values ($Iter = 200$ and $\alpha = 5$) remain stable and effective for the vehicle segmentation task in traffic video frames. These values consistently yield satisfactory results, as demonstrated by both statistical analyses and the absence of significant performance differences across various hyperparameter configurations.

Table 5.7: Stadistical Results and Average Friedman's Rankings and Holm's p Values (0.05) for traffic video frames.

$Iter$	α	Ranking	No.	p_{Holm}	Fitness		PSNR		SSIM		FSIM	
					AVG	STD	AVG	STD	AVG	STD	AVG	STD
50	1	8.375	2	0.5524	2.17E-01	6.10E-04	2.49E+01	5.58E-02	8.67E-01	1.37E-03	9.48E-01	5.82E-04
	3	10.375	3	0.2347	2.18E-01	8.03E-04	2.49E+01	7.24E-02	8.67E-01	1.63E-03	9.48E-01	7.75E-04
	5	10.375	3	0.2347	2.18E-01	8.78E-04	2.49E+01	7.76E-02	8.67E-01	1.73E-03	9.48E-01	7.91E-04
	10	12.375	4	0.0747	2.18E-01	1.01E-03	2.49E+01	7.71E-02	8.67E-01	1.73E-03	9.47E-01	7.21E-04
100	1	6.375	**1**		2.17E-01	5.61E-04	2.49E+01	4.72E-02	8.68E-01	1.20E-03	9.48E-01	5.12E-04
	3	8.375	2	0.5524	2.17E-01	7.49E-04	2.49E+01	6.60E-02	8.67E-01	1.54E-03	9.48E-01	6.69E-04
	5	8.375	2	0.5524	2.17E-01	8.27E-04	2.49E+01	6.99E-02	8.67E-01	1.57E-03	9.48E-01	6.97E-04
	10	10.375	3	0.2347	2.18E-01	9.22E-04	2.49E+01	6.81E-02	8.67E-01	1.59E-03	9.48E-01	6.64E-04
200	1	6.375	**1**	1	2.17E-01	**5.12E-04**	2.49E+01	4.21E-02	8.68E-01	1.09E-03	9.48E-01	4.23E-04
	3	8.375	2	0.5524	2.17E-01	6.31E-04	2.49E+01	5.09E-02	8.67E-01	1.28E-03	9.48E-01	5.32E-04
	5	8.375	2	0.5524	2.17E-01	7.71E-04	2.49E+01	5.69E-02	8.67E-01	1.38E-03	9.48E-01	5.43E-04
	10	8.375	2	0.5524	2.17E-01	8.69E-04	2.49E+01	6.05E-02	8.67E-01	1.46E-03	9.48E-01	5.78E-04
300	1	6.375	**1**	1	**2.17E-01**	5.16E-04	2.49E+01	**4.08E-02**	**8.68E-01**	**1.04E-03**	**9.48E-01**	**3.87E-04**
	3	6.375	**1**	1	2.17E-01	6.60E-04	2.49E+01	5.12E-02	8.68E-01	1.24E-03	9.48E-01	4.93E-04
	5	8.375	2	0.5524	2.17E-01	7.80E-04	**2.49E+01**	5.33E-02	8.67E-01	1.37E-03	9.48E-01	5.29E-04
	10	8.375	2	0.5524	2.17E-01	7.66E-04	2.49E+01	5.26E-02	8.67E-01	1.37E-03	9.48E-01	4.98E-04

Table 5.8 presents a comprehensive overview of the AVG performance metrics alongside their respective STD values for the vehicle segmentation methodology. The values highlighted in bold indicate the algorithms with the best AVG performance for the evaluated metrics and the values with the results with the minimum STD. Notably, for DSC and IoU metrics, the proposed HHGATSD emerges as the leader, achieving AVG scores of 0.82 and 0.70, respectively. It also demonstrates the lowest STD values for these metrics.

Concerning the P metric, K-means emerges as the top-performing algorithm with an AVG value of 0.89 and a STD of 0.12. However, it is worth noting that HHGATSD closely

follows with an AVG of 0.87 and a STD of 0.13, demonstrating only a slight variation between the two. For the R and ACC metrics, HHGATSD once again showcases the highest AVG values and the smallest STD values among all algorithms tested.

Regarding computational time, it is essential to highlight that Otsu achieved the fastest segmentation time, with an average of 0.46 seconds per image. HHGATSD demonstrated notable efficiency in close succession with an average of 0.49 seconds. Although K-means exhibited a slightly higher average of 0.50 seconds, Fuzzy IterAg presented significantly higher segmentation time, with an average of 5.58 seconds per image. Importantly, the observed differences in computational time between the proposed HHGATSD approach and alternative algorithms, such as Otsu and K-means, do not indicate any statistically significant differences. This underscores the efficiency of our methodology for vehicle segmentation.

Table 5.8: Statistical Results of the Performance Metrics in Vehicle Segmentation.

Metric		HHGATSD	Otsu	K-means	Fuzzy IterAg
DSC	AVG	**0.82**	0.74	0.76	0.73
	STD	**0.08**	0.13	0.10	0.15
IoU	AVG	**0.70**	0.60	0.62	0.60
	STD	**0.12**	0.15	**0.12**	0.16
P	AVG	0.87	0.88	**0.89**	0.83
	STD	0.13	**0.12**	**0.12**	0.22
R	AVG	**0.80**	0.66	0.68	0.72
	STD	**0.11**	0.16	0.13	0.13
ACC	AVG	**0.96**	0.95	0.95	0.95
	STD	**0.02**	0.03	0.03	0.03
Time	AVG	0.49	**0.46**	0.50	5.58
	STD	0.12	**0.03**	0.09	1.45

Figures 5.6 and 5.7 offer an in-depth illustration of the effectiveness of our proposed methodology, utilizing the HHGATSD algorithm for multilevel segmentation to segment vehicles in the traffic video sequence. Each of the eight frames represents a different scenario, with each row representing the process of obtaining the mask for each one. Meanwhile, the columns present a series of key images, showcasing the most critical stages of our proposed methodology. This visual representation illustrates the gradual transformation of the original image into a mask that segments the vehicles.

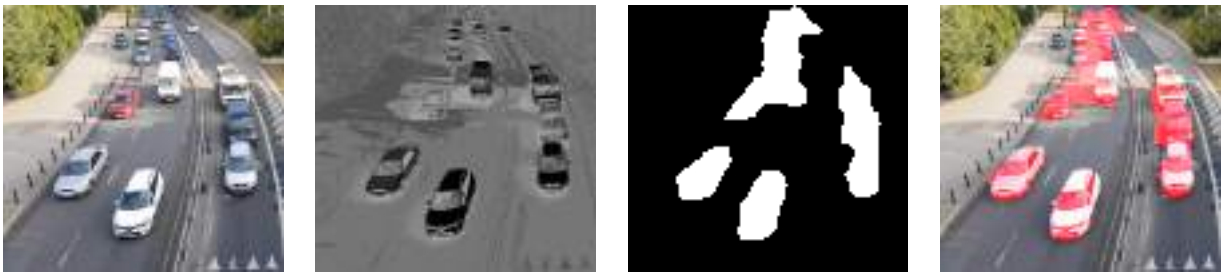

(a) 87

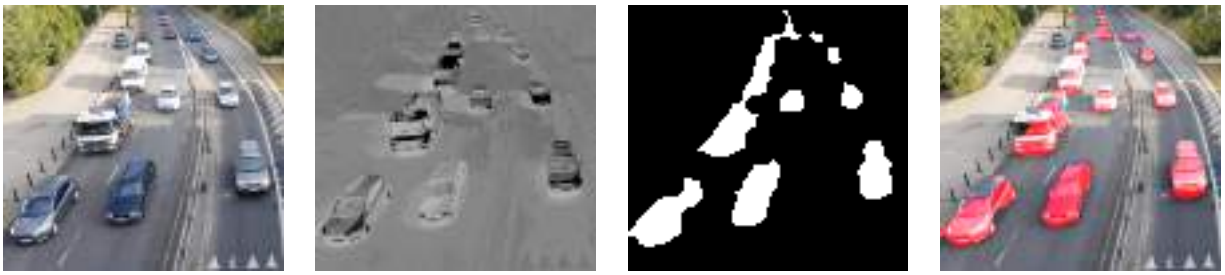

(b) 141

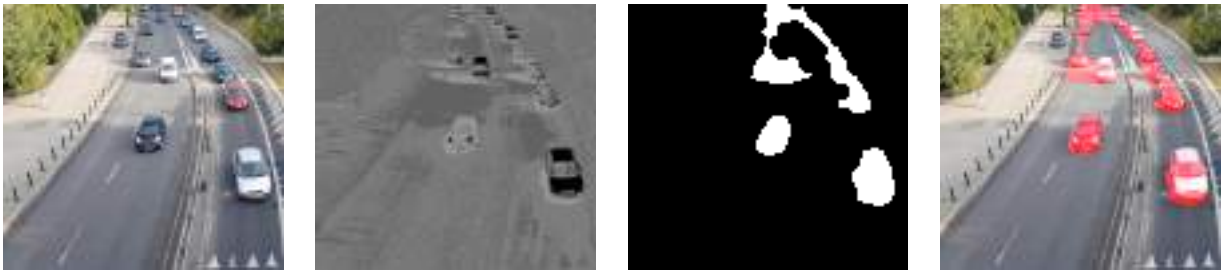

(c) 308

(d) 389

Figure 5.6: Visual Examples of the Proposed Methodology.

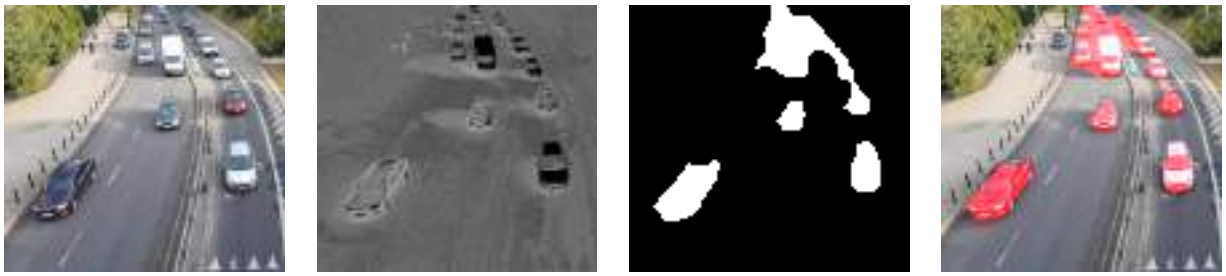

(a) 416

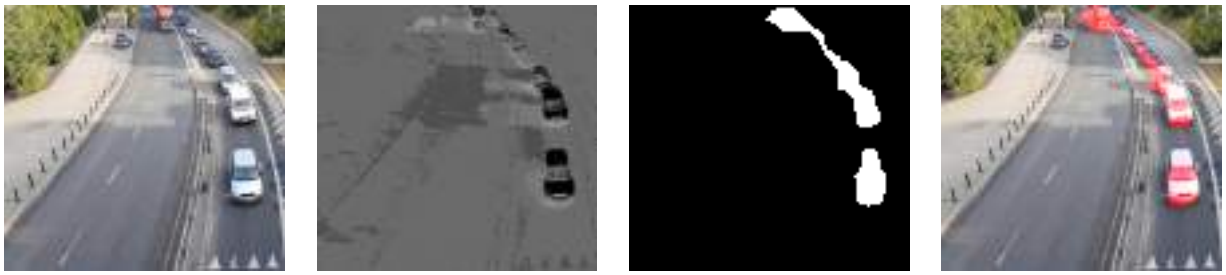

(b) 441

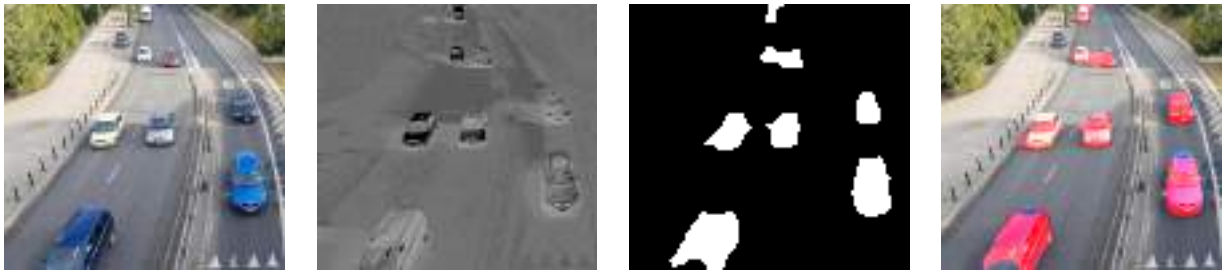

(c) 507

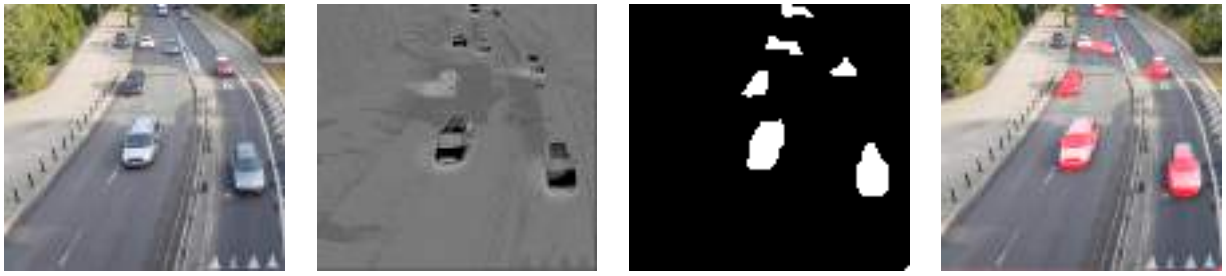

(d) 534

Figure 5.7: Visual Examples of the Proposed Methodology.

The first column displays the original $\boldsymbol{I_{th}}$ image of the traffic scene captured by the surveillance camera. The second column reveals the component image L, acquired through the RobustPCA process, which captures the image's underlying structural information. This component undergoes multilevel segmentation with five thresholds ($\boldsymbol{I_{th}}$).

In the third column, we present the mask obtained by applying binarization and morphological operations ($\boldsymbol{I_{seg}}$). This mask accentuates the regions corresponding to the vehicles within the frames. Finally, the fourth column displays the original image once more, overlaying the final segmentation mask ($\boldsymbol{I_{seg}}$) in red. This red overlay facilitates the identification of segmented areas.

It is important to mention that as vehicles draw closer to the camera, their spatial distance increases, leading to a proportional increase in the number of pixels they occupy. Consequently, in such scenarios, the segmentation becomes more refined and accurate, capturing more delimited details with greater precision. On the other hand, it is worth emphasizing that due to the method's capability to perform segmentation without prior background or vehicle-labeled information, automobiles positioned far from the camera are not delineated as separate entities. Still, they contribute significantly to understanding traffic dynamics, especially vehicular density. Thus, despite not being isolated, their presence is vital for comprehensive traffic analysis.

5.5 Conclusions and Future Work

This work presents a novel HH approach, including a method for segmenting vehicles in video frames captured by traffic cameras, which were rigorously tested through three comprehensive sets of experiments.

The study commences by subjecting HHGATSD to a rigorous evaluation, testing it on 29 functions from the IEEE CEC2017 benchmark for optimization problems. The results consistently showcase its robustness and competitive performance in 30 and 50 dimensions, surpassing seven state-of-the-art optimization algorithms. Results validate the proposal's performance through convergence graph analysis and Friedman's non-parametric statistical test, establishing it as the highest-ranked algorithm for both dimensions.

Next, an experiment focused on image segmentation with implications for object recognition and scene analysis was applied. Multilevel segmentation was applied to ten random images selected from the BSDS500. In these experiments, 2, 4, 6, 6, 8, and 10 thresholds were used, in which the proposed approach consistently outperformed the other optimization algorithms in terms of fitness, PSNR, SSIM, and FSIM. Notably, it secures the top-rank in Friedman's non-parametric test for objective function minimization and the FSIM metric, attesting to its efficacy in accurately delineating object boundaries in various imaging contexts. However, due to the low dimensionality of the problems used, it did not exhibit significant differences in most cases during the Holm test.

The culmination of our research trials involves the application of our methodology to vehicle segmentation in traffic video sequences, yielding promising results. HHGATSD plays a pivotal role in multilevel image segmentation, outperforming three commonly used techniques in overlap metrics by comparing the obtained mask against ground truth, particularly in DSC, IoU, R, and ACC. These results underscore its suitability for moving object segmentation in complex traffic environments, and its ability to maintain low STD values in these metrics highlights its consistency, a critical aspect in object tracking applications.

6

Conclusions and Future Work

This final chapter provides a summary of the main contributions, limitations, and future research directions that arise from this thesis. Firstly, Section 6.1 presents a comprehensive overview of the results and contributions. Next, the limitations of these contributions are identified, and potential areas for future research are discussed in Section 6.2. Finally, Section 6.3 lists the publications carried out as a co-author that derived from the knowledge gained during the Ph.D.

6.1 Summary of Contributions

The surge in e-commerce has underscored the critical role of Last-Mile Logistics (LML). The rapid expansion of online shopping, coupled with the COVID-19 pandemic, has brought to the forefront the need for efficient and resilient LML systems within urban environments. These systems connect businesses with consumers and have a significant impact on urban infrastructure and the efficiency of logistics.

This thesis aimed to investigate the evolving challenges and social impacts faced by Logistics Service Providers (LSPs) in urban settings, highlighting the growing need for effective and sustainable solutions.

To tackle the challenges associated with urban logistics, strategic policies are essential to facilitate its development. These policies are designed to enhance the efficiency and sustainability of urban logistics, focusing on their economic, social, and environmental impacts.

The research examined three policies for optimizing LML: Vehicle Fleet Electrification, Demand Aggregation Infrastructure, and Enhanced Traffic Management. Each policy introduces different challenges and opportunities for improving urban logistics efficiency. Vehicle Fleet Electrification aims to reduce emissions and operational costs. In contrast, Demand Aggregation Infrastructure seeks to refine delivery systems and reduce the failed

delivery rate. On the other hand, Enhanced Traffic Management is designed to mitigate urban congestion and improve mobility. These policies are instrumental in shaping the future of urban logistics, addressing specific objectives and challenges within each domain.

The contributions made in this doctoral thesis within the LML optimization field for the policies targeting LSPs and urban societal benefits are summarized below. These contributions provide insights into the research questions posed in Section 1.1, and are structured accordingly:

- *Is it possible to develop a new optimization method based on Hyper-heuristics (HHs) that are more efficient and scalable than existing state-of-the-art methods for solving the Capacitated Electric Vehicle Routing Problem (CEVRP), addressing the challenges associated with high-dimensional instances?*

  In this Ph.D. thesis, the HH algorithm the Hyper-Heuristic Adaptive Simulated Annealing and Reinforcement Learning (HHASA_{RL}) has been proposed to address the optimization challenges of high-dimensional CEVRP, overcoming the limitations of existing state-of-the-art methods. This approach hybridized the well-established Metropolis criterion from the self-adaptive Simulated Annealing (SA) as a movement acceptance mechanism with the Reinforcement Learning (RL) algorithm as a heuristic selection mechanism. Experimental results demonstrated the superior performance of the HHASA_{RL} on the IEEE WCCI2020 competition benchmark, outperforming all comparative state-of-the-art algorithms using the same dataset. Notably, the algorithm identified multiple new best-known solutions for high-dimensional instances. Among the three variations of the HHASA_{RL} algorithm, HHASA_{TS} is distinguished as the top-performing algorithm, as evidenced by average results and non-parametric tests. HHASA_{TS} employs the Thompson Sampling method to address the Multi-Armed Bandit (MAB) problem. Consequently, the findings affirmatively conclude that the answer to the research question is positive.

- *Could a more realistic model for the Stationary Parcel Locker (SPL) problem be developed that incorporates stochastic demand, costs, locker capacities, dynamic collection periods, and the prediction of customer acceptance choices?* and *Is the Genetic Algorithm (GA) a competitive method to solve this more realistic and complex model of the SPL problem?*

  In this thesis, the Locker Location Problem with Constraints on the Luce Threshold Model (CLLPTLM) is formulated to handle the challenges of locker allocation, incorporating more realistic factors to enhance the strategic positioning of SPLs. The goal is to maximize the profit for LSPs by optimizing the balance between generated revenue and service costs. To achieve this, an adapted GA has been designed specifically to address the SPL location problem with capacity constraints. This modification allows the algorithm to efficiently process large-scale problem instances, a capability substantiated through extensive computational experiments. The effectiveness of the proposed method is validated using both synthetic and real datasets, demonstrating that the adapted GA consistently yields highly efficient solutions for the CLLPTLM optimization problem across a range of testing scenarios. Such results underscore the adaptability and scalability of the method, proving its competence

in tackling complex real-world problems. Furthermore, a comprehensive sensitivity analysis is performed to elucidate the influence of various problem parameters on the obtained solutions. With this contribution, positive responses to both posed research questions regarding the development of a more realistic SPL model and the competitiveness of GA in solving this enhanced model are conclusively established.

- *Can an efficient HH algorithm be developed for optimizing vehicle segmentation in image-based traffic monitoring that accounts for the variability of environmental conditions and real-time traffic dynamics?*

  This dissertation introduces the Hyper-heuristic Genetic Algorithm based on Thompson Sampling with Diversity (HHGATSD) algorithm, designed to be integrated into a vehicle segmentation methodology, that uses advanced image processing techniques to improve the accuracy and efficiency of vehicle detection in dynamic urban traffic environments, considering light variability and real-time traffic dynamics. The algorithm is tested and validated on multiple datasets, demonstrating its effectiveness and robustness, outperforming all comparative algorithms. To validate the performance is evaluated against the IEEE CEC2017 benchmark in 30 and 50 dimensions to address optimization challenges. In the domain of image segmentation, a random selection of images from the BSDS500 dataset is analyzed to evaluate the capabilities of the algorithm in object recognition and scene analysis. Moreover, the application of HH to vehicle segmentation in traffic video frames is studied, and the results are compared with ground-truth data to confirm the accuracy and reliability. The results showed that the proposed algorithm outperforms other methods in vehicle segmentation, providing a positive answer to the research question.

In summary, the advancements detailed in this thesis reflect significant strides in addressing the complex challenges of LML within urban environments. By developing and validating innovative algorithms like HHASA$_{RL}$ and HHGATSD and refining models such as CLLPTLM, this research contributes valuable insights and tools to the field of urban logistics. These contributions not only enhance the operational efficiency of LML but also consider the broader implications for sustainability and urban mobility.

6.2 Limitations and Future Work

Despite the significant contributions, this thesis also identifies areas for further research and potential limitations that future work could address:

- While the HHASA$_{RL}$ algorithm demonstrates considerable success in optimizing the high-dimensional CEVRP and outperforms existing state-of-the-art methods, there is potential for further refinement and expansion. Future studies could integrate advanced machine learning predictive models to enhance decision-making processes within the algorithm, particularly in anticipating charging needs and optimizing routes. Another study line could be incorporating deep RL techniques for a more accurate heuristic selection mechanism, thereby extending the adaptability of the algorithm and effectiveness to a broader range of complex routing scenarios, including various constraints and dynamic environments such as CEVRP with time windows.

- The CLLPTLM model incorporates more realistic elements than the existing state-of-the-art models, such as stochastic demand, dynamic collection periods, locker capacity constraints, and the consideration of customer acceptance probability for the strategic positioning of SPLs. Despite these advancements, further research opportunities exist to enhance its realism and applicability. Future developments could explore environmental factors, like congestion and energy usage, extending beyond the spatial configuration of lockers to reduce delivery distances and associated costs. Moreover, the model could prioritize locations that are more accessible to public transportation, thereby boosting its sustainability.

- Although the HHGATSD algorithm shows effective and robust performance in vehicle segmentation methodology for traffic video frames and optimization benchmarks for 30 and 50 dimensions, there is potential for further enhancement to ensure its applicability in real-world settings since its current testing is limited to 2D view. Future studies could broaden the applicability of the HHGATSD by incorporating data from multiple camera angles, thereby improving the precision of road occupancy rates and traffic density analysis. Moreover, testing the algorithm with datasets comprising images obtained in adverse weather conditions, such as during snowfall or rain, would be advantageous.

In future work, the directions for subsequent research highlight the opportunity to expand upon the foundational insights presented in this thesis. By addressing the identified limitations and exploring the proposed enhancements and new application domains, future studies can broaden the scope and influence of this work. Advancing these methodologies and models will contribute to the development of more intelligent and sustainable urban logistics systems, providing significant benefits to both LSPs and society.

6.3 Other Publications

In addition to the scientific publications that underpin this research, this section presents additional works derived from the insights gained in the area of MH and HH algorithms throughout this doctoral thesis. These collaborative publications, developed in conjunction with fellow researchers, are listed below by year:

- **2021:**
  Journals:
  - O. Ramos-Soto, **E. Rodríguez-Esparza**, S. E. Balderas-Mata, D. Oliva, A. E. Hassanien, R. K. Meleppat and R. J. Zawadzki, "An efficient retinal blood vessel segmentation in eye fundus images by using optimized top-hat and homomorphic filtering", *Computer Methods and Programs in Biomedicine*. [180]
    (IF = 7.02 → Q1)
  - H. Ayaz, **E. Rodríguez-Esparza**, M. Ahmad, D. Oliva, M. Pérez-Cisneros and R. Sarkar, "Classification of Apple Disease based on Non-linear Deep Features", *Applied Science*. [181]
    (IF = 2.83 → Q2)

Conferences:

- O. Ramos-Soto, **E. Rodríguez-Esparza**, M. Pérez-Cisneros and S. E. Balderas-Mata, "Inner limiting membrane segmentation and surface visualization method on retinal OCT images", SPIE in Medical Imaging: Biomedical Applications in Molecular, Structural, and Functional Imaging, California, U.S.A. [182]
- M. S. R. Martins, D. Oliva, **E. Rodriguez-Esparza**, M. Delgado, R. Lüders, M. El Yafrani, L. L. M. Melo Junior, M. Abd Elaziz and M. Pérez-Cisneros, "A selection hyperheuristic guided by Thompson Sampling for numerical optimization", Genetic and Evolutionary Computation Conference, Lille, France. [183]

Book Chapter:

- J. Murillo-Olmos, **E. Rodríguez-Esparza**, M. Pérez-Cisneros, D. Zaldivar, E. Cuevas, G. Trejo-Caballero, A. A. Juan, "Thresholding algorithm applied to Chest X-Ray images with Pneumonia", in Metaheuristics in Machine Learning: Theory and Applications, Springer International Publishing. [184]

- **2022:**
  Journal:
  - N. Ortega-Sánchez, **E. Rodríguez-Esparza**, D. Oliva, M. Pérez-Cisneros A. Wagdy Mohamed and G. Dhiman, "Identification of apple diseases in digital images by using the Gaining-sharing knowledge based algorithm for multilevel thresholding", *Soft Computing*. [185]
    (IF = 3.73 → Q2)

  Book Chapter:
  - A. Acosta, A. Ochoa, **E. Rodríguez-Esparza**, D. Oliva, A. A. Juan, G. Pajares, "Classification System to Detect Diseases in Apples by Using a Convolutional Neural Network", in Technological and Industrial Applications Associated With Industry 4.0, Springer International Publishing. [186]

- **2023:**
  Conferences:
  - B. Morales-Castañeda, **E. Rodríguez-Esparza**, D. Oliva, A. Casas-Ordaz, A. Valdivia, M. A. Navarro, A. Ramos-Michel and S. Jalaleddin Mousavirad, "A novel diversity-aware inertia weight and velocity control for particle swarm optimization", IEEE Congress on Evolutionary Computation (CEC), Chicago, U.S.A. [187]
  - M. A. Navarro, **E. Rodríguez-Esparza**, B. Morales-Castañeda, A. Ramos-Michel, D. Oliva, A. Valdivia and A. Casas-Ordaz, "An hyper-heuristic based population management through statistical analysis and phases optimization", IEEE Congress on Evolutionary Computation (CEC), Chicago, U.S.A. [188]

  - B. Morales-Castañeda, D. Oliva, M. A. Navarro, A. Ramos-Michel, A. Valdivia, A. Casas-Ordaz, **E. Rodríguez-Esparza** and S. Jalaleddin Mousavirad, "Improving the convergence of the PSO algorithm with a stagnation variable and fuzzy logic", IEEE Congress on Evolutionary Computation (CEC), Chicago, U.S.A. [189]
  - E. Perez-Zarate, O. Ramos-Soto, **E. Rodriguez-Esparza** and G. Aguilar, "LoLi-IEA: Low-Light image enhancement algorithm", SPIE in Medical Imaging: Biomedical Applications in Molecular, Structural, and Functional Imaging, San Diego U.S.A. [190]

- **2024:**
  Journal:

  - **E. Rodríguez-Esparza**, B. Morales-Castañeda, A. Casas-Ordaz, D. Oliva, M. A. Navarro, A. Valdivia and E. H. Houssein, "Handling the balance of operators in evolutionary algorithms through a weighted Hill Climbing approach", *Knowledge-Based Systems*. [191]
    (IF = 8.8 → Q1)
  - E. Perez-Zarate, O. Ramos-Soto, **E. Rodríguez-Esparza** and D. Oliva, "AFEN: Multi-Channel Residual Blocks for Enhanced Low-Light Underwater Vision", *IEEE Transactions on Image Processing*. **Under review**
    (IF = 10.6 → Q1)
  - O. Ramos-Soto, J. A. Ramos-Frutos, **E. Rodríguez-Esparza**, D. Oliva and S. E. Balderas-Mata, "Visual enhancement of chest X-ray scans through metaheuristic-based optimization of Gamma correction and CLAHE", *IEEE Transactions on Image Processing*. **Under review**
    (IF = 7.7 → Q1)

  Conferences:

  - A. Casas-Ordaz, A. Valdivia, E. H. Haro, D. Oliva, L. A. Beltrán, I. Aranguren, **E. Rodríguez-Esparza** and D. Campos-Peña, "IDEL: An Improved Differential Evolution with Lissajous Mutation", IEEE Congress on Evolutionary Computation (CEC), Yokohama, Japan.
  - B. Morales-Castañeda, **E. Rodríguez-Esparza**, D. Oliva, M. A. Navarro, I. Aranguren, A. Casas Ordaz, L. A. Beltran and S. Zapotecas-Martinez, "Adaptability and Efficiency in Population Management: A multi-population CMA-ES Strategy for High-Dimensional Optimization", International Conference on Knowledge-Based and Intelligent Information & Engineering Systems (KES), Seville, Spain.

  Book Chapter:

  - O. Ramos-Soto, **E. Rodríguez-Esparza**, F. Carrasco-Hernández and S. E. Balderas-Mata, "A Hybrid Approach for Optic Disc Localization in Eye Fundus

Images", in Metaheuristics in Machine Learning: Theory and Applications, Springer International Publishing. **Under Review**

Bibliography

[1] Y. Vakulenko, P. Shams, D. Hellström, and K. Hjort, "Service innovation in e-commerce last mile delivery: Mapping the e-customer journey," *Journal of Business Research*, vol. 101, pp. 461–468, 2019.

[2] C. Archetti and L. Bertazzi, "Recent challenges in routing and inventory routing: E-commerce and last-mile delivery," *Networks*, vol. 77, no. 2, pp. 255–268, 2021.

[3] N. Boysen, S. Fedtke, and S. Schwerdfeger, "Last-mile delivery concepts: a survey from an operational research perspective," *Or Spectrum*, vol. 43, pp. 1–58, 2021.

[4] S. M. Patella, G. Grazieschi, V. Gatta, E. Marcucci, and S. Carrese, "The adoption of green vehicles in last mile logistics: A systematic review," *Sustainability*, vol. 13, no. 1, 2021. [Online]. Available: https://www.mdpi.com/2071-1050/13/1/6

[5] A. Bhatti, H. Akram, H. M. Basit, A. U. Khan, S. M. Raza, and M. B. Naqvi, "E-commerce trends during covid-19 pandemic," *International Journal of Future Generation Communication and Networking*, vol. 13, no. 2, pp. 1449–1452, 2020.

[6] D. Miljenović and B. Beriša, "Pandemics trends in e-commerce: drop shipping entrepreneurship during covid-19 pandemic," *Pomorstvo*, vol. 36, no. 1, pp. 31–43, 2022.

[7] S. Singh, R. Kumar, R. Panchal, and M. K. Tiwari, "Impact of covid-19 on logistics systems and disruptions in food supply chain," *International Journal of Production Research*, vol. 59, no. 7, pp. 1993–2008, 2021.

[8] N. Giuffrida, J. Fajardo-Calderin, A. D. Masegosa, F. Werner, M. Steudter, and F. Pilla, "Optimization and machine learning applied to last-mile logistics: A review," *Sustainability*, vol. 14, no. 9, 2022. [Online]. Available: https://www.mdpi.com/2071-1050/14/9/5329

[9] R. W. Goodman, "Whatever you call it, just don't think of last-mile logistics, last," *Global Logistics & Supply Chain Strategies*, vol. 9, no. 12, 2005.

[10] P. Martin. (2018) Statista. Supply chain: share of total costs by type worldwide 2018. [Online]. Available: https://www.statista.com/statistics/1043253/share-of-total-supply-chain-costs-by-type-worldwide/

[11] R. Gevaers, E. Van de Voorde, and T. Vanelslander, "Characteristics and typology of last-mile logistics from an innovation perspective in an urban context," in *City distribution and urban freight transport*. Edward Elgar Publishing, 2011.

[12] J. N. Gonzalez, L. Garrido, and J. M. Vassallo, "Exploring stakeholders' perspectives to improve the sustainability of last mile logistics for e-commerce in urban areas," *Research in Transportation Business & Management*, vol. 49, p. 101005, 2023.

[13] I. M. Fund, "Macroeconomic issues in small states and implications for fund engagement," *Strategy, Policy, and Review Department, in collaboration with other IMF Departments*, 2013.

[14] A. Can and P. Aumond, "Estimation of road traffic noise emissions: The influence of speed and acceleration," *Transportation Research Part D: Transport and Environment*, vol. 58, pp. 155–171, 2018.

[15] M. Awwad, A. Shekhar, and A. Iyer, "Sustainable last-mile logistics operation in the era of e-commerce," in *Proceedings of the International Conference on Industrial Engineering and Operations Management*, 2018, pp. 584–591.

[16] V. Monteiro, J. A. Afonso, J. C. Ferreira, and J. L. Afonso, "Vehicle electrification: New challenges and opportunities for smart grids," *Energies*, vol. 12, no. 1, p. 118, 2018.

[17] S. Moslem and F. Pilla, "Planning location of parcel lockers using group analytic hierarchy process in spherical fuzzy environment," *Transportation Research Interdisciplinary Perspectives*, vol. 24, p. 101024, 2024.

[18] S. Maerivoet, K. Carlier, B. Ons, A. Wijbenga, S. Boerma, J. Vreeswijk, E. Mintsis, D. Koutras, V. Karagounis, X. Zhang *et al.*, "Enhanced traffic management procedures of connected and autonomous vehicles in transition areas," 2020.

[19] E. B. Bayarçelik and H. B. Bumin Doyduk, "Digitalization of business logistics activities and future directions," *Digital Business Strategies in Blockchain Ecosystems: Transformational Design and Future of Global Business*, pp. 201–238, 2020.

[20] M. Woschank, E. Rauch, and H. Zsifkovits, "A review of further directions for artificial intelligence, machine learning, and deep learning in smart logistics," *Sustainability*, vol. 12, no. 9, p. 3760, 2020.

[21] M. Sánchez, J. M. Cruz-Duarte, J. carlos Ortíz-Bayliss, H. Ceballos, H. Terashima-Marin, and I. Amaya, "A systematic review of hyper-heuristics on combinatorial optimization problems," *IEEE Access*, vol. 8, pp. 128 068–128 095, 2020.

[22] F. Peres and M. Castelli, "Combinatorial optimization problems and metaheuristics: Review, challenges, design, and development," *Applied Sciences*, vol. 11, no. 14, p. 6449, 2021.

[23] P. P. Oteiza, J. I. Ardenghi, and N. B. Brignole, "Parallel hyper-heuristics for process engineering optimization," *Computers & Chemical Engineering*, vol. 153, p. 107440, 2021.

[24] C.-C. Lu, S. Yan, H.-C. Li, A. Diabat, and H.-T. Wang, "Optimal fleet deployment for electric vehicle sharing systems with the consideration of demand uncertainty," *Computers & Operations Research*, vol. 135, p. 105437, 2021.

[25] C. Büsing, T. Gersing, and S. Wrede, "Analysing the complexity of facility location problems with capacities, revenues, and closest assignments." in *INOC*, 2022, pp. 1–6.

[26] A. Chaudhuri, "Smart traffic management of vehicles using faster r-cnn based deep learning method," *arXiv preprint arXiv:2311.10099*, 2023.

[27] A. Kutlimuratov, J. Khamzaev, T. Kuchkorov, M. S. Anwar, and A. Choi, "Applying enhanced real-time monitoring and counting method for effective traffic management in tashkent," *Sensors*, vol. 23, no. 11, p. 5007, 2023.

[28] E. Rodríguez-Esparza, A. D. Masegosa, D. Oliva, and E. Onieva, "A new hyper-heuristic based on adaptive simulated annealing and reinforcement learning for the capacitated electric vehicle routing problem," *arXiv preprint arXiv:2206.03185*, 2022.

[29] E. Rodríguez-Esparza, E. Kampitakis, A. D. Masegosa, E. Onieva, and E. I. Vlahogianni, "A two-phase metaheuristic approach for the parcel locker location problem: First select then merge," in *2023 8th International Conference on Models and Technologies for Intelligent Transportation Systems (MT-ITS)*. IEEE, 2023, pp. 1–6.

[30] E. Rodríguez-Esparza, O. Ramos-Soto, A. D. Masegosa, E. Onieva, D. Oliva, A. Arriandiaga, and A. Ghosh, "Optimizing road traffic surveillance: A robust hyper-heuristic approach for vehicle segmentation," *IEEE Access*, vol. 12, pp. 29 503–29 524, 2024.

[31] M. Kress *et al.*, "Operational logistics," *The Art and Science of Sustaining Military Operations*, 2002.

[32] H. Cherevko, V. Kolodiichuk, and I. Kolodiichuk, "Historical and meritorical genesis of logistics," *Zeszyty Naukowe Szkoły Głównej Gospodarstwa Wiejskiego w Warszawie. Ekonomika i Organizacja Logistyki*, no. 4 [4, pp. 5–12, 2019.

[33] H. Zijm, M. Klumpp, A. Regattieri, S. Heragu *et al.*, *Operations, logistics and supply chain management*. Springer, 2019.

[34] J. F. Magee, W. C. Copacino, and D. B. Rosenfield, *Modern logistics management: Integrating marketing, manufacturing and physical distribution*. John Wiley & Sons, 1985, vol. 22.

[35] A. Rushton, P. Croucher, and P. Baker, *The handbook of logistics and distribution management: Understanding the supply chain*. Kogan Page Publishers, 2022.

[36] L. Li, *Managing supply chain and logistics: Competitive strategy for a sustainable future*. World Scientific Publishing Company, 2014.

[37] M. Kmiecik, "Logistics coordination based on inventory management and transportation planning by third-party logistics (3pl)," *Sustainability*, vol. 14, no. 13, p. 8134, 2022.

[38] M. Klumpp and S. Heragu, "Outbound logistics and distribution management," *Operations, Logistics and Supply Chain Management*, pp. 305–330, 2019.

[39] A. M. Caunhye, X. Nie, and S. Pokharel, "Optimization models in emergency logistics: A literature review," *Socio-economic planning sciences*, vol. 46, no. 1, pp. 4–13, 2012.

[40] R. Farahani, *Logistics operations and management: concepts and models*. Elsevier, 2011.

[41] V. Sanchez-Rodrigues, A. Potter, and M. M. Naim, "The impact of logistics uncertainty on sustainable transport operations," *International Journal of Physical Distribution & Logistics Management*, vol. 40, no. 1/2, pp. 61–83, 2010.

[42] R. Sarraj, E. Ballot, S. Pan, D. Hakimi, and B. Montreuil, "Interconnected logistic networks and protocols: simulation-based efficiency assessment," *International Journal of Production Research*, vol. 52, no. 11, pp. 3185–3208, 2014.

[43] W. Van Heeswijk, M. Mes, and M. Schutten, "Transportation management," *Operations, Logistics and supply chain management*, pp. 469–491, 2019.

[44] S. Lim, X. Jin, and J. Srai, "Last-mile logistics structures: a literature review and design guideline," *Institute for Manufacturing, Cambridge University*, 2016.

[45] H. S. Na, S. J. Kweon, and K. Park, "Characterization and design for last mile logistics: A review of the state of the art and future directions," *Applied Sciences*, vol. 12, no. 1, p. 118, 2021.

[46] R. Raj, A. Singh, V. Kumar, T. De, and S. Singh, "Assessing the e-commerce last-mile logistics' hidden risk hurdles," *Cleaner Logistics and Supply Chain*, vol. 10, p. 100131, 2024.

[47] T. Bosona, "Urban freight last mile logistics—challenges and opportunities to improve sustainability: a literature review," *Sustainability*, vol. 12, no. 21, p. 8769, 2020.

[48] D. Oliva, M. Abd Elaziz, and S. Hinojosa, *Metaheuristic algorithms for image segmentation: theory and applications*. Springer, 2019.

[49] D. Oliva, E. H. Houssein, and S. Hinojosa, *Metaheuristics in machine learning: theory and applications*. Springer, 2021, vol. 967.

[50] B. Chopard and M. Tomassini, *An introduction to metaheuristics for optimization*. Springer, 2018.

[51] S. Salhi, "Handbook of metaheuristics," *Journal of the Operational Research Society*, vol. 65, no. 2, pp. 320–320, 2014.

[52] F. Bennis and R. K. Bhattacharjya, *Nature-Inspired Methods for Metaheuristics Optimization: Algorithms and Applications in Science and Engineering*. Springer, 2020, vol. 16.

[53] M. Iqbal, M. Azam, M. Naeem, A. S. Khwaja, and A. Anpalagan, "Optimization classification, algorithms and tools for renewable energy: A review," *Renewable and sustainable energy reviews*, vol. 39, pp. 640–654, 2014.

[54] B. E. Woodworth and N. Srebro, "Tight complexity bounds for optimizing composite objectives," *Advances in neural information processing systems*, vol. 29, 2016.

[55] M. Fathi, M. Khakifirooz, A. Diabat, and H. Chen, "An integrated queuing-stochastic optimization hybrid genetic algorithm for a location-inventory supply chain network," *International Journal of Production Economics*, vol. 237, p. 108139, 2021.

[56] M. Abdel-Basset, L. Abdel-Fatah, and A. K. Sangaiah, "Metaheuristic algorithms: A comprehensive review," *Computational intelligence for multimedia big data on the cloud with engineering applications*, pp. 185–231, 2018.

[57] Y. F. Yiu, J. Du, and R. Mahapatra, "Evolutionary heuristic a* search: Heuristic function optimization via genetic algorithm," in *2018 IEEE First International Conference on Artificial Intelligence and Knowledge Engineering (AIKE)*. IEEE, 2018, pp. 25–32.

[58] B. Morales-Castañeda, D. Zaldivar, E. Cuevas, F. Fausto, and A. Rodríguez, "A better balance in metaheuristic algorithms: Does it exist?" *Swarm and Evolutionary Computation*, vol. 54, p. 100671, 2020.

[59] A. L. B. Almeida, J. d. C. Lima, and M. A. M. Carvalho, "Systematic literature review on parallel trajectory-based metaheuristics," *ACM Computing Surveys*, vol. 55, no. 8, pp. 1–34, 2022.

[60] G. Wu, R. Mallipeddi, and P. N. Suganthan, "Ensemble strategies for population-based optimization algorithms–a survey," *Swarm and evolutionary computation*, vol. 44, pp. 695–711, 2019.

[61] D. H. Wolpert and W. G. Macready, "No free lunch theorems for optimization," *IEEE transactions on evolutionary computation*, vol. 1, no. 1, pp. 67–82, 1997.

[62] L. Serafino, "The no free lunch theorem: What are its main implications for the optimization practice?" in *Black Box Optimization, Machine Learning, and No-Free Lunch Theorems*. Springer, 2021, pp. 357–372.

[63] J. McDermott, "When and why metaheuristics researchers can ignore "no free lunch" theorems," *SN Computer Science*, vol. 1, no. 1, p. 60, 2020.

[64] T. Dokeroglu, T. Kucukyilmaz, and E.-G. Talbi, "Hyper-heuristics: A survey and taxonomy," *Computers & Industrial Engineering*, p. 109815, 2023.

[65] J. H. Drake, A. Kheiri, E. Özcan, and E. K. Burke, "Recent advances in selection hyper-heuristics," *European Journal of Operational Research*, vol. 285, no. 2, pp. 405–428, 2020.

[66] P. Ross, "Hyper-heuristics," *Search methodologies: introductory tutorials in optimization and decision support techniques*, pp. 529–556, 2005.

[67] E. K. Burke, M. R. Hyde, G. Kendall, G. Ochoa, E. Özcan, and J. R. Woodward, "A classification of hyper-heuristic approaches: revisited," *Handbook of metaheuristics*, pp. 453–477, 2019.

[68] E. K. Burke, M. Hyde, G. Kendall, G. Ochoa, E. Özcan, and J. R. Woodward, "A classification of hyper-heuristic approaches," *Handbook of metaheuristics*, pp. 449–468, 2010.

[69] E. K. Burke, M. Gendreau, M. Hyde, G. Kendall, G. Ochoa, E. Özcan, and R. Qu, "Hyper-heuristics: A survey of the state of the art," *Journal of the Operational Research Society*, vol. 64, pp. 1695–1724, 2013.

[70] S. Erdoğan and E. Miller-Hooks, "A green vehicle routing problem," *Transportation research Part E: logistics and transportation review*, vol. 48, no. 1, pp. 100–114, 2012.

[71] G. Clarke and J. W. Wright, "Scheduling of vehicles from a central depot to a number of delivery points," *Operations research*, vol. 12, no. 4, pp. 568–581, 1964.

[72] M. Ester, H.-P. Kriegel, J. Sander, X. Xu *et al.*, "A density-based algorithm for discovering clusters in large spatial databases with noise," in *kdd*, vol. 96, no. 34, 1996, pp. 226–231.

[73] S. Pelletier, O. Jabali, and G. Laporte, "50th anniversary invited article—goods distribution with electric vehicles: review and research perspectives," *Transportation science*, vol. 50, no. 1, pp. 3–22, 2016.

[74] T. Erdelić and T. Carić, "A survey on the electric vehicle routing problem: variants and solution approaches," *Journal of Advanced Transportation*, vol. 2019, 2019.

[75] M. Schneider, A. Stenger, and D. Goeke, "The electric vehicle-routing problem with time windows and recharging stations," *Transportation science*, vol. 48, no. 4, pp. 500–520, 2014.

[76] H. Mao, J. Shi, Y. Zhou, and G. Zhang, "The electric vehicle routing problem with time windows and multiple recharging options," *IEEE Access*, vol. 8, pp. 114 864–114 875, 2020.

[77] J. Shi, Y. Gao, W. Wang, N. Yu, and P. A. Ioannou, "Operating electric vehicle fleet for ride-hailing services with reinforcement learning," *IEEE Transactions on Intelligent Transportation Systems*, vol. 21, no. 11, pp. 4822–4834, 2019.

[78] B. Lin, B. Ghaddar, and J. Nathwani, "Deep reinforcement learning for electric vehicle routing problem with time windows," *arXiv preprint arXiv:2010.02068*, 2020.

[79] J. Zhao, M. Mao, X. Zhao, and J. Zou, "A hybrid of deep reinforcement learning and local search for the vehicle routing problems," *IEEE Transactions on Intelligent Transportation Systems*, 2020.

[80] A. Bogyrbayeva, S. Jang, A. Shah, Y. J. Jang, and C. Kwon, "A reinforcement learning approach for rebalancing electric vehicle sharing systems," *IEEE Transactions on Intelligent Transportation Systems*, 2021.

[81] M. Keskin and B. Çatay, "Partial recharge strategies for the electric vehicle routing problem with time windows," *Transportation Research Part C: Emerging Technologies*, vol. 65, pp. 111–127, 2016.

[82] ——, "A matheuristic method for the electric vehicle routing problem with time windows and fast chargers," *Computers & operations research*, vol. 100, pp. 172–188, 2018.

[83] A. Montoya, C. Guéret, J. E. Mendoza, and J. G. Villegas, "A multi-space sampling heuristic for the green vehicle routing problem," *Transportation Research Part C: Emerging Technologies*, vol. 70, pp. 113–128, 2016.

[84] ——, "The electric vehicle routing problem with nonlinear charging function," *Transportation Research Part B: Methodological*, vol. 103, pp. 87–110, 2017.

[85] M. Peppel and S. Spinler, "The impact of optimal parcel locker locations on costs and the environment," *International Journal of Physical Distribution & Logistics Management*, vol. 52, no. ahead-of-print, 2022.

[86] Y. Deutsch and B. Golany, "A parcel locker network as a solution to the logistics last mile problem," *International Journal of Production Research*, vol. 56, no. 1-2, pp. 251–261, 2018.

[87] Y. H. Lin, Y. Wang, D. He, and L. H. Lee, "Last-mile delivery: Optimal locker location under multinomial logit choice model," *Transportation Research Part E: Logistics and Transportation Review*, vol. 142, p. 102059, 2020.

[88] G. Yang, Y. Huang, Y. Fu, B. Huang, S. Sheng, L. Mao, S. Huang, Y. Xu, J. Le, Y. Ouyang *et al.*, "Parcel locker location based on a bilevel programming model," *Mathematical Problems in Engineering*, vol. 2020, 2020.

[89] R. Luo, S. Ji, and Y. Ji, "An active-learning pareto evolutionary algorithm for parcel locker network design considering accessibility of customers," *Computers & Operations Research*, vol. 141, p. 105677, 2022.

[90] Z.-H. Che, T.-A. Chiang, and Y.-J. Luo, "Multiobjective optimization for planning the service areas of smart parcel locker facilities in logistics last mile delivery," *Mathematics*, vol. 10, no. 3, 2022.

[91] Y. Lin, Y. Wang, L. H. Lee, and E. P. Chew, "Profit-maximizing parcel locker location problem under threshold luce model," *Transportation Research Part E: Logistics and Transportation Review*, vol. 157, p. 102541, 2022.

[92] M. Kahr, "Determining locations and layouts for parcel lockers to support supply chain viability at the last mile," *Omega*, vol. 113, p. 102721, 2022.

[93] S. Mancini, M. Gansterer, and C. Triki, "Locker box location planning under uncertainty in demand and capacity availability," *Omega*, p. 102910, 2023.

[94] P. Yunusoglu and M. G. Avci, "Optimizing parcel locker locations with pricing decisions in last-mile delivery," in *Towards Industry 5.0: Selected Papers from ISPR2022, October 6–8, 2022, Antalya*. Springer, 2023, pp. 641–648.

[95] A. Khassiba and D. Delahaye, "Simulated-annealing hyper-heuristic for demand-capacity balancing in air traffic flow management," in *SESAR Innovation Days*, 2022.

[96] X.-C. Liao, Y.-H. Jia, X.-M. Hu, and W.-N. Chen, "Uncertain commuters assignment through genetic programming hyper-heuristic," *IEEE Transactions on Computational Social Systems*, 2023.

[97] W. Zheng, L. Jinlong, and Z. Jingling, "Hyper-heuristic algorithm for traffic flow-based vrp with simultaneous delivery and pickup," *Journal of Computational Design and Engineering*, p. qwad097, 2023.

[98] P. B. Prakoso and Y. Sari, "Vehicle detection using background subtraction and clustering algorithms," *TELKOMNIKA (Telecommunication Computing Electronics and Control)*, vol. 17, no. 3, pp. 1393–1398, 2019.

[99] X. Hu, X. Xu, Y. Xiao, H. Chen, S. He, J. Qin, and P.-A. Heng, "Sinet: A scale-insensitive convolutional neural network for fast vehicle detection," *IEEE transactions on intelligent transportation systems*, vol. 20, no. 3, pp. 1010–1019, 2018.

[100] V. S. Sindhu, "Vehicle identification from traffic video surveillance using yolov4," in *2021 5th international conference on intelligent computing and control systems (ICICCS)*. IEEE, 2021, pp. 1768–1775.

[101] A. Kashevnik and A. Ali, "3d vehicle detection and segmentation based on efficientnetb3 and centernet residual blocks," *Sensors*, vol. 22, no. 20, p. 7990, 2022.

[102] X. Huang, D. Mu, and Z. Li, "Intelligent traffic analysis: A heuristic high-dimensional image search algorithm based on spatiotemporal probability for constrained environments," *Alexandria Engineering Journal*, vol. 59, no. 3, pp. 1413–1423, 2020.

[103] C. S. Priya and F. S. Francis, "A novel lorawan-based real-time traffic analysis approach for vehicle congestion estimation," in *2023 Winter Summit on Smart Computing and Networks (WiSSCoN)*. IEEE, 2023, pp. 1–6.

[104] P. Menga, R. Buccianti, M. Bedogni, and S. Moroni, "Promotion of freight mobility in milan: Environmental, energy and economical aspects," *World Electric Vehicle Journal*, vol. 6, no. 4, pp. 1014–1020, 2013.

[105] C. Wang, F. Qin, X. Xiang, H. Jiang, and X. Zhang, "A dual-population based co-evolutionary algorithm for capacitated electric vehicle routing problems," *IEEE Transactions on Transportation Electrification*, 2023.

[106] M. Mavrovouniotis, G. Ellinas, and M. Polycarpou, "Ant colony optimization for the electric vehicle routing problem," in *2018 IEEE Symposium Series on Computational Intelligence (SSCI)*. IEEE, 2018, pp. 1234–1241.

[107] M. Mavrovouniotis, C. Menelaou, S. Timotheou, G. Ellinas, C. Panayiotou, and M. Polycarpou, "A benchmark test suite for the electric capacitated vehicle routing problem," in *2020 IEEE Congress on Evolutionary Computation (CEC)*. IEEE, 2020, pp. 1–8.

[108] S. Kirkpatrick, C. D. Gelatt, and M. P. Vecchi, "Optimization by simulated annealing," *science*, vol. 220, no. 4598, pp. 671–680, 1983.

[109] D. Delahaye, S. Chaimatanan, and M. Mongeau, "Simulated annealing: From basics to applications," in *Handbook of metaheuristics*. Springer, 2019, pp. 1–35.

[110] B. Morales-Castaneda, D. Zaldivar, E. Cuevas, O. Maciel-Castillo, I. Aranguren, and F. Fausto, "An improved simulated annealing algorithm based on ancient metallurgy techniques," *Applied Soft Computing*, vol. 84, p. 105761, 2019.

[111] P. Auer, N. Cesa-Bianchi, and P. Fischer, "Finite-time analysis of the multiarmed bandit problem," *Machine learning*, vol. 47, no. 2, pp. 235–256, 2002.

[112] J. Gittins, K. Glazebrook, and R. Weber, *Multi-armed bandit allocation indices*. John Wiley & Sons, 2011.

[113] T. Yang, S. Zhang, and C. Li, "A multi-objective hyper-heuristic algorithm based on adaptive epsilon-greedy selection," *Complex & Intelligent Systems*, vol. 7, no. 2, pp. 765–780, 2021.

[114] D. Russo, B. Van Roy, A. Kazerouni, I. Osband, and Z. Wen, "A tutorial on thompson sampling," *arXiv preprint arXiv:1707.02038*, 2017.

[115] I. Umami and L. Rahmawati, "Comparing epsilon greedy and thompson sampling model for multi-armed bandit algorithm on marketing dataset," *Journal of Applied Data Sciences*, vol. 2, no. 2, 2021.

[116] T. Vidal, T. G. Crainic, M. Gendreau, and C. Prins, "Heuristics for multi-attribute vehicle routing problems: A survey and synthesis," *European Journal of Operational Research*, vol. 231, no. 1, pp. 1–21, 2013.

[117] M. Mavrovouniotis, C. Menelaou, S. Timotheou, C. Panayiotou, G. Ellinas, and M. Polycarpou, "Benchmark set for the ieee wcci-2020 competition on evolutionary computation for the electric vehicle routing problem," *KIOS CoE, University of Cyprus, Cyprus, Tech. Rep*, 2020.

[118] D. Woller, V. Kozák, and M. Kulich, "The grasp metaheuristic for the electric vehicle routing problem," in *International Conference on Modelling and Simulation for Autonomous Systems*. Springer, 2020, pp. 189–205.

[119] Y.-H. Jia, Y. Mei, and M. Zhang, "A bilevel ant colony optimization algorithm for capacitated electric vehicle routing problem," *IEEE Transactions on Cybernetics*, 2021.

[120] M. Scoczynski, M. Delgado, R. Lüders, D. Oliva, M. Wagner, I. Sung, and M. El Yafrani, "Saving computational budget in bayesian network-based evolutionary algorithms," *Natural Computing*, vol. 20, no. 4, pp. 775–790, 2021.

[121] S. J. Mousavirad, D. Oliva, R. K. Chakrabortty, D. Zabihzadeh, and S. Hinojosa, "Population-based self-adaptive generalised masi entropy for image segmentation: A novel representation," *Knowledge-Based Systems*, p. 108610, 2022.

[122] N. A. Aziz, Z. Ibrahim, S. Razali, and N. A. A. Aziz, "Estimation-based metaheuristics: a new branch of computational intelligence," in *The national conference for postgraduate research*, 2016, pp. 469–476.

[123] L. K. de Oliveira, E. Morganti, L. Dablanc, and R. L. M. de Oliveira, "Analysis of the potential demand of automated delivery stations for e-commerce deliveries in belo horizonte, brazil," *Research in Transportation Economics*, vol. 65, pp. 34–43, 2017.

[124] S. Schwerdfeger and N. Boysen, "Who moves the locker? a benchmark study of alternative mobile parcel locker concepts," *Transportation Research Part C: Emerging Technologies*, vol. 142, p. 103780, 2022.

[125] A. Seghezzi, C. Siragusa, and R. Mangiaracina, "Parcel lockers vs. home delivery: a model to compare last-mile delivery cost in urban and rural areas," *International Journal of Physical Distribution & Logistics Management*, vol. 52, no. 3, pp. 213–237, 2022.

[126] A. Lagorio, R. Pinto *et al.*, "The parcel locker location issues: An overview of factors affecting their location," in *Proceedings of the 8th International Conference on Information Systems, Logistics and Supply Chain: Interconnected Supply Chains in an Era of Innovation, ILS*, 2020, pp. 414–421.

[127] E. K. Leung, Z. Ouyang, and G. Q. Huang, "Community logistics: a dynamic strategy for facilitating immediate parcel delivery to smart lockers," *International Journal of Production Research*, vol. 61, no. 9, pp. 2937–2962, 2023.

[128] M. A. Navarro, D. Oliva, A. Ramos-Michel, B. Morales-Castañeda, D. Zaldívar, and A. Luque-Chang, "A review of the use of quasi-random number generators to initialize the population in meta-heuristic algorithms," *Archives of Computational Methods in Engineering*, pp. 1–36, 2022.

[129] Y. Huang and K. M. Kockelman, "Electric vehicle charging station locations: Elastic demand, station congestion, and network equilibrium," *Transportation Research Part D: Transport and Environment*, vol. 78, p. 102179, 2020.

[130] R. Mangiaracina, A. Perego, A. Seghezzi, and A. Tumino, "Innovative solutions to increase last-mile delivery efficiency in b2c e-commerce: a literature review," *International Journal of Physical Distribution & Logistics Management*, vol. 49, no. 9, pp. 901–920, 2019.

[131] Valhalla Project, "Valhalla matrix api reference," https://valhalla.github.io/valhalla/api/matrix/api-reference/, 2023, august 1.

[132] M. Ding, N. Ullah, S. Grigoryan, Y. Hu, and Y. Song, "Variations in the spatial distribution of smart parcel lockers in the central metropolitan region of tianjin, china: A comparative analysis before and after covid-19," *ISPRS International Journal of Geo-Information*, vol. 12, no. 5, p. 203, 2023.

[133] T. Drezner and Z. Drezner, "Lost demand in a competitive environment," *Journal of the Operational Research Society*, vol. 59, no. 3, pp. 362–371, 2008.

[134] Y. Gao, J. Li, Z. Xu, Z. Liu, X. Zhao, and J. Chen, "A novel image-based convolutional neural network approach for traffic congestion estimation," *Expert Systems with Applications*, vol. 180, p. 115037, 2021.

[135] Y. Liu, C. Yang, and Q. Sun, "Thresholds based image extraction schemes in big data environment in intelligent traffic management," *IEEE transactions on intelligent transportation systems*, vol. 22, no. 7, pp. 3952–3960, 2020.

[136] S. Wan, S. Ding, and C. Chen, "Edge computing enabled video segmentation for real-time traffic monitoring in internet of vehicles," *Pattern Recognition*, vol. 121, p. 108146, 2022.

[137] A. Valada, J. Vertens, A. Dhall, and W. Burgard, "Adapnet: Adaptive semantic segmentation in adverse environmental conditions," in *2017 IEEE International Conference on Robotics and Automation (ICRA)*. IEEE, 2017, pp. 4644–4651.

[138] D. Oliva, S. Hinojosa, V. Osuna-Enciso, E. Cuevas, M. Pérez-Cisneros, and G. Sanchez-Ante, "Image segmentation by minimum cross entropy using evolutionary methods," *Soft Computing*, vol. 23, pp. 431–450, 2019.

[139] E. Rodríguez-Esparza, L. A. Zanella-Calzada, D. Oliva, A. A. Heidari, D. Zaldivar, M. Pérez-Cisneros, and L. K. Foong, "An efficient harris hawks-inspired image segmentation method," *Expert Systems with Applications*, vol. 155, p. 113428, 2020.

[140] S. Hinojosa, D. Oliva, E. Cuevas, M. Pérez-Cisneros, and G. Pájares, "Real-time video thresholding using evolutionary techniques and cross entropy," in *2018 IEEE Conference on Evolving and Adaptive Intelligent Systems (EAIS)*. IEEE, 2018, pp. 1–8.

[141] S. Kullback, *Information theory and statistics*. Courier Corporation, 1968.

[142] D. Oliva, S. Hinojosa, E. Cuevas, G. Pajares, O. Avalos, and J. Gálvez, "Cross entropy based thresholding for magnetic resonance brain images using crow search algorithm," *Expert Systems with Applications*, vol. 79, pp. 164–180, 2017.

[143] P.-Y. Yin, "Multilevel minimum cross entropy threshold selection based on particle swarm optimization," *Applied mathematics and computation*, vol. 184, no. 2, pp. 503–513, 2007.

[144] P. W. Shaikh, M. El-Abd, M. Khanafer, and K. Gao, "A review on swarm intelligence and evolutionary algorithms for solving the traffic signal control problem," *IEEE transactions on intelligent transportation systems*, vol. 23, no. 1, pp. 48–63, 2020.

[145] G. Corriveau, R. Guilbault, A. Tahan, and R. Sabourin, "Review and study of genotypic diversity measures for real-coded representations," *IEEE transactions on evolutionary computation*, vol. 16, no. 5, pp. 695–710, 2012.

[146] A. Shukla, H. M. Pandey, and D. Mehrotra, "Comparative review of selection techniques in genetic algorithm," in *2015 international conference on futuristic trends on computational analysis and knowledge management (ABLAZE)*. IEEE, 2015, pp. 515–519.

[147] A. Lipowski and D. Lipowska, "Roulette-wheel selection via stochastic acceptance," *Physica A: Statistical Mechanics and its Applications*, vol. 391, no. 6, pp. 2193–2196, 2012.

[148] A. Slivkins *et al.*, "Introduction to multi-armed bandits," *Foundations and Trends® in Machine Learning*, vol. 12, no. 1-2, pp. 1–286, 2019.

[149] S. De, A. Ghosh, and S. K. Pal, "Fitness evaluation in genetic algorithms with ancestors' influence," in *Genetic algorithms for pattern recognition*. CRC Press, 2017, pp. 1–24.

[150] D. Oliva, E. Rodriguez-Esparza, M. S. Martins, M. Abd Elaziz, S. Hinojosa, A. A. Ewees, and S. Lu, "Balancing the influence of evolutionary operators for global optimization," in *2020 IEEE Congress on Evolutionary Computation (CEC)*. IEEE, 2020, pp. 1–8.

[151] I. Ono and S. Kobayashi, "A real-coded genetic algorithm for function optimization using unimodal normal distribution," in *Proceedings of International Conference on Genetic Algorithms*, 1999, pp. 246–253.

[152] K. Deb, D. Joshi, and A. Anand, "Real-coded evolutionary algorithms with parent-centric recombination," in *Proceedings of the 2002 Congress on Evolutionary Computation. CEC'02 (Cat. No. 02TH8600)*, vol. 1. IEEE, 2002, pp. 61–66.

[153] L. J. Eshelman and J. D. Schaffer, "Real-coded genetic algorithms and interval-schemata," in *Foundations of genetic algorithms*. Elsevier, 1993, vol. 2, pp. 187–202.

[154] R. Poli and W. B. Langdon, "Schema theory for genetic programming with one-point crossover and point mutation," *Evolutionary Computation*, vol. 6, no. 3, pp. 231–252, 1998.

[155] S. C. Esquivel and C. C. Coello, "On the use of particle swarm optimization with multimodal functions," in *The 2003 Congress on Evolutionary Computation, 2003. CEC'03.*, vol. 2. IEEE, 2003, pp. 1130–1136.

[156] R. Storn and K. Price, "Differential evolution–a simple and efficient heuristic for global optimization over continuous spaces," *Journal of global optimization*, vol. 11, no. 4, pp. 341–359, 1997.

[157] I. BoussaïD, J. Lepagnot, and P. Siarry, "A survey on optimization metaheuristics," *Information sciences*, vol. 237, pp. 82–117, 2013.

[158] H. R. Tizhoosh, "Opposition-based learning: a new scheme for machine intelligence," in *Computational intelligence for modelling, control and automation, 2005 and international conference on intelligent agents, web technologies and internet commerce, international conference on*, vol. 1. IEEE, 2005, pp. 695–701.

[159] G. Wu, R. Mallipeddi, and P. N. Suganthan, "Problem definitions and evaluation criteria for the cec 2017 competition on constrained real-parameter optimization," *National University of Defense Technology, Changsha, Hunan, PR China and Kyungpook National University, Daegu, South Korea and Nanyang Technological University, Singapore, Technical Report*, 2017.

[160] P. Arbelaez, M. Maire, C. Fowlkes, and J. Malik, "Contour detection and hierarchical image segmentation," *IEEE Trans. Pattern Anal. Mach. Intell.*, vol. 33, no. 5, pp. 898–916, May 2011. [Online]. Available: http://dx.doi.org/10.1109/TPAMI.2010.161

[161] F. A. Hashim, E. H. Houssein, K. Hussain, M. S. Mabrouk, and W. Al-Atabany, "Honey badger algorithm: New metaheuristic algorithm for solving optimization problems," *Mathematics and Computers in Simulation*, vol. 192, pp. 84–110, 2022.

[162] R. Eberhart and J. Kennedy, "A new optimizer using particle swarm theory," in *MHS'95. Proceedings of the Sixth International Symposium on Micro Machine and Human Science*. Ieee, 1995, pp. 39–43.

[163] P. Civicioglu and E. Besdok, "Bernstain-search differential evolution algorithm for numerical function optimization," *Expert Systems with Applications*, vol. 138, p. 112831, 2019.

[164] S. Mirjalili, S. M. Mirjalili, and A. Lewis, "Grey wolf optimizer," *Advances in engineering software*, vol. 69, pp. 46–61, 2014.

[165] A. A. Heidari, S. Mirjalili, H. Faris, I. Aljarah, M. Mafarja, and H. Chen, "Harris hawks optimization: Algorithm and applications," *Future Generation Computer Systems*, vol. 97, pp. 849–872, 2019.

[166] J. Zhang and A. C. Sanderson, "Jade: Self-adaptive differential evolution with fast and reliable convergence performance," in *2007 IEEE congress on evolutionary computation*. IEEE, 2007, pp. 2251–2258.

[167] X. Chen, H. Tianfield, C. Mei, W. Du, and G. Liu, "Biogeography-based learning particle swarm optimization," *Soft Computing*, vol. 21, pp. 7519–7541, 2017.

[168] M. Abd Elaziz, D. Oliva, A. A. Ewees, and S. Xiong, "Multi-level thresholding-based grey scale image segmentation using multi-objective multi-verse optimizer," *Expert Systems with Applications*, vol. 125, pp. 112–129, 2019.

[169] N. Otsu, "A threshold selection method from gray-level histograms," *IEEE transactions on systems, man, and cybernetics*, vol. 9, no. 1, pp. 62–66, 1979.

[170] C. Saha and M. F. Hossain, "Mri brain tumor images classification using k-means clustering, nsct and svm," in *2017 4th IEEE Uttar Pradesh Section International Conference on Electrical, Computer and Electronics (UPCON)*. IEEE, 2017, pp. 329–333.

[171] S. Aja-Fernández, A. H. Curiale, and G. Vegas-Sánchez-Ferrero, "A local fuzzy thresholding methodology for multiregion image segmentation," *Knowledge-Based Systems*, vol. 83, pp. 1–12, 2015.

[172] P. Ghamisi, M. S. Couceiro, J. A. Benediktsson, and N. M. Ferreira, "An efficient method for segmentation of images based on fractional calculus and natural selection," *Expert Systems with Applications*, vol. 39, no. 16, pp. 12 407–12 417, 2012.

[173] A. Hore and D. Ziou, "Image quality metrics: Psnr vs. ssim," in *2010 20th International Conference on Pattern Recognition*. IEEE, 2010, pp. 2366–2369.

[174] D. R. I. M. Setiadi, "Psnr vs ssim: imperceptibility quality assessment for image steganography," *Multimedia Tools and Applications*, vol. 80, no. 6, pp. 8423–8444, 2021.

[175] L. Zhang, L. Zhang, X. Mou, and D. Zhang, "Fsim: A feature similarity index for image quality assessment," *IEEE transactions on Image Processing*, vol. 20, no. 8, pp. 2378–2386, 2011.

[176] E. R. Arce-Santana, A. R. Mejia-Rodriguez, E. Martinez-Peña, A. Alba, M. Mendez, E. Scalco, A. Mastropietro, and G. Rizzo, "A new probabilistic active contour region-based method for multiclass medical image segmentation," *Medical & biological engineering & computing*, vol. 57, no. 3, pp. 565–576, 2019.

[177] J. Zhang, J. Du, H. Liu, X. Hou, Y. Zhao, and M. Ding, "Lu-net: An improved u-net for ventricular segmentation," *IEEE Access*, vol. 7, pp. 92 539–92 546, 2019.

[178] O. J. Bastidas, B. Garcia-Zapirain, A. L. Totoricagüena, S. Zahia, and J. U. Carpio, "Feature analysis and prediction of complications in ostomy patients based on laboratory analytical data using a machine learning approach," in *2021 International Conference BIOMDLORE*. IEEE, 2021, pp. 1–8.

[179] O. Jossa-Bastidas, S. Zahia, A. Fuente-Vidal, N. Sánchez Férez, O. Roda Noguera, J. Montane, and B. Garcia-Zapirain, "Predicting physical exercise adherence in fitness apps using a deep learning approach," *International Journal of Environmental Research and Public Health*, vol. 18, no. 20, p. 10769, 2021.

[180] O. Ramos-Soto, E. Rodríguez-Esparza, S. E. Balderas-Mata, D. Oliva, A. E. Hassanien, R. K. Meleppat, and R. J. Zawadzki, "An efficient retinal blood vessel segmentation in eye fundus images by using optimized top-hat and homomorphic filtering," *Computer Methods and Programs in Biomedicine*, vol. 201, p. 105949, 2021.

[181] H. Ayaz, E. Rodríguez-Esparza, M. Ahmad, D. Oliva, M. Pérez-Cisneros, and R. Sarkar, "Classification of apple disease based on non-linear deep features," *Applied Sciences*, vol. 11, no. 14, p. 6422, 2021.

[182] O. Ramos-Soto, E. Rodríguez-Esparza, M. Pérez-Cisneros, and S. E. Balderas-Mata, "Inner limiting membrane segmentation and surface visualization method on retinal oct images," in *Medical Imaging 2021: Biomedical Applications in Molecular, Structural, and Functional Imaging*, vol. 11600. SPIE, 2021, pp. 262–274.

[183] M. Scoczynski, D. Oliva, E. Rodríguez-Esparza, M. Delgado, R. Lüders, M. E. Yafrani, L. Ledo, M. A. Elaziz, and M. Peréz-Cisnero, "A selection hyperheuristic guided by thompson sampling for numerical optimization," in *Proceedings of the Genetic and Evolutionary Computation Conference Companion*, 2021, pp. 1394–1402.

[184] J. Murillo-Olmos, E. Rodríguez-Esparza, M. Pérez-Cisneros, D. Zaldivar, E. Cuevas, G. Trejo-Caballero, and A. A. Juan, "Thresholding algorithm applied to chest x-ray images with pneumonia," in *Metaheuristics in Machine Learning: Theory and Applications*. Springer, 2021, pp. 359–407.

[185] N. Ortega-Sánchez, E. Rodríguez-Esparza, D. Oliva, M. Pérez-Cisneros, A. W. Mohamed, G. Dhiman, and R. Hernández-Montelongo, "Identification of apple diseases in digital images by using the gaining-sharing knowledge-based algorithm for multilevel thresholding," *Soft Computing*, pp. 1–37, 2022.

[186] A. Acosta, A. Ochoa, E. Rodriguez-Eparza, D. Oliva, A. A. Juan, and G. Pajares, "Classification system to detect diseases in apples by using a convolutional neural network," *Technological and Industrial Applications Associated With Industry 4.0*, vol. 347, p. 331, 2021.

[187] B. Morales-Castañeda, D. Oliva, A. Casas-Ordaz, A. Valdivia, M. A. Navarro, A. Ramos-Michel, E. Rodríguez-Esparza, and S. J. Mousavirad, "A novel diversity-aware inertia weight and velocity control for particle swarm optimization," in *2023 IEEE Congress on Evolutionary Computation (CEC)*. IEEE, 2023, pp. 1–8.

[188] M. A. Navarro, B. Morales-Castañeda, A. Ramos-Michel, D. Oliva, A. Valdivia, A. Casas-Ordaz, and E. Rodríguez-Esparza, "An hyper-heuristic based population management through statistical analysis and phases optimization," in *2023 IEEE Congress on Evolutionary Computation (CEC)*. IEEE, 2023, pp. 1–8.

[189] B. Morales-Castañeda, D. Oliva, M. A. Navarro, A. Ramos-Michel, A. Valdivia, A. Casas-Ordaz, E. Rodríguez-Esparza, and S. J. Mousavirad, "Improving the convergence of the pso algorithm with a stagnation variable and fuzzy logic," in *2023 IEEE Congress on Evolutionary Computation (CEC)*. IEEE, 2023, pp. 1–8.

[190] E. Perez-Zarate, O. Ramos-Soto, E. Rodríguez-Esparza, and G. Aguilar, "Loli-iea: low-light image enhancement algorithm," in *Applications of Machine Learning 2023*, vol. 12675. SPIE, 2023, pp. 230–245.

[191] E. Rodríguez-Esparza, B. Morales-Castañeda, A. Casas-Ordaz, D. Oliva, M. A. Navarro, A. Valdivia, and E. H. Houssein, "Handling the balance of operators in evolutionary algorithms through a weighted hill climbing approach," *Knowledge-Based Systems*, vol. 294, p. 111784, 2024.